STRESS CORROSION CRACKING OF NUCLEAR GRADE STEELS.

by

M.A. Gammon

A thesis submitted to the Faculty of Engineering, University of Cape Town, in fulfilment of the degree of Master of Science in Engineering.

Department of Materials Engineering
University of Cape Town

December 1992

TABLE OF CONTENTS

TABLE OF CONTENTS

ACKNOWLEDGMENTS 1

ABSTRACT 2

1 INTRODUCTION 3

2 LITERATURE REVIEW 4

2.1 Introduction 4
2.1.1 The Nuclear Power Industry 4

2.2 Stress Corrosion Cracking 6

2.3 Passivating Materials 7
2.3.1 Measuring Sensitization – ASTM 262 9
2.3.2 Measuring Sensitization – The EPR Method 10

2.4 Crack Initiation 11

2.5 Factors Influencing Crack Growth 12
2.5.1 Mechanical Factors 12
2.5.2 Electrochemical Factors 14
2.5.3 Metallurgical Factors 17

2.6 Mechanisms of Stress Corrosion 18
2.6.1 Pre-Existing Active Path Mechanism 18
2.6.2 Deformation Assisted Active Path Mechanism 19
2.6.3 Adsorption Mechanism 20
2.6.4 Film Induced Cleavage 20

2.7 Stress Corrosion Cracking Test Methods 21
2.7.1 Constant Displacement 22
2.7.2 Constant Load 23
2.7.3 Slow Strain Rate 23
2.7.4 Fracture Mechanics Approaches 26

2.8 Stress corrosion cracking of 316L 27

2.9 Stress corrosion cracking of type 508 steel 29

3 EXPERIMENTAL METHOD 32
3.1 Material 32
3.1.1 316NG Stainless Steel 32
3.1.1.1 Microstructure 34
3.1.1.2 Mechanical Properties 35
3.1.2 A508 Pressure Vessel Steel 36
3.1.2.1 Microstructure 39
3.1.2.2 Mechanical Properties 40
3.2 Experimental Method 41
3.2.1 Slow Strain Rate Testing 41
3.2.1.1 Slow Strain Rate Test Apparatus. 42
3.2.1.2 Experimental Procedure 44
3.2.2 Rising Load Fracture Mechanics Testing 45
3.2.2.1 Rising Load Test Apparatus 46
3.2.2.2 Experimental Procedure 48
3.2.3 Electrochemical Tests 49

4 RESULTS 51
4.1 316NG MATERIAL 51
4.1.1 Slow Strain Rate Tests 51
4.1.1.1 Mechanical Properties 51
4.1.1.2 Fractography 53
4.1.2 Corrosion Properties 55
4.1.3 Electrochemical Potentiodynamic Reactivation 56
4.2 A508 MATERIAL 58
4.2.1 Slow Strain Rate Tests 58
4.2.1.1 Mechanical Properties 58
508 – A, Condition HT1 58
508 – A, Condition HT2 59
508 – A, Condition HT3 60
508 – B, Condition HT3 61
4.2.1.2 Fractography 62
508 – A, Condition HT1 62
508 – A, Condition HT2 66
508 – A, Condition HT3 69
508 – B, Condition HT3 70
4.2.2 Rising Load Tests 72
4.2.2.1 Mechanical Properties 72
4.2.2.2 Fractography 73

5. DISCUSSION 75
5.1 316NG Material 75
5.1.1 General Observations 75
5.1.2 Sensitization and Corrosion Properties 75
5.1.3 Slow Strain Rate Testing 76
5.2 508 Material 79
5.2.1 General Observations 79
5.2.2 Heat Treatments 80
5.2.3 Slow Strain Rate Testing 80
5.2.4 Rising Load Testing 85

6. CONCLUSIONS 87

REFERENCES 88

APPENDIX A

APPENDIX B

APPENDIX C

APPENDIX D

ACKNOWLEDGMENTS

I would like to express my appreciation to all those who assisted me during the course of this project, in particular:

Professor A Ball, my supervisor, for his advice and support.

Dr RD Knutsen for his advice and assistance at various stages through the project.

Mr N Dreze and Mr G Newins for their technical assistance.

My wife, Susan, for encouragement, support and understanding.

The staff and my fellow students for their support, encouragement and guidance.

Finally, the Council for Nuclear Safety are gratefully acknowledged for their funding and assistance.

Dedicated to my parents

ABSTRACT

A nuclear grade 316L stainless steel and a 508–III quenched and tempered pressure vessel steel were studied for their stress corrosion cracking susceptibility. Cylindrical tensile specimens were subjected to slow strain rate testing at 75°C in aerated, aqueous solutions (distiled water with 1000ppm Cl^- or $SO_4^=$ ions in solution) in a range of corrosion potentials. The 316L has been examined for sensitization and stress corrosion resistance. This study has shown that the peak degree of sensitization attainable in this material is well within the limits considered as safe by the nuclear power industry. This material is not susceptible to environmentally assisted cracking as long as the potential is kept below the pitting potential for the material. A single instance of intergranular stress corrosion cracking was noted when this material was tested in 1000ppm Cl^- solution at 440mV (SHE). Two casts of 508–III have been examined: 508–A has been tested in the as quenched condition as well as after two tempering heat treatments, while 508–B has been tested in the fully tempered condition only. The mechanical properties of the 508 type materials are strongly influenced by the heat treated condition and mildly influenced by the service environment. In the quenched condition anodic intergranular stress corrosion cracking is severe in the chloride solution and it is argued that the absence of intergranular cracking in the sulphate solution is due to the over aggressiveness of this environment. In all three heat treated conditions loss of ductility is more pronounced in sulphate solutions than in chlorides. Transgranular cleavage is evident in strongly cathodic conditions and this is ascribed to the ingress of hydrogen. The transgranular hydrogen embrittlement seems to be independant of heat treated condition. Rising load tests on fatigue precracked specimens have indicated that environmentally enhanced crack growth of existing defects does not occur for the conditions tested.

1 INTRODUCTION

Stress corrosion cracking is a time dependent process in which the synergistic effect of a tensile stress, a susceptible microstructure and a corrosive environment causes macroscopically brittle failure of a component. The most disturbing thing about this phenomenon is that the component often fails at loads well below the design strength, after a period of insidious slow crack growth. For a given situation, stress corrosion cracking can be reduced by changing the microstructure, or the environment, thus eliminating one of the components of the synergism mentioned earlier.

In the nuclear power industry failure of a reactor pressure vessel would obviously constitute a major disaster. Stress corrosion cracking is a constant concern in this context because the detection of small cracks is no trivial matter. A sound understanding of the causes and processes of stress corrosion cracking is required by industry so that circumstances conducive to crack initiation and growth can be avoided in opperating reactors.

In an effort to develop a local nuclear power industry the South African Atomic Energy Corperation has developed the capability to manufacture steels for use in nuclear power plants. This study seeks to evaluate the microstructural susceptibility of two such locally manufactured steels to stress corrosion cracking. A cast of nuclear grade AISI 316L and a cast of ASTM A508-III pressure vessel steel are examined using the slow strain rate method. Small cylindrical tensile specimens were used for all test conditions, while precracked compact tension (CT) specimens were used to investigate initiation vs propagation phenomina in the A508 steel in one of the heat treated conditions.

2 LITERATURE REVIEW

2.1 Introduction

The integrity of the reactor pressure vessel is of fundamental importance to the safe operation of nuclear plant, however, the list of potential problems associated with the design, construction and operation of a reactor are numerous. These problems, in conjunction with the in service degradation of operating reactors, has demanded research. It follows that the literature dealing with the environmental degradation of pressure vessels is extensive and complex. The complexity is partly due to problems associated with finding realistic test conditions (those giving results which can confidently be extrapolated to plant conditions) and partly because of the range of materials and operating environments in use within the industry.

Environmentally assisted cracking is an umbrella term encompassing stress corrosion cracking, (the subject of this study), hydrogen embrittlement, liquid metal embrittlement and corrosion fatigue. While it is helpful to draw theoretical distinctions between these facets of environmental failure, there is often a degree of overlap with more than one process in operation in a given situation.

2.1.1 The Nuclear Power Industry

Commercial boiling water reactors [1-3] (BWR) use high purity water at a feed temperature of about 190°C to produce 1.7 tonnes per second of turbine steam at 288°C. Pressure within the system is maintained at 7 MPa and water is re-circulated through the reactor at 13 tonnes per second. Under these conditions (BWR), nuclear reactions within the cooling water produce oxidizing radiolysis products (O_2 and H_2O_2).

Tests have shown that these can be controlled by injection of hydrogen gas into the feed water – so called Hydrogen Water Chemistry (HWC). For protection against intergranular stress corrosion cracking of feedwater piping, 2 – 3 ppm H_2 is adequate, however, impractically high doses would be required to protect the main reactor pressure vessel [3].

Pressurised water reactors [4] (PWR) operate at higher temperatures and pressures than boiling water reactors. In these machines water is circulated through the reactor at 18 tonnes per second and heated from 290°C to 325°C at a pressure of 15.5 MPa. This is used to produce 1.5 tonnes per second of steam at 275°C and 5.7 MPa in heat exchanges called steam generators. Up to 6000 ppm boron and 5 ppm lithium can be added to the water in PWR reactors depending on the current state of the fuel cycle [5]. These are used to control the neutron flux within the reactor core.

There is a wide range of construction materials in use in commercial water cooled reactors [1,6-8]. A508 – II and A508 – III forgings, together with A533 – B and A333 – 6 rolled plate make up the majority of the reactor pressure vessels, usually weld overlaid with 308 and 309 stainless steels. Primary piping is normally 304L, 316L or, less commonly, 321L stainless steels with cast duplex stainless elbows and pump housings. In PWR systems the steam generator tubing is Inconel 600, Inconel 800, Inconel 690, Monel 400, Zr – II or Zr 2,5 Nb. In every case, the control of manufacturing process variables during construction and assembly is of fundamental importance to the safety of the finished reactor and particular attention has to be paid to welding and heat treatment operations. The vast majority of in-service failures can be directly attributed to these two areas.

2.2 Stress Corrosion Cracking

Stress corrosion cracking is a time dependent failure in which a susceptible material fails at loads well below the normal material's yield strength due to the synergistic action of a sustained local tensile stress and a corrosive environment. This failure mode achieved engineering significance with the 'season cracking' of brass cartridge cases in India and with the 'caustic cracking' of early riveted steel locomotive boilers.

Stress corrosion cracking is difficult to study because of the interplay between a wide range of controlling variables. In aqueous tests, significant problems are associated with:

- control of water chemistry,
- control and monitoring of dissolved oxygen concentration,
- potentiostatic control together with reference electrode design,
- seals for dynamically loaded test cells,
- so called "inert salts" for high temperature conductivity,
- electrical isolation of the specimen,
- crack growth monitoring systems,
- effects of water flow rates (laminar or turbulent flow) [1].

Due to the restrictions on solution mixing afforded by the crack geometry, the environment within the crack enclave can differ markedly from that of the bulk solution. The free corrosion potential of the crack tip differs from that of the general material surface because of a drop in electrochemical potential along the length of the crack (a result of the ohmic resistance of the solution within the crack), and the change in free corrosion potential caused by changing solution concentrations along the crack length. Macroscopically, stress corrosion cracks propagate on a plane perpendicular to the principle tensile stress in an inter or transgranular manner depending on the specific material-environment combination. In severe stress corrosion cracking failures there is no macroscopic plastic deformation.

The interpretation of test results can often be difficult, especially when the indications of stress corrosion cracking are not clear. Payer, Berry and Boyd [9] suggest the classification of test results into one of three catagories: clear indications of stress corrosion cracking, clear absence of stress corrosion cracking and "ambiguous indications", the latter usually being shallow surface events. Severe stress corrosion cracking is indicated by substantial loss of ductility together with metallographic and fractographic observations of cracks propagating in an inter or transgranular manner perpendicularly to the principal tensile stress.

Metallographic and fractographic examinations are the only conclusive methods for confirming the presence or absence of stress corrosion cracking. Once confirmation is obtained by one or other of these techniques other parameters can be used to quantify the severity of the effect.

2.3 Passivating Materials

Some metals have very low general corrosion rates due to the formation of a tenacious, impermeable oxide layer on their surfaces which prevents further corrosion. Aluminium alloys and stainless steels are examples of this phenomenon. The protection afforded by this layer is a function of how strongly it adheres to the surface of the metal and whether or not it prevents the ingress of further oxygen to the underlying metal. If the oxide exhibits a volume change on formation then it is unlikely that it will be able to form a permanent continuous layer.

This passive layer is only able to form over a specific potential range as illustrated in fig. 1. It has been found that the critical potential ranges for stress corrosion cracking of passivating materials lie in the regions of active to passive transition [10,11].

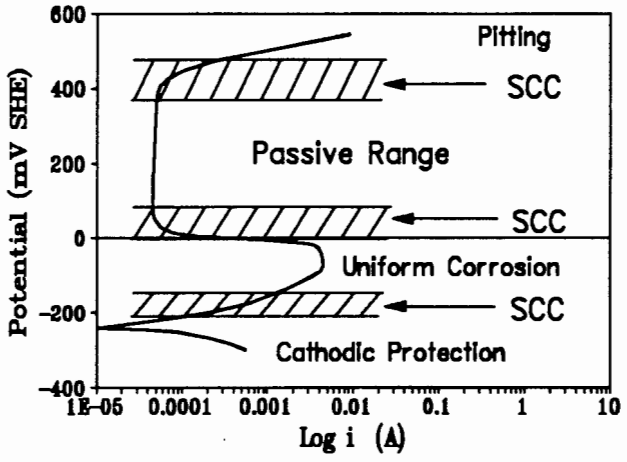

Figure 1 Stress corrosion cracking occurs near the active to passive transition potentials in passivating steels. Schematic for 304 in 1M H_2SO_4 solution. (after Staehle [11])

In stainless steels the corrosion protection layer is an oxide of chromium and a continuous layer will form if the steel has more than 12 wt% chromium. Stainless steels can be sensitized by heat treatments through the formation of $M_{23}C_6$ chromium rich carbides at the grain boundaries [12-14] and at dislocation sites within the grain interiors [15-19] resulting in a loss of chromium in the regions adjacent to the carbides. These steels thus loose their ability to form a continuous protective layer and therefore develop active intergranular or transgranular corrosion paths. In this condition the steel is said to be sensitized and, depending on the service environment, could fail due to stress corrosion cracking.

The kinetics of sensitization are diffusion controlled and are therefore temperature and time dependent. In this process the diffusion of chromium to the grain boundary leaves the metal adjacent to the grain boundary denuded of chromium, thus establishing a chromium concentration gradient between the interior and exterior of the grains. If the metal is held at elevated temperatures for longer times, chromium from the grain interiors will diffuse down this concentration gradient into the depleted regions [12] thus levelling out the concentration gradient. This will eventually lead to a situation where the grain interiors have a lower bulk chromium content but no isolated regions which are unacceptably depleted of chromium. This process is called healing and is illustrated in fig. 2.

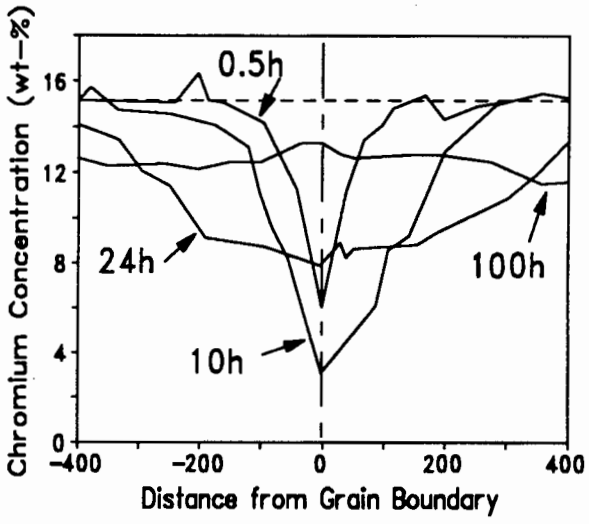

Figure 2 Variation in grain boundary Cr depletion in Ni-14.7 Cr-7 Fe-0.03 C alloy annealed for 20 mins at 1100°C and aged at 700°C for the times shown. (After Sedriks [20])

2.3.1 Measuring Sensitization – ASTM 262

Sensitization of stainless steels is a major engineering problem because of the unavoidable use of welding in the manufacture of plant and equipment. Several procedures have been developed to detect sensitization, and the most commonly used methods form the basis of ASTM A262 [21]. This standard consists of five standardized tests for the identification of sensitization in a range of stainless steels.

ASTM 262 Practice A is a quantitative test which is used for acceptance of material but not for rejection. It provides a simple method of screening out those specimens which are certain to be free of rapid intergranular attack in the other four test methods. In this test, polished specimens are etched in 10% oxalic acid solution at a current density of $1A/cm^2$ for 90 seconds. The etched surface is then classified as either stepped, duel or ditched. Those specimens which are duel or ditched are then tested using one or more of the boiling acid tests which make up Practices B, C, D and E of ASTM 262. Metals with a stepped structure have traditionally been accepted as being free of sensitization.

Etching in oxalic acid under these conditions *initially* causes attack of the chromium rich regions [10], not the chromium depleted regions around them. This is due to a complex chain of reactions which occurs when a strongly oxidizing potential is impressed on the strongly reducing solution [22]. The chromium rich phases are attacked to give off hexavalent chromium ions, which in turn are reduced by the oxalic acid to give $CrOH^{2-}$ [22]. This causes an increase in the oxidizing power within the crevice and attack of the regions adjacent to the grain boundaries follows. Due to this mechanism, material which is in the fully healed condition (as shown by the 100 hour line in fig. 2), and not susceptible to IGSCC, will fail the oxalic acid etch test because the chromium rich carbides are still present [22].

2.3.2 Measuring Sensitization – The EPR Method

The electrochemical potentiodynamic reactivation (EPR) test technique [23-25] has been developed in an attempt to find a rapid, non destructive and quantitative method of measuring the degree of sensitization (DOS) of stainless steels. In some applications [26] it has been found that intergranular failure has occurred in steel which has passed the ASTM 262 test while in other, less critical applications it may be acceptable for economic reasons to use a "moderately" sensitized stainless steel which would fail the ASTM test. The EPR technique is much more sensitive than the ASTM tests and has been successfully used to measure radiation induced sensitization of stainless steels [27].

The EPR technique as proposed by Clarke [23] involves the measurement of the total charge Q that flows when a metal is scanned from a passive potential through to the free corrosion potential. If the material is depleted in chromium then the oxide film will heal slowly and a larger total charge will be required to achieve film healing than that required for material which does not have any chromium depletion [28]. This charge is normalized with respect to the assumed total grain boundary area, GBA, (a function of grain size) and is then a

measure of the ease with which the protective oxide film is able to repair itself at active potentials. In his recommendations for standardising this process, Clarke proposed that the degree of sensitization, Pa, be calculated as:

$$Pa = Q / GBA$$

where the grain boundary area (GBA) is calculated from the area of the specimen, A_S, and the ASTM grain size number, X, according to the following formula:

$$GBA = A_S \left[5.09544 \times 10^3 \exp^{(0.34696\ X)} \right]$$

The assumption inherent in this is that all of the corrosion current flowing during the reactivation scan comes from 2μm on either side of the grain boundaries.

There are several variations on this concept. The early work by Cihal [24] employed a double loop scan in which the ratio of the total charge flowing during a cathodic scan to that of an anodic scan over the same potential range is a measure of the degree of sensitization of the material. More recently [25] the ratio of the peak currents during cathodic and anodic scans has been used in a similar way. Each of these approaches is based on the same underlying principle, that of measuring the total charge or current needed to break and reform the passive layer.

2.4 Crack Initiation

The initiation phase of stress corrosion cracking typically accounts for most of the time to failure, and the mechanism of initiation differs from one situation to another. In severe cases bad design or poor control of manufacturing methods results in surface roughness and crevice situations so that local corrosive attack is progressing even before the plant is commissioned.

On smooth surfaces exposed to an aggressive environment, stress corrosion cracking is often preceded by some form of local attack. It has been shown that pitting attack occurs preferentially on surface or near surface inclusions and MnS inclusions are particularly aggressive in this regard [29].

Film rupture by slip is an alternate agent for the initiation process in situations where the operating loads in conjunction with residual stresses cause localised plastic deformation of the surface exposed to the environment. This is especially severe in materials which have a low stacking fault energy. The presence of aggressive ionic species in the electrolyte, such as Cl^- and $SO_4^=$, enhances the breakdown of the passive layer and contributes significantly to crack initiation.

2.5 Factors Influencing Crack Growth

2.5.1 Mechanical Factors

Environmentally assisted cracking is driven by tensile stresses. These stresses are static in the case of stress corrosion cracking, or cyclic in the case of corrosion fatigue. Residual stresses from the manufacturing process can often exceed the yield stress of the material [30] and are thus of great significance when evaluating the nominal operating loads on a component; residual stresses alone can cause stress corrosion cracking. Careful attention must also be paid to stress concentrating effects such as changes in geometry and surface or near surface defects in the material [43].

The loading rate is also an important mechanical parameter in the study of stress corrosion cracking. The crack tip strain rate controls the rate at which fresh metal is exposed to the environment, while the passivation rate is a measure of how fast the surface oxide layer is formed. If the mechanical action of breaking the oxide layer is an important step in the crack advancement process then these two time dependent processes must be balanced for an optimum crack growth rate. Slow loading rates allow passivity to dominate while excessively high loading rates cause ductile tearing and crack blunting. This is indicated in fig. 3.

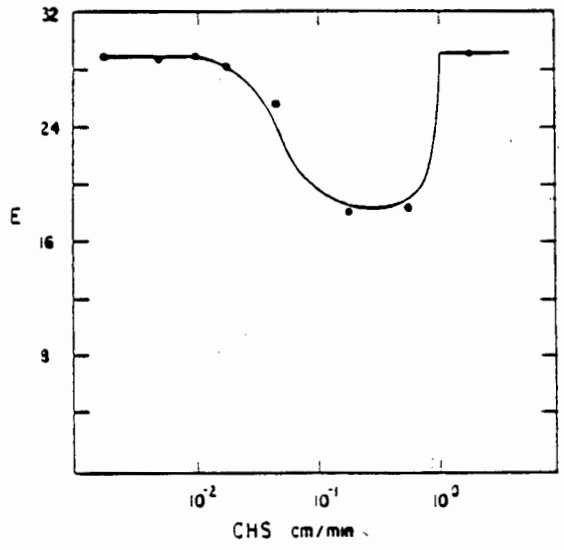

Figure 3 The influence of crosshead speed (strain rate) on the sensitivity (E = strain to fracture) to stress corrosion cracking. (After Kim and Wilde [31])

Buzzanca, Caretta, Meini, Pascal and Ronchetti [32] have conducted a study of the strain rate effect on IGSCC which highlights this relationship between material susceptibility, environmental aggressiveness and strain rate. They identify three categories of strain rate dependance. At the two extremes, no environmental effect is evident while at intermediate strain rates (between 10^{-4} and 10^{-8} s^{-1}) the severity of the effect depends on the specific situation. If the material is very susceptible or the environment very aggressive then stress corrosion cracking will occur at the upper end of this range. Conversely, if the material is mildly susceptible or the environment relatively benign then strain rates at the bottom end of this range produce environmental cracking.

A round robin testing programme co-ordinated by the International Cyclic Crack Growth Rate Collaborative Group has investigated the effect of water flow rate on cyclic crack growth rates in PWR environments [8]. This work has shown a significant relationship between this test variable and crack velocities. Under low flow rates (i.e. lamina flow conditions) crack growth rates have been orders of

magnitude higher than for dry conditions, while under high flow rates (i.e. turbulent conditions) no appreciable effect of PWR environment was observed.

In developing a mixed potential model to analyse the effectiveness of hydrogen water chemistry for protecting boiling water reactor stainless steel components against IGSCC, Macdonald [33] has shown that for high dissolved oxygen contents the water flow dynamics are not significant. In contrast, at low oxygen contents the predicted electrochemical potential is highly sensitive to hydrodynamic conditions, because under these conditions the limiting current for reduction of the active species in the electrolyte is of the same order of magnitude as the passive current of the stainless steel.

2.5.2 Electrochemical Factors

It is well known that any corrosion process involves the dissolution of metal atoms into the electrolyte through the release of electrons:

$$M \rightleftharpoons M^{n+} + ne^-$$

The left to right reaction can be encouraged by removing the reaction products, that is the M^{n+} and e^-. Any accumulation of M^{n+} ions would slow down the corrosion rate and in severe cases could halt the reaction. This is known as concentration overpotential.

In the same way, if a net negative charge is allowed to accumulate on the metal the reaction will be slowed down and eventually halted, a fact exploited in cathodic protection processes. The potential at which this happens can be measured relative to some reference (usually the standard hydrogen electrode) and is known as the Standard Single Cell Potential, which forms the basis of the Electrochemical Series.

For corrosion of a single metal in solution the anodic reaction listed above is accompanied by one of the cathodic reactions:

$$4H^+ + O_2 + 4e^- \rightleftharpoons 4H_2O^-$$

(OXYGEN REDUCTION REACTION)

$$2H^+ + 2e^- \rightleftharpoons H_2$$

(HYDROGEN EVOLUTION REACTION)

In their forward directions both of these reactions lead to an increase in the solutions pH by removing H^+ ions. This means that both of these reactions are encouraged by acidic conditions. In addition, the oxygen reduction reaction is enhanced by free oxygen in the solution.

During general corrosion, anodic and cathodic reactions are simultaneously occurring at different sites on the surface of the metal. In materials that form a protective oxide layer, the formation of local corrosion sites (pitting, crevice corrosion or stress corrosion cracking) leads to a situation where the cathodic current is spread over a large passive area, while the anodic surface area is comparatively small and very high anodic dissolution rates are thus sustained.

The environments encountered in commercial reactors can be devided into two categories. In boiling water reactors oxygen cannot be avoided (because it is produced in the reactor during opperation) so very pure water has to be used, while in pressurised water reactors the water is de-oxygenated and alkali treated usually to a room temperature pH of 9 (1).

The reason for this can best be understood with the aid of fig. 4. Here we see that at low dissolved oxygen levels the material has a very low free corrosion potential (fig. 4a), but a small increase in oxygen concentration can shift this anodically by about 500mV. If we combine this with the Pourbaix diagram for iron in water at 300°C (fig. 4b) one can see that while the oxygen concentration is less than 10ppb the free corrosion potential is hydrogen redox controlled and is in the

immune region. However, if there is more than 10ppb dissolved oxygen then the free corrosion potential shifts anodically by about 500mV (fig. 4a) to an oxygen redox controlled regime where the metal is in a passive region (fig. 4b) and is thus susceptible to local attack.

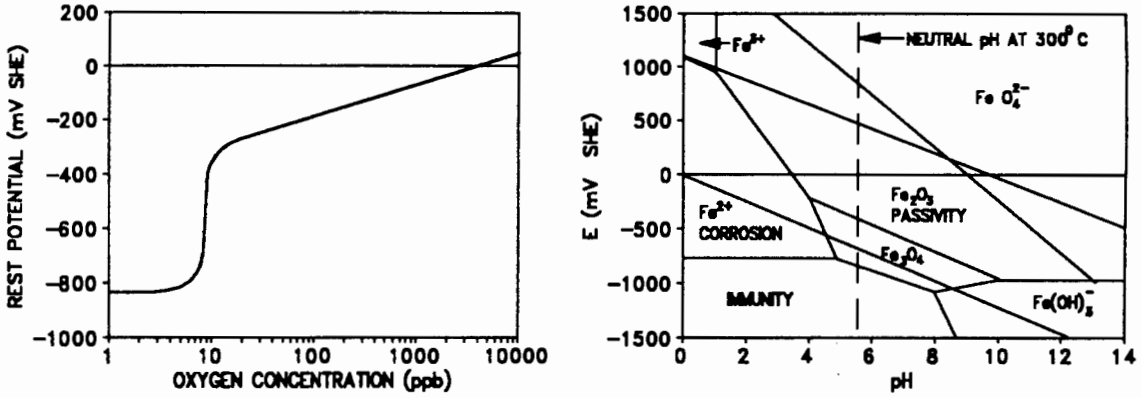

(a) (b)

Figure 4 (a) The equilibrium corrosion potential of A533-B in pure water as a function of dissolved oxygen concentration, (b) Pourbaix diagram for iron in water at 300°C (after Scott [1]).

The work of Hurst *et al* [5] has demonstrated the significance of potential and dissolved oxygen concentration on the initiation of stress corrosion cracking in smooth tensile specimens of A508-III material tested in PWR water at 290°C. In this case cracking was observed in the potential range -250mV to +100mV SHE, this potential being achieved both potentiostatically and by dosing the water with about 200 ppb of oxygen.

In a test program involving slow strain rate testing of 304, 316NG and A533 B pressure vessel steels, Ljungberg, Cubicciotti and Trille [34] investigated the effect of various water impurities on stress corrosion cracking. They found that sulphate and chloride ions significantly enhanced the intergranular stress corrosion cracking of 304, while hydrogen peroxide and copper at low concentrations aggravated the detrimental effect of chlorides. Nitrates and carbon dioxide had no effect on 304 stainless steel.

They found that transgranular stress corrosion cracking of A533-B was enhanced by all impurities tested (sulphate, chloride, carbon dioxide and sodium carbonate), while none of these impurities (including chlorides with copper added) produced any stress corrosion cracking of the 316NG tested in this program [34].

2.5.3 Metallurgical Factors

Material modifications, through adjustments in alloying elements or heat treatment, can affect stress corrosion crack initiation and growth rates. Changes in composition, microstructure and dislocation densities can alter the mechanism and/or rate of the processes controlling propagation, leading to significant changes in cracking susceptibility.

Variations in the intergranular stress corrosion cracking behaviour of different heats of 304 stainless steel have been discussed by Szklarska-Smialowska and Cragnolino [35]. It is clear that significant differences in susceptibility are evident after identical thermo-mechanical histories. This they attribute to the collective effect of changes in inclusion size and shape distributions and minor changes in impurity levels.

Coleman *et al* [36] found that the relationship between stress corrosion cracking susceptibility and grain size is in general agreement with the Petch model for brittle failure, that is, the fracture stress is inversely proportional to $\sqrt{d}$, where d is the average grain size. Thus a fine grain sized steel is more resistant to stress corrosion cracking than a coarse grained steel.

Stress concentrations are formed in an alloy where coplanar dislocation arrays pile up against intergranular or transgranular barriers [37]. These arrays are regions of higher disorder and higher internal energy, and thus act as sites for selective dissolution. Plastic deformation increases the number of sites of this type, thus increasing the stress corrosion cracking susceptibility of the material. Diffusion rates are also higher in these planar dislocation "pipes" and this can

lead to deformation induced chromium carbide precipitation within stacking fault planes, intersections of twin faults and regions of high dislocation densities [18].

Dislocation cell structures are not as prone as planar structures to stress corrosion cracking and hydrogen embrittlement in austenitic stainless steels [38]. Kowaka [37] has shown that at very low phosphorus levels (P = 0.003wt%), the dislocation structure of 304 is cellular, while at higher levels (P = 0.071wt%) it is planar. This may account for the adverse effect of phosphorus on the stress corrosion cracking of austenitic stainless steels.

In a study of several high strength steels in 3.5% NaCl solution Kerr et al [39] found that untempered, twinned and dislocated martensitic microstructures were susceptible to stress corrosion cracking while a highly tempered martensitic microstructure containing no residual austenite was found to be the most stress corrosion resistant material condition.

2.6 Mechanisms of Stress Corrosion

Stress corrosion cracking begins with the formation of an occluded cell in which the environment is concentrated. This process can be the result of bad design (the formation of crevices etc.), bad manufacturing (rough machining), local corrosion (pitting), or deformation induced (the rupture of a passive layer due to persistent slip lines). Initiation is followed by crack growth which is usually slow and insidious.

There are four major schools of thought about the mechanisms involved in stress corrosion cracking, and these are outlined below.

2.6.1 Pre-Existing Active Path Mechanism

Grain boundaries have energy fields which make them favourable sites for impurity segregation and solute precipitation. The activity of this region is further increased by the mis-orientation of grains and the pile up of grain boundary dislocations. This strain energy can

encourage dissolution reactions and thus be a driving force for stress assisted intergranular corrosion cracking. In certain instances precipitation of impurities within grains can lead to transgranular stress corrosion cracking [16]. For stainless steels, the formation of chromium carbides at grain boundaries or at deformation sites within the grains [17] can lead to stress corrosion cracking by this mechanism, while in low alloy steels the precipitation of such impurities as sulphur and phosphorus can have the same effect [40-42]. For martensitic steels the active path can be along the prior austenite grain boundaries.

2.6.2 Deformation Assisted Active Path Mechanism

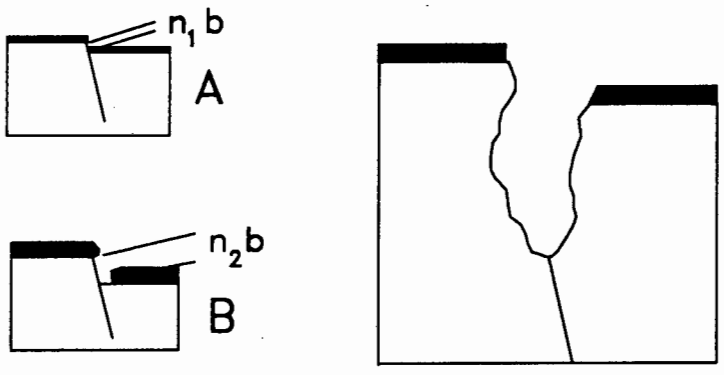

Figure 5 Film rupture of a metal with a low stacking fault energy. Thin films (A) rupture easier than thick ones (B). $n_1 < n_2$
b = Burges vector. (After Kowaka [37]).

The stress concentrating effect of a crack or other defect causes a region of plastic deformation. This encourages the eggression of dislocations which manifest themselves by the appearance of slip steps at the defect [43]. These dislocations disrupt the protective passive film and expose bare metal to the environment, thus starting the crack. In metals with a low stacking fault energy the eggression of persistent slip bands on an otherwise smooth surface can be enough to initiate cracking. This process is illustrated in figure 5.

2.6.3 Adsorption Mechanism

In this theory [37,44], impurity atoms (often hydrogen or sulphur) diffuse to the crack tip and become adsorbed to the surface (fig. 6), thus locally weakening the interatomic bonding of the metal. Dislocations initiate here and are injected into the metal along the planes of maximum shear stress (*i.e.* 45° to the principle tensile stress). This leads to an incremental crack growth process [26,27] similar in nature to fatigue crack growth.

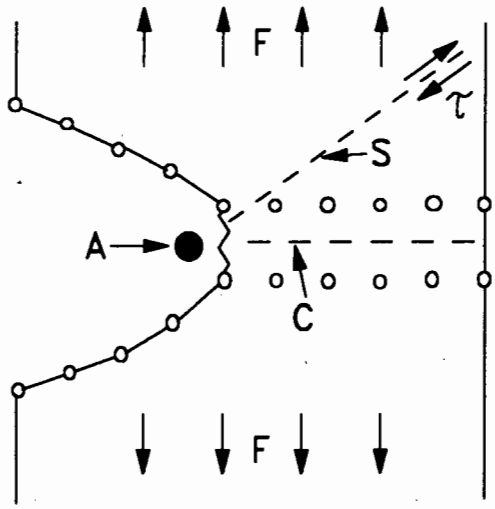

Figure 6 Adsorption of atom A at the crack tip causes a weakening of the interatomic bonding in the base metal. (After Kowàka [37])

2.6.4 Film Induced Cleavage

Sieradzki and Newman [45] developed an explanation for transgranular stress corrosion cracking based on evidence [46] that a spongy layer is formed within cracks which is not an oxide layer but a de-alloyed metallic layer with (for stainless steels Fe-Ni alloy) a continually varying composition through its thickness. They propose that the presence of this film at a crack tip can modify local deformation processes.

The main interfacial factors between the film and the underlying metal, governing the behaviour of the material are:

- lattice parameter misfit (coherency of the two lattices)
- elastic modulus mismatch
- toughness of the film
- interfacial bonding
- geometric shape of the film around the inner edge of the crack
- porosity of the film

If the film is tough, then at some specific stress intensity it will fracture [47], while if it is ductile it will undergo high speed ductile tearing and initiate shock wave microcleavage in the bulk of the material.

In this model, the problem of high crack velocities in the presence of low anodic dissolution rates is eliminated since the anodic process accounts for about 1% of the total crack advance, and the fractography arises naturally from the stepwise microcleavage process.

2.7 Stress Corrosion Cracking Test Methods

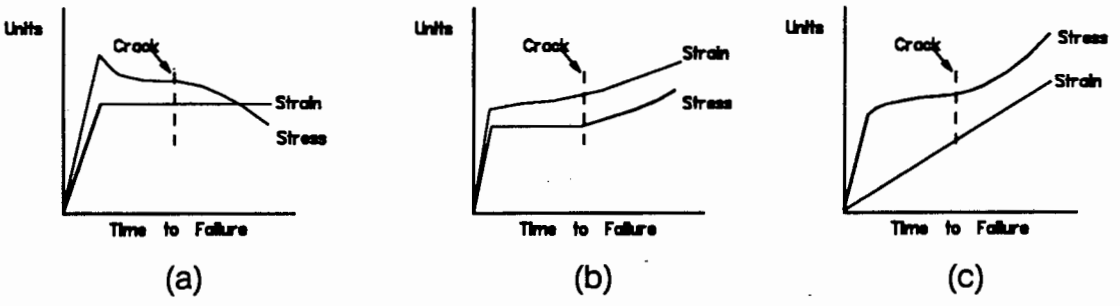

Figure 7 The variation of stress and strain during the main test methods is illustrated in these schematic diagrams. (a) = Constant displacement (bent beam testing), (b) = Constant load, (c) = Slow strain rate testing. (after Kowaka [37])

Stress corrosion cracking occurs only when specific conditions of environment, material and stress apply simultaneously. Several loading

methods are employed in the study of stress corrosion cracking and the more common ones are dealt with in the following sections. The variation of stress and strain with time during these test methods is illustrated in fig. 7.

2.7.1 Constant Displacement

The simplest form of loading is to hold a specimen at a predefined elastic or plastic strain and examine it for signs of intergranular attack after a specific time of immersion in the corrosive environment. There are two commonly employed specimen geometries for constant displacement testing: the bent beam test and the U-bend test, and these are illustrated in fig. 8.

The bent beam test [48] commonly uses three supports in which case the maximum stress is given by

$$\text{Stress} = 6\,E\,t\,y\,/\,L^2$$

where Stress is in MPa, E is the elastic modulus in MPa, t the thickness of the specimen in mm, y the deflection in mm and L the distance between the outer supports in mm.

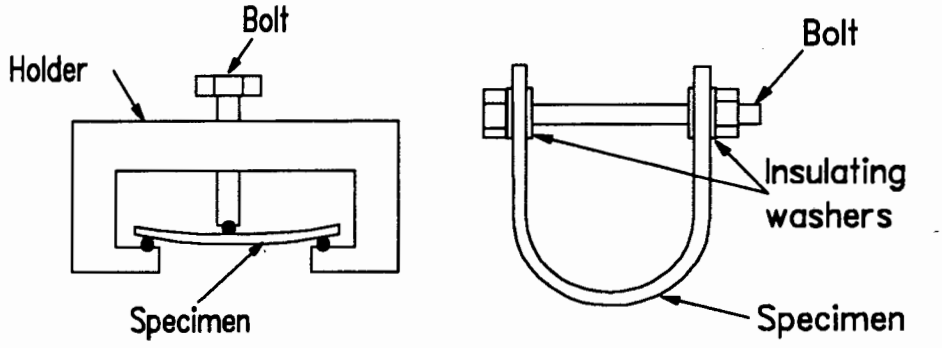

Figure 8 The bent beam and U-bend test methods employ specimens statically strained to a predefined deflection and immersed in a corrosive solution.

The U-bend test is widely used, the details being given in ASTM G30 – 72 [49]. In this test the stress profile is complex with the maximum stress being in the work hardening region above the yield point. There is a stress gradient through the thickness of the specimen with a maximum tensile stress on the outer surface and a

maximum compressive stress on the inner surface. Additionally, there is a stress gradient along the length of the specimen from zero at the outer supports to a maximum in the centre. Finally, there may also be a variation of stress across the width of the specimen.

Constant displacement specimens are popular because they are easy to produce and test, and high temperature tests can be conducted in an autoclave without the necessity of the sliding seals required for the other test methods. However, there are two major disadvantages with this test methods. Firstly, tests can take a long time and, in the absence of stress corrosion cracking, still give inconclusive results. Secondly, the complex stress profile can make quantative analysis of the results difficult.

2.7.2 Constant Load

In this test method a tensile specimen is subject to a constant load, usually by suspending a mass from the one end, and the time to failure is recorded. In some instances a small cyclic load (±5%) is superimposed on the static load as this greatly reduces the initiation time for stress corrosion cracking [37]. For high temperature work these tests can be performed in an autoclave where the pressure in the autoclave is used to produce the constant load on the specimen through the use of metal bellows [50]. These tests are more expensive than constant displacement tests and also suffer the possibility of inconclusive results if the test is terminated after some cut-off time without specimen failure.

2.7.3 Slow Strain Rate

This test method was first suggested by Nikoforova in 1961 and subsequently Parkins and Scully have used it extensively . In the early days it was referred to as constant extension rate testing (CERT), however the standard term slow strain rate testing is now used [51]. One of the chief advantages of the method is that it is relatively quick and always results in failure of the specimen. It is, however, an

unusually aggressive test method and therefore the results obtained in SSR tests can not easily be extrapolated to true plant conditions.

For stress corrosion cracks to propagate the strain rate has to fall within a certain range; both faster and slower loading rates lead to ductile failure (fig. 3 on page 13). This has been discussed in section 2.5.1.

In slow strain rate testing the degree of stress corrosion cracking can be indexed in a number of different ways [52]:

- The strain ratio: $\epsilon_{f(scc)}/\epsilon_{f(air)}$
- The stress ratio: $UTS_{(scc)}/UTS_{(air)}$
- The reduction of area ratio: $A_{f(scc)}/A_{f(air)}$
- The energy to fracture ratio: $\int \epsilon\sigma_f \, d\epsilon \; / \; \int \epsilon\sigma_f \, d\epsilon$
- The proportion of the fracture surface area that is due to SCC (*i.e.* inter or transgranular fracture regions)
- The number and length of secondary cracks penetrating the gauge length
- Time to failure
- Crack growth rates (usually with precracked specimens)

Parkins [53] has published the results of comparative tests in which low alloy ferritic and carbon-manganese steels were tested using both constant displacement and slow strain rate test methods. In this study, as with others involving non-passivating metals [54,55], the stress corrosion cracking susceptibility as indexed by these two methods are in good agreement.

In their comparative study between U-bend and slow strain rate testing of 304 stainless steel in high temperature water, Yang, Zhang, Zhao and Congleton [56] found that the susceptibility to stress corrosion cracking decreased with increasing temperature for U-bend

specimens, but peaked at 250°C for slow strain rate testing. This they ascribed to dynamic straining of the oxide layer which exhibits a different morphology and mechanical properties depending on the temperature at which in forms.

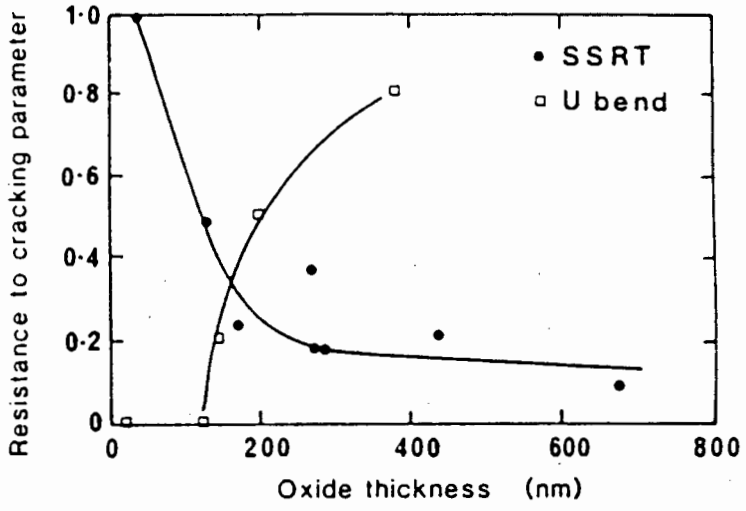

Figure 9 Resistance to cracking vs oxide thickness for U-bend and SSR test data. (UNS S31600 in water with 5ppm Cl^- at 265°C) (After Yang *et al* [57])

The same authors have published results [57] of an investigation into the oxide layers that form on 304 and 316NG stainless steels in U-bend and slow strain rate tests. From their results (fig. 9) it is obvious that in situations where a stable passive oxide layer offers protection against general corrosion the mechanical properties of the film will be important where dynamic straining of the material occurs throughout the duration of the test.

The slow strain rate test method has been adapted by Maiya [58] to make the study of crack initiation easier. He modified the specimen geometry by drilling a small diameter hole into or through the gauge length of smooth cylindrical tensile specimens. This serves to localise strain and, when used in conjunction with microscopic examination, has proved to be a sensitive way to study crack initiation processes. Additionally, when stainless steel pins are forced into the hole, crevice effects can easily be investigated. While this may seem on face value to be a good approach, it must be realised that when strain is localised into a sub-section of the gauge length the crosshead speed must be reduced accordingly, in order to achieve a *local* strain rate which is

low enough to allow for stress corrosion cracking. The lowest crosshead speed attainable on the machine used in this study produces a nominal strain rate of $3x10^{-6}$ s^{-1} for a gauge length of 15mm, and so this method could not be tried in the present work.

Beavers and Koch [59] have conducted a survey based on the literature and questionnaires sent to members of the Materials Technology Institute, the National Association on Corrosion Engineers, and the American Society for Testing and Materials. From this study they showed that the main variables of importance in slow strain rate testing are strain rate and test potential. Additionally, they found that most reported cases of anomalous results could be attributed directly to inadequate control or measurement of one or both of these parameters.

2.7.4 Fracture Mechanics Approaches

Constant load precracked fracture mechanics specimens have been used in stress corrosion cracking studies [60] to determine the threshold stress intensity for environmentally accelerated crack growth.

The use of precracked specimens simplifies the investigation of crack growth phenomena since no initiation process need be considered. Fatigue precracked specimens can be loaded in each of three modes viz:

- constant strain (using wedge opening CT specimens),
- sustained static load, and
- slow strain rate (usually referred to as rising load tests).

The variations of stress and strain with time for each of these three loading methods is the same as those shown schematically in fig. 7.

2.8 Stress corrosion cracking of 316L

It is generally accepted that type 316 stainless steel is more corrosion resistant than type 304 in chloride contaminated environments due to its higher nickel content and the addition of molybdenum. These both contribute to the formation of a more stable oxide layer and thus result in greater resistance to stress corrosion crack initiation. It is therefore advantageous to use 316 stainless steel in power generating systems where the risk of chloride contamination exists.

In an effort to limit the chances of sensitization, nuclear grade stainless steels have been developed. These have a low carbon content (<0.03 wt% max) with additions of nitrogen (0.06-0.1 wt%) to maintain strength through solid solution strengthening [61].

Nitrogen is also beneficial in preventing sensitization of stainless steels. Berneke and Sandenbergh [62] have conducted an investigation into the effects of nitrogen and molybdenum on the sensitization properties of 316L, in which nine heats, with nitrogen levels between 0.029 wt% and 0.155 wt% were hot rolled, solution annealed and subjected to a range of sensitization heat treatments between 600 and 850°C. The electrochemical potentiodynamic reactivation technique was used in conjunction with the oxalic acid etch test to investigate the degree of sensitization. In this work it was found that nitrogen improves the resistance of 316 stainless steel to sensitization for both high and low carbon steels. Their results are summarized in fig. 10 in which it can be seen that small additions of nitrogen have a pronounced effect on sensitization resistance.

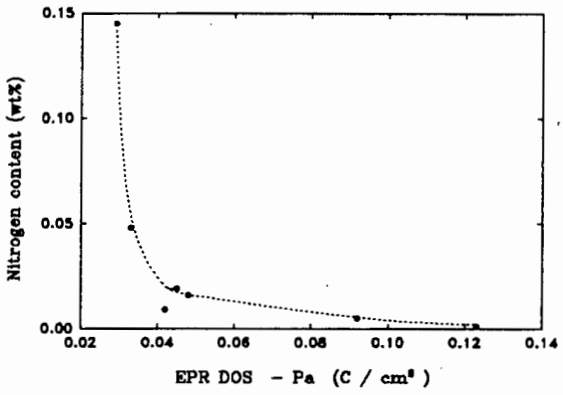

Figure 10 The effect of nitrogen on the sensitization of 316L with 2.2% Mo after heat treatment at 750°C for 6 hours. (After Berneke et al [62])

Briant *et al* (14) have found the same trend in their study and attribute the effect to segregation of nitrogen to the grain boundary regions and a possible retarding effect of nitrogen on the growth kinetics of chromium carbides, although a causative link between N_2 content and carbide growth kinetics has not been demonstrated yet.

The stress corrosion cracking of 316L in 290°C water has been studied over a number of years by Congleton and various co-workers. In their early work [63] they established that transgranular and intergranular failure occurs in annealed and sensitized steels respectively, depending on the test potential, itself a function of both dissolved oxygen and chloride ion concentrations. They found that at very low oxygen contents transgranular failure can still occur in annealed type 316 stainless steel tested at 288°C.

Later, Congleton, Zheng and Hua [64] showed that in high temperature water stress corrosion cracks will initiate in 316 stainless steel at potentials above 50mV (SHE) due to anodic dissolution, while cracks will form in the range −450 to −200mV due to fracture of the thick oxide layer that forms in this potential range.

In subsequent work [65] the effect of temperature was investigated. Figure 11 summarizes the findings of this study. The results indicate that for the clean 316L which they studied the chances of stress corrosion cracking occurring at temperatures below 100°C are remote because the oxide layer which forms at these temperatures is thin and ductile. Fracture of the thicker layer which forms at higher temperatures is responsible for initiating the stress corrosion cracking found under these conditions.

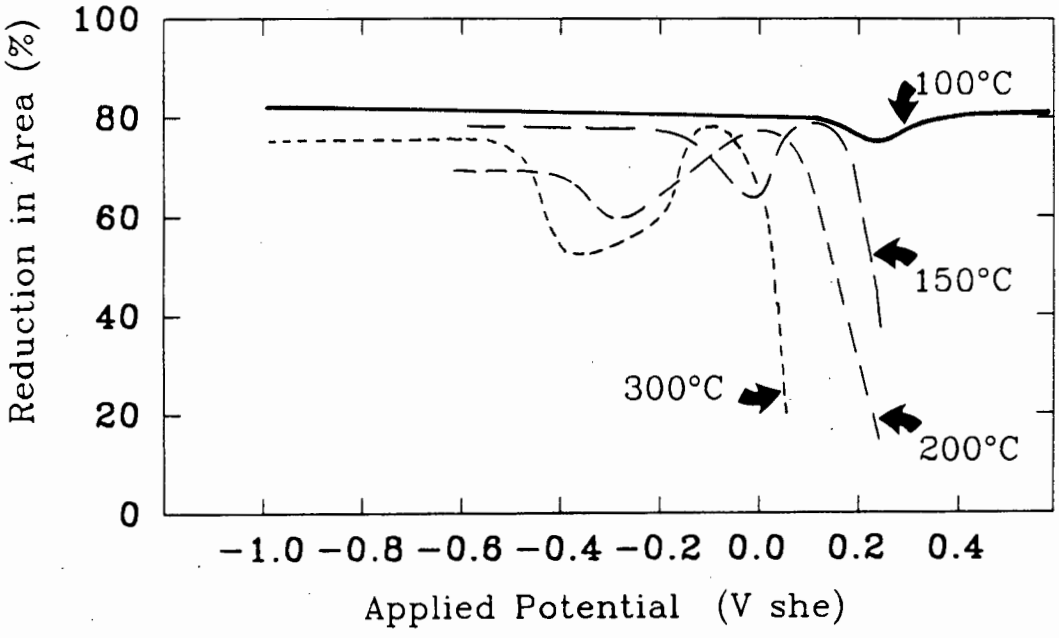

Figure 11 The effect of temperature on the stress corrosion cracking of 316L in PWR water.
(After Congleton *et al* [65]).

2.9 Stress corrosion cracking of type 508 steel

Research into environmentally assisted crack growth of ferritic pressure vessel steels has focused mainly on corrosion fatigue. Extensive work has been conducted to assure the safety of operating reactors and much of this has been coordinated by the International Cyclic Crack Growth Rate Collaborative Group. This body coordinates a large inter-laboratory collaborative testing programme in the United Kingdom which has three primary objectives [8]:

To verify the safety of the ASME XIA (1980) wet fatigue crack growth curves for UK plant conditions,

To confirm the lack of stress corrosion cracking susceptibility when subjected to static loads,

To establish an understanding of the mechanisms of crack growth in order that the interpretation of plant conditions can be intelligently reasoned.

This investigation has established a significant dependency of crack growth rate on the water flow conditions. The enhanced crack growth rates found for A508 steel in reactor water at 290°C under low flow conditions are not found when tests are conducted under high flow conditions [8]. This effect could be the result of a change in passivation rate or free corrosion potential caused by the solution flow rate or simply because of the flushing away of locally concentrating ions from the crack tip.

Atkinson [66] has investigated the effect of corrosion potential on crack growth rates of a low sulphur (S=0.005 wt%) A508-III in PWR primary water at 290°C, where the test potential was controlled both potentiostatically and by regulating the dissolved oxygen content. He found that control of water oxygen content could lead to crack growth rate enhancements, with the most severe cracking at -100mV (SHE). Potentiostatic control led to a more complex scenario with hysteresis effects apparent as the direction of potential stepping was reversed. The range of potentials for environmentally accelerated cracking was found to be -250 to +20 mV SHE. The work of Hurst et al [5] has demonstrated a clear dependence of cracking on potential and dissolved oxygen for slow strain rate specimens of A-508 steel in PWR water at 293°C. Both of these studies report an absence of significant cracking under cathodic polarisation.

Many workers have documented an effect of sulphur on the crack growth rates of pressure vessel steels. Combrade, Foucault, Marcus and Slama [67] have shown that in stagnant conditions such as in a crack, a monoatomic layer of sulphur can adsorb to the surface of steel and significantly increase the anodic dissolution current in PWR water. Their work indicates a substantial enhancement of crack growth rates for corrosion fatigue, however, slow strain

rate tests did not indicate any sulphur induced cracking enhancement. From this they conclude that the build up of an adsorbed layer of sulphur atoms on steel surfaces is more efficient in a sheltered crack than on a smooth surface. This means that sulphur will have a less significant effect on cylindrical tensile specimens than on precracked CT type specimens.

This is consistent with the work of Scott, Treswell and Druce [68] who examined the effect of steel sulphur content on corrosion fatigue crack growth rates. They found that high (0.055 wt%) sulphur steels which had shown enhanced cracking when tested in another laboratory did not show enhanced cracking when tested in their high flow rate (turbulent) test rig. The effect of sulphur is not associated with local corrosion cells around MnS inclusions as is the case in other material/environment pairs, but rather with adsorption of sulphur to the steel surface [67].

3 EXPERIMENTAL METHOD

3.1 Material

Two classes of steel used in the nuclear power industry were investigated. The aim of the study is to confirm the quality of locally manufactured steels by comparing their corrosion and stress corrosion cracking properties with comparable steels manufactured overseas. In the case of the A508 – III steel, some material from a French manufactured reactor was supplied for comparative purposes. All steels were supplied by the South African Atomic Energy Corporation (AEC).

3.1.1 316NG Stainless Steel

The 316NG material tested in this study was supplied in the form of compact tension (CT) specimens which had been used for fatigue crack growth rate tests. Slow strain rate specimens were machined from these in the same orientation with respect to the CT specimens, however, the CT specimens had been machined in two orientations namely parallel and perpendicularly to the forging direction.

The metallurgy of stainless steels is largely controlled by the iron-chromium-nickel ternary phase diagrams (Shown in Appendix A [Adapted from 69]). The effects of most alloying elements on this phase diagram can be accounted for in the equations for the chromium and nickel equivalents derived by Hull [70]. If Cr^* and Ni^* are the chromium and nickel equivalents respectively then

$$Cr^* = \%Cr + 1.21(\%Mo) + 0.48(\%Si) + 2.27(\%V) + 0.72(\%W) + 2.2(\%Ti) + 0.14(\%Nb) + 0.21(\%Ta) + 2.48(\%Al)$$

$$Ni^* = \%Ni + 0.11(\%Mn) - 0.0086(\%Mn)^2 + 0.41(\%Co) + 0.44(\%Cu) + 18.4(\%N) + 24.5(\%C)$$

The 316NG used in this study was manufactured by the AEC and the chemical composition is listed in Table 1 together with AISI specifications for this class of steel, and the Cr^* and Ni^* equivalents as calculated from the previous equations.

Element	316NG	AISI 316L
Carbon	0.013	0.03 max
Chromium	16.67	16.0-18.0
Nickel	10.49	10.0-14.0
Molybdenum	2.10	2.0-3.0
Manganese	1.09	2.00 max
Phosphorus	0.020	0.045 max
Sulphur	0.015	0.030 max
Silicon	0.58	1.00 max
Copper	0.120	
Cobalt	0.037	
Titanium	0.002	
Vanadium	0.040	
Cr^*	23.1	18.4-23.5
Ni^*	11.88	10-15

Table 1 Composition of the 316NG material used in this study together with the AISI specification for this class of steel. Chromium and Nickel equivalents calculated from the equations given in the previous section. (Composition analysis courtesy of Middleburg Steel and Alloys SA)

The composition is within specifications for a low carbon 316 stainless steel. Both the chromium and the nickel concentrations are near the lower limits allowed but impurity levels, perticularly sulphur and phosphorous, are well controlled.

The chromium and nickel equivalents can be used in conjunction with the Fe-Ni-Cr ternary phase diagrams of Appendix A to construct a pseudo binary phase diagram of Cr-Ni for this iron composition. This has been done and is shown in figure 12. This diagram represents a slice through the ternary phase diagram and therefore is calculated for a specific composition of steel, namely the steel used in this investigation. However, it is obvious from the last two lines of table 1 that the Cr^* for this steel is near to the upper limits allowed, while the Ni^* is close to the lower limits. This means that the composition *range* covered by the standard (the shaded region on the two dimensional binary phase diagram) lies predominantly to the right of the

composition of the steel used in this study, *i.e.* the composition of the 316 used is towards the ferritic extreme of what the standard allows.

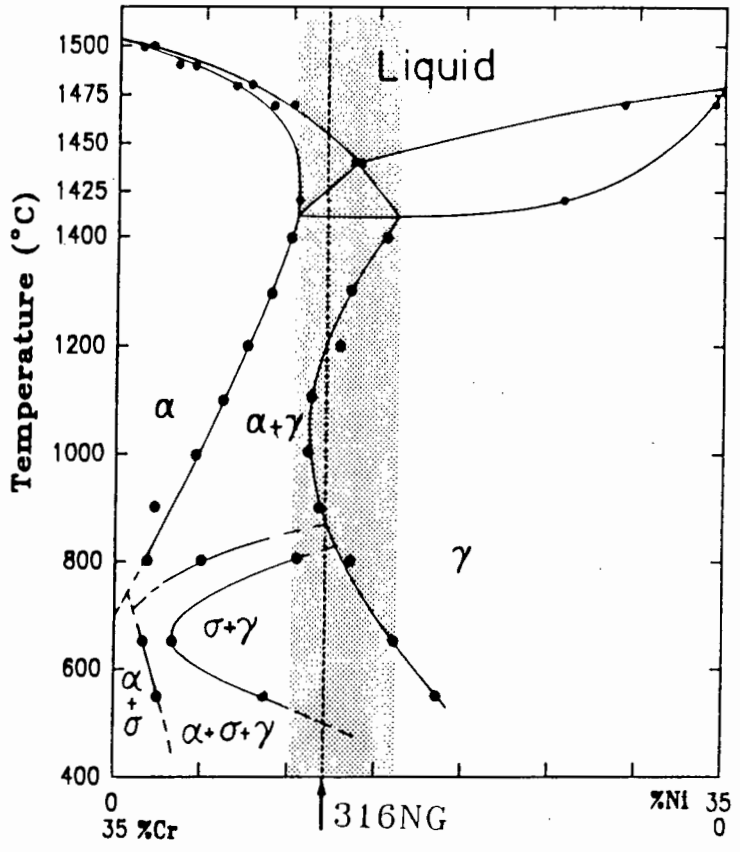

Figure 12 Pseudo binary Cr-Ni phase diagram for 77 Wt% Fe stainless steel drawn from isothermal data presented in Appendix A. The shaded region covers the range of compositions allowed by the standard while the vertical line indicates the composition of the 316NG used in this study (Ni and Cr equivalents)

3.1.1.1 Microstructure

The pseudo binary phase diagram (fig. 12) indicates that on slow cooling from the liquid phase, ferrite solidifies first. This ferrite is stable above 1200°C, but below this temperature the equlibrium condition of the material is the fully austenitic state. However, the composition of the 316NG only just passes through the nose of the fully austenitic phase region of this diagram (which is subject to errors arising from both the data of Appendix A and the calculation of Cr and Ni equivalents),

and in reality the delta ferrite may well be stable down to room temperature.

It is interesting to note that prolonged heat treatment in the temperature range 600-800°C could lead to the formation of the hard intermetallic sigma phase. This will have important repercussions when designing a heat treatment aimed at inducing sensitization. Sigma is known to cause a loss of ductility in stainless steels.

The annealed (1050°C, 0.5Hr., water quench) microstructure of the 316NG material (fig. 13) after electrochemical etching in oxalic acid reveals a stepped microstructure of austenite, with some delta ferrite stringers oriented perpendicular to the direction of forging.

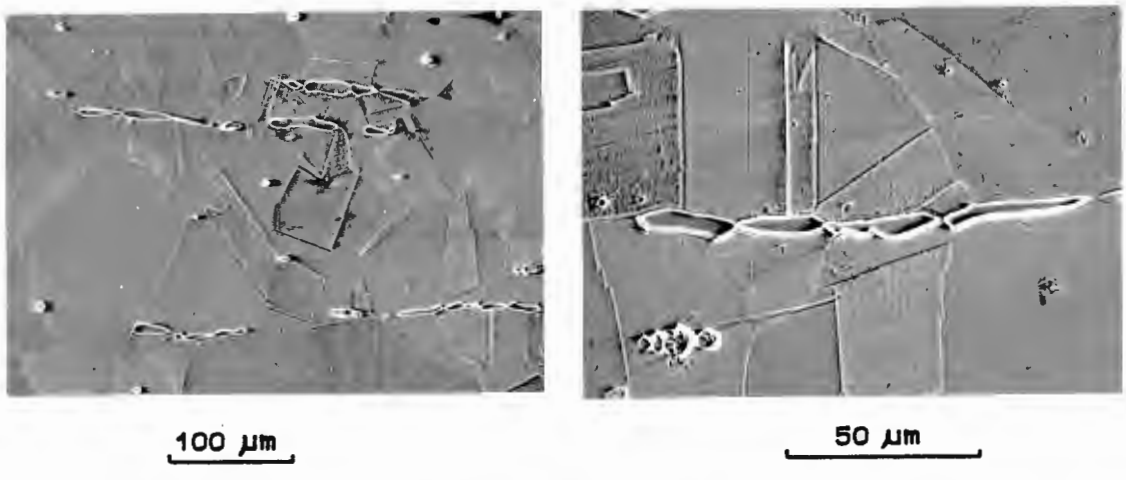

Figure 13 The microstructure of the 316NG stainless steel (after annealing at 1050°C for 0.5Hr and then quenching) shows an austenitic microstructure with some retained delta ferrite. (Electrochemically Etched in 10% oxalic acid)

3.1.1.2 Mechanical Properties

The measured mechanical properties for this steel together with the AISI specifications are listed in Table 2. This data was generated from a single specimen oriented in the forging direction. Slow strain rate results indicate that while the strength is orientation independant, the ductility is lower in this

orientation than in the perpendicular direction. The elongation to fracture is marginally below specification for this orientation but it is envisaged that this would not be the case for specimens oriented across the forging direction.

Mechanical Property	316NG	AISI (Standard)
UTS (MPa)	740	610 min
Yield (MPa)	288	240 min
Ef (%)	54	55 min
ROA (%)	77	--

Table 2 Mechanical properties of the 316NG used in this study. Data from a specimen oriented in the forging direction.

3.1.2 A508 Pressure Vessel Steel

The ASTM specification for "Quenched and tempered vacuum-treated carbon and alloy steel forgings for pressure vessels" is standard A508/A508M – 86 [71]. This specification covers quenched and tempered forgings for vessel closures, shells, flanges, tube sheets, rings, heads and similar parts. It governs the composition, mechanical properties, non destructive evaluation, welding, and various other aspects of production for eight classes of alloy steels. This study involves class three (A508 – III) from this family of tempered martensitic steels.

The standard specifies a tempering heat treatment of 595-675°C for one half hour per inch of maximum section thickness. This is sufficient to cause recovery and spheroidization of iron carbides (fig. 14). In practice these forgings are usually welded together and so this tempering is typically followed by a post weld heat treatment which would cause further recovery of the microstructure.

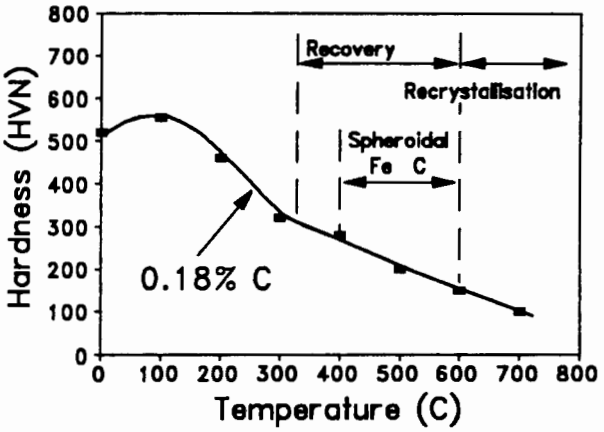

Figure 14 Hardness of martensitic steel when tempered for 1 hour at a range of temperatures. (After Honeycombe [72])

Two casts of A508-III pressure vessel steel were investigated. The material manufactured by the AEC is designated 508-A, while that manufactured in France is designated 508-B.

The chemical composition of the two casts is compared to the ASTM specification in Table 3. Both the 508-A and 508-B steels are well within specifications in every regard with the exception of the chromium content. Chromium is minimised in these steels to aid weldability.

Element	508-A	508-B	ASTM Standard
Carbon	0.201	0.154	0.25 max
Manganese	1.39	1.39	1.20-1.50
Phosphorus	0.008	0.007	0.025 max
Sulphur	0.005	0.005	0.025 max
Silicon	0.30	0.24	0.15-0.40
Nickel	0.66	0.75	0.40-1.00
Chromium	0.31	0.41	0.25 max
Molybdenum	0.56	0.52	0.45-0.60
Vanadium	0.004	0.004	0.05 max
Titanium	0.005	0.006	--

Table 3 Chemical composition of the two casts of A508-III used in this study, together with the ASTM specification for this class of steel. (Composition analysis courtesy of Middleburg Steel and Alloys SA.)

The 508-A was received in the forged and quenched condition, and examined in three heat treated conditions designated HT1, HT2 and

HT3 (Table 4), while the 508-B material was received in the post weld heat treated condition (equivalent to HT3) and was tested in this condition only (ie. as received).

Name	Treatment	508-A	508-B
HT1	Quenched from 1000°C	488Hv	--
HT2	Quenched + Temp. 1hr-650°C	287Hv	--
HT3	Quenched + Temp. 1hr-650°C + 5hr - 615°C FC (30°C/Hr)	216Hv	220Hv

Table 4 Table showing the conditions in which each of the two 508 type steels were tested and giving the Hv_{30} hardness values resulting from these heat treatments.

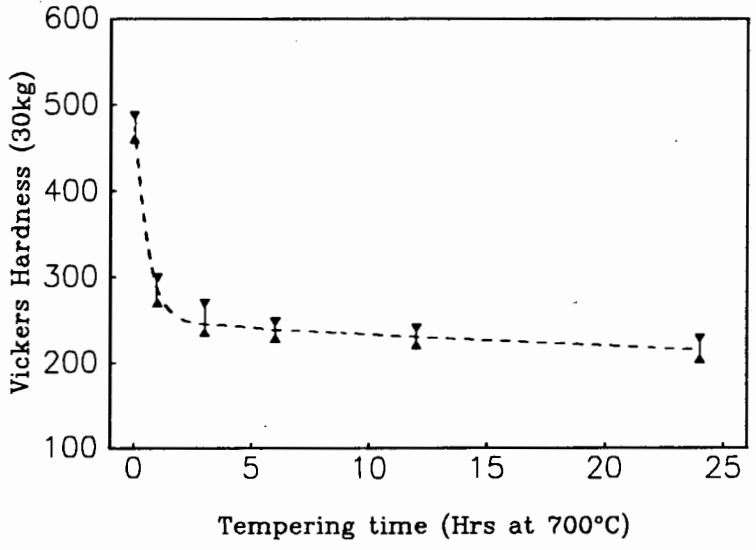

Figure 15 The effect of tempering time at 700°C on the bulk hardness of the quenched 508-A steel.

The effect of tempering at 700°C on the bulk hardness of the 508-A material was investigated and the results are shown in fig. 15. The hardness drops rapidly at first, and then levels off at around 220-250Hv.

3.1.2.1 Microstructure

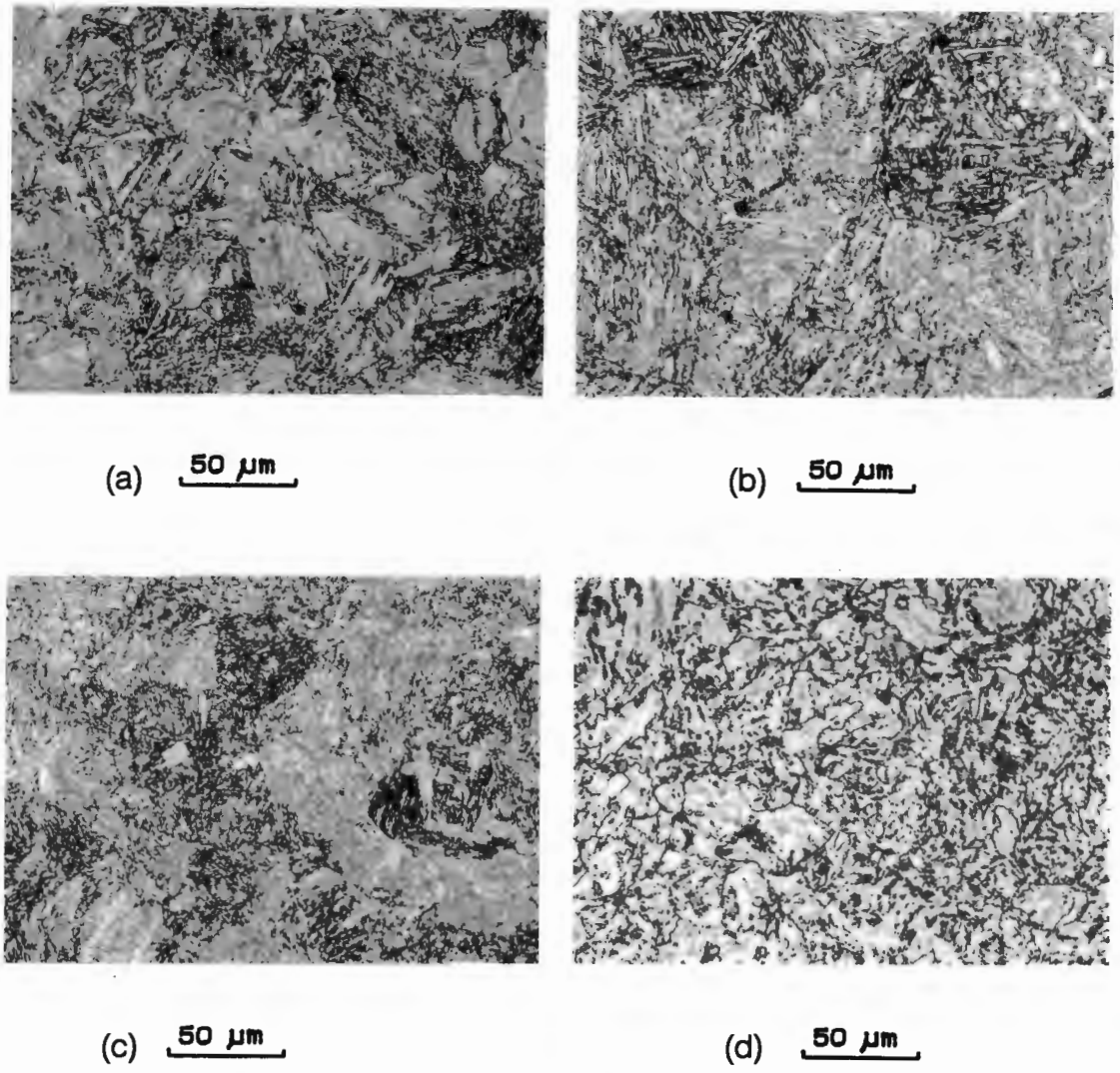

Figure 16 The microstructure of 508–A after the three heat treatments, and 508–B in condition HT3.
(a) 508–A, HT1 (b) 508–A, HT2
(c) 508–A, HT3 (d) 508–B HT3.

The microstructures of the 508 steels in the heat treated conditions of interest are shown in fig. 16. The quenched microstructure consists of martensite, and tempering leads to recovery with the formation of an extensive distribution of spheroidal carbides. The 508–A material in the HT3 condition

consists of very fine dispersion of such carbides in a recovered martensite matrix. In this condition the prior austenite grain boundaries are not visible.

The 508 – B material shown in fig. 16d has been subjected to a commercial post weld heat treatment, the specific details of which are unknown. The microstructure has recovered to the spheroidized condition. The prior austenite grain boundaries are evident, while the prior austenite grain size is less than half that of the 508 – A material.

3.1.2.2 Mechanical Properties

Property	508A HT1 *	508A HT2 *	508A HT3 *	508B HT3 *	ASTM Standard
UTS (MPa)	**1200**	**833**	660	590	550-725
Yield Strength (MPa)	530	520	480	350	345 min
Str. to Fracture (%)	**15.7**	20.5	21.5	24.7	18 min
ROA (%)	48	70	71	75	38 min

Table 5 The room temperature mechanical properties of the 508 materials in the 3 heat treated conditions.
* Heat treatments as shown in Table 4

The mechanical properties of the pressure vessel steels investigated are listed in Table 5, together with the ASTM specifications for this class of steel. The effect of tempering on the mechanical properties is evident. The ASTM specifications for this steel demand a tempering heat treatment of 1 hour per inch of maximum section thickness, at 650°C. Thus it is not surprising that the HT1 condition is out of specification, with very high strength and a lack of ductility. Of greater concern is the fact that the HT2 condition (which has been tempered in accordance with the standard) still exhibits excessive strength. In the HT3 condition the 508 – A material is within the limits of the ASTM specifications.

3.2 Experimental Method

3.2.1 Slow Strain Rate Testing

The slow strain rate test for stress corrosion cracking involves straining a tensile specimen, at a uniform extension rate, in a corrosive environment. Several experimental parameters are important and these are dealt with now:

A nominal strain rate of $3x10^{-6}$ s^{-1} is chosen for the testing because this is the slowest that the equipment can attain with the chosen test specimen geometry.

Tests have been conducted on the 316 material in distiled water and in 1000ppm Cl^- solution while the 508-III material has been tested in distiled water, 1000ppm Cl^- and 1000ppm $SO_4^=$ solutions. All testing was conducted at 75°C. Solutions were prepared using analytical grade $MgCl_2$ and Na_2SO_4 salts.

The need to conserve material necessitated the use of small specimens. The chosen geometry has a gauge length of 15mm and a diameter of 3mm, with 6mm diameter extensions to M6 threaded grips. The specimen geometry is shown in fig. 17.

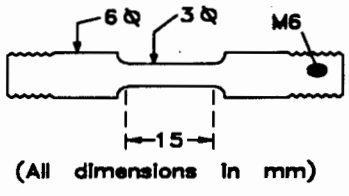

Figure 17 Specimen geometry for the slow strain rate tests. The threaded sections attach to the load frame grips through "O" ring seals in the water bath. (not to scale)

The range of different environments and materials tested leads to a wide spectrum of free corrosion potentials, and so for each "material/environment" combination, slow strain rate testing has been conducted at a series of potentials above and below the free corrosion potential for that situation. In most instances of material and solution testing has been conducted from 300mV below through to 150mV

above the free corrosion potential. The absolute range of all tests has involved a spread from −960mV up to +440mV (SHE scale).

3.2.1.1 Slow Strain Rate Test Apparatus.

Load Frame

The test rig used for this investigation is shown in fig. 18. The variable speed direct current electric motor is coupled to two fixed ratio reduction gear boxes followed by a set of toothed belt reduction pulleys. The drive is then passed through a worm and screw gear and to the crosshead. Crosshead speed can thus be controlled by a ten turn potentiometer and for this study was held at 4.5×10^{-5} mm s^{-1} which gives a nominal strain rate of 3×10^{-6} s^{-1} . The upper end of the specimen is coupled through a universal joint to the crosshead frame while the lower end is joined via an extension rod to a load cell and rose bearing.

Figure 18 Photograph of the slow strain rate rig used in this investigation. A. Computer used for data capture; B. Load frame; C. electric motor; D. Water bath; E. Test cell; F. Potentiostat; G. Control electronics.

Test Cell and Environment Conditioning.

The test cell is illustrated in fig. 19. It consists of a polymethyl methacrylate (PMMA) cylinder with a volume of 400cm^3. The specimen passes through "O" ring seals in the base of the test cell and in the upper tube, to the threaded grips. The cell has a PMMA lid to limit evaporation and to hold the four high purity graphite counter electrodes. The salt bridge to the reference electrode passes through the side of the test cell and ends 5mm from the gauge length of the test piece.

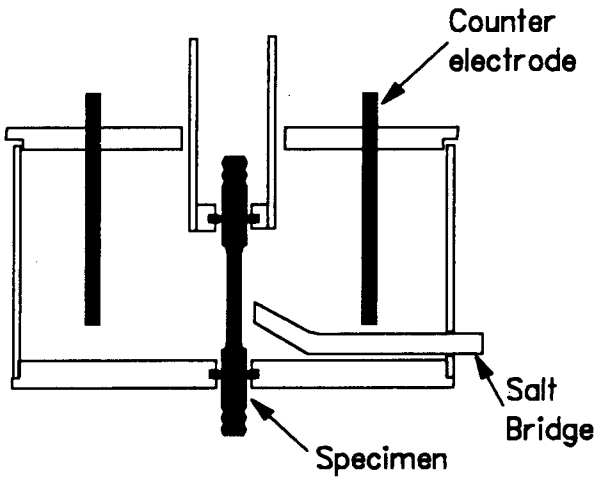

Figure 19 Schematic diagram of the test cell design used for the slow strain rate tests.

The test solution is held in a 6 litre constant temperature water bath. This volume of solution was used to provide a buffer against temperature change, evaporation and contamination from the anodic dissolution of the specimen. The solution is pumped through silicone rubber tubing into the test cell at a rate of about 500cm^3 min^{-1} by a thermoregulating pumping unit. An aquarium pump is used to continually aerate the test solution in the holding tank.

Potential Control and Corrosion Current Monitoring

The test potential of the specimen is controlled using a Wenking LT-78 potentiostat which is used both to set the test potential as well as to monitor the corrosion current during testing. The potential is set relative to a saturated calomel electrode using a ten turn potentiometer allowing 2mV accuracy, and the corrosion current is continuously monitored using a strip chart recorder.

Ancillary Equipment

The test rig is equipped with a 10kN load cell and a plunger type linear variable displacement transducer (LVDT) for monitoring the load and crosshead displacement respectively. The output of these two sensors is amplified by simple instrument amplifiers to give an output between 0 and 10 volts. Data capture is performed using an 8088 based PC equipped with a PC-30 analog/digital multifunction board. This card has a resolution of 2.5mV over the 10 volt range for which it is configured. Software was written in Turbo Pascal to control and monitor the equipment and is listed in Appendix B. The computer is used to gather instantaneous readings for the load and displacement at 1 minute intervals during testing and store the data in a text file for later spreadsheet analysis. Additionally the computer will shut down the motor, the waterbath and all instrumentation in the event of a loadcell overload or when the specimen breaks.

3.2.1.2 Experimental Procedure

The test solution is mixed and placed in the water bath to be heated to the test temperature. The gauge length of the specimen is polished to a 600 grit finish in a drill, then cleaned in alcohol and measured using a vernier calliper. The test specimen is then mounted through the "O" rings and a small

preload is applied to remove any slackness in the loading chain. The solution is introduced into the test cell and the potentiostat and reference electrodes connected. After the specimen has reached equilibrium (usually about 20 minutes) the specimen is polarised to the test potential and straining is commenced. At the end of the test the equipment shuts down and the specimen is cleaned in di-amonium hydrogen citrate to remove any corrosion product. It is then rinsed in alcohol, and stored in a desicator for microscopic investigation.

Fractographic evaluation is conducted in a Cambridge S – 200 scanning electron microscope (SEM) to characterise the fracture mode. SEM micrographs were recorded of the fracture surfaces and analysed to identify any intergranular or transgranular fracture regions. Additionally, some of the specimens were sectioned and the gauge length cross section examined by optical microscopy to investigate secondary cracking.

3.2.2 Rising Load Fracture Mechanics Testing

The rising load test method is used to study the effects of the corrosive environment on the growth of an existing crack using fatigue pre-cracked compact tension specimens. The specimen is immersed in the solution of interest and subjected to a slowly increasing load while the crack length and load are monitored. This test is used to identify the critical stress intensity for environmentally induced crack growth, and to study crack growth phenomenon without the added complication of crack initiation processes.

One half sized CT – 1 compact tension specimens were used in this study. The specimen geometry is shown in fig. 20.

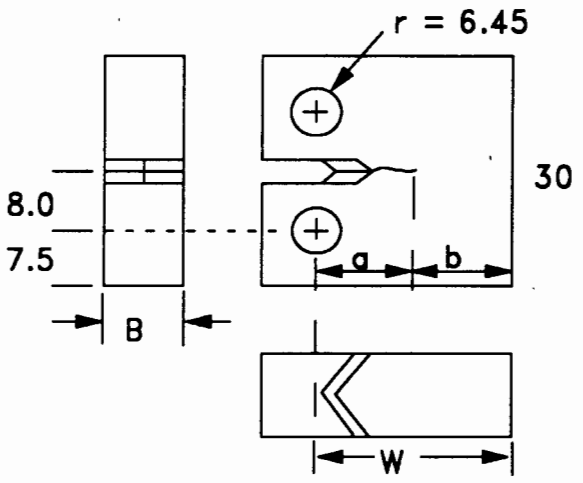

Figure 20 Specimen geometry for the riding load tests. The pull rod grips attach to the load frame through "O" rings in the water bath.

The slowest loading rate attainable with the equipment is 1.07 N s^{-1} and this is used for all tests. Due to a shortage of material the rising load tests have been conducted on the 508-A material in the HT2 condition only. All rising load tests have been conducted at the free corrosion potential for the various solutions.

Tests have been conducted in 1000ppm Cl^- and 1000ppm $SO_4^=$ solutions at 75°C. Solutions were prepared using analytical grade $MgCl_2$ and Na_2SO_4 salts.

3.2.2.1 Rising Load Test Apparatus

Load Frame

A 50kN Electro-Servo Hydraulic (ESH) universal fatigue testing machine is used for these tests. A voltage scan generator is used to generate a slowly rising voltage as the control signal which is fed into the load cell servo amplifier of the ESH machine. Tests were conducted in load control mode.

Test Cell and Environment Conditioning.

The test cell is illustrated in fig. 21. It consists of a PMMA box with a volume of 1200cm^3. The specimen is held by pins to the grips which pass through "O" ring seals in the base of the test cell. The cell has a PMMA lid to limit evaporation.

As with the slow strain rate tests, the test solution is held in a 6 litre tank and pumped to the test cell using a thermoregulating pump. The holding tank is aerated continually using an aquarium pump.

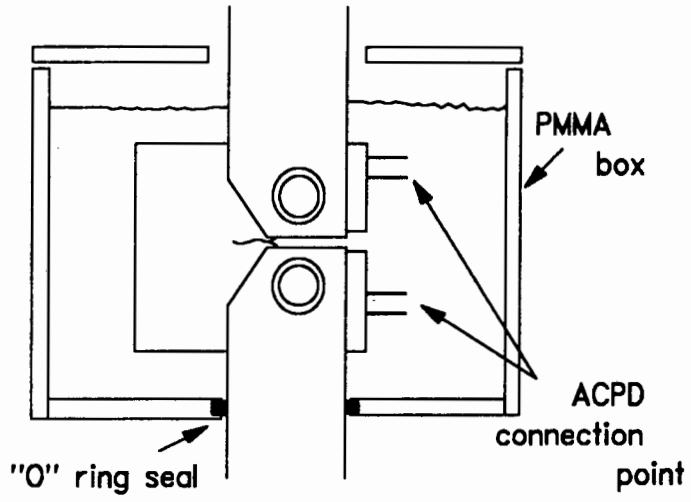

Figure 21 Schematic diagram of the test cell design used for the rising load tests.

Ancillary Equipment

Several attempts were made to monitor crack length during testing. An alternating current potential drop (ACPD) crack growth system was used initially. This equipment has an operating frequency of 179 Hz and thus the AC current flows almost exclusively in the surface 2mm of the specimen. Crack growth in the centre of the CT specimen can not be measured with this setup. The ACPD system was checked using a blank specimen in which the growing crack was simulated by cutting the specimen on a band saw and crack length changes of

0.25mm could easily be measured. After two tests in which the output of this system did not change measurably until sudden specimen failure, crack opening displacement (COD) measurements were attempted using a strain gauge based clip gauge. In both of the tests conducted using this system the hot solution penetrated the sealing on the strain gauges and caused failure of the clip gauge. The lack of change in ACPD output during testing could be because crack growth, if present on the surface of the specimen, was not of this order of magnitude. Fractographic investigation confirm that there was no crack growth prior to sudden failure.

During the rising load tests the load, crosshead position and either ACPD or clip gauge voltage are recorded at one minute intervals using the same computer based data logging equipment as the slow strain rate tests except that the PC-30 card is configured to cover the range from -10 to +10 volts. Dedicated software was written to facilitate this process and is listed in Appendix B. The data is stored in a text file for subsequent spreadsheet analysis and graphing.

3.2.2.2 Experimental Procedure

The specimens were fatigue precracked using the limiting load method. This involves fatigue loading at an R ratio of 0.2 up to a maximum which is calculated according to the equation:

$L_{max} = Bb\sigma_y/(2W+a)$ (Dimentions as per fig. 20).

Using this approach precracks were grown to a length of about 5mm in 2 hours (about 70 000 cycles).

The precracked specimens were cleaned in arklone and alcohol and stored in a desicator. The solution is prepared and heated. The specimen is mounted in the test cell using stainless steel dowel pins, and the solution is introduced. The load is cycled for 100 pulses at 20% of the fatigue precracking

load to aid the ingress of solution into the precrack. The data capture programme is started and the load slowly ramped from an initial load of about 200N.

The tests ended with sudden specimen failure after 7-10 hours. The specimens were cleaned with di-ammonium hydrogen citrate and alcohol an then stored in a desicator for fractographic examination.

3.2.3 Electrochemical Tests

Potential scans and electrochemical potentiodynamic reactivation (EPR) tests were conducted using an EG&G Princeton Applied Research 173 potentiostat in conjunction with an external voltage scan generator. A disk of the material is ground and polished finishing on a 0.25μm diamond impregnated cloth. These are then held in a standard teflon specimen holder which exposes 1cm^2 of the disk surface to the test solution. The specimen holder, graphite counter electrodes, purge gas inlet and reference electrode salt bridge are held in a one litre five necked corrosion flask. For the EPR tests computer controlled data capture is again employed because the total charge flowing during a scan can not be measured directly with existing equipment and a numerical integration of a large data set is thus employed. The accuracy of the equipment was checked by performing the ASTM G5-78 (1980) test using AISI 430 in 1N H_2SO_4. Good agreement with the standard ASTM curve was obtained.

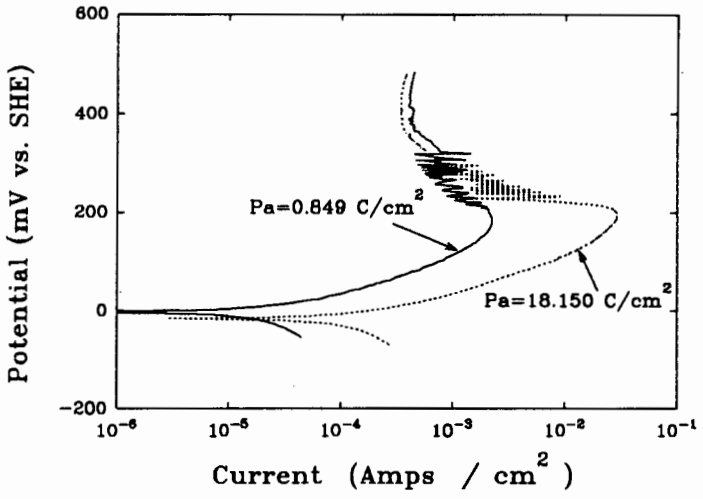

Figure 22 The results of an EPR scan of commercial grade 304 stainless steel after annealing at 1100°C for 1 hour followed by quenching (solid line) and sensitizing at 650°C for 1 hour (dashed line).

A set of EPR tests was conducted on commercial grade 304 after solution annealing and sensitizing at 650°C for 1 hour. The results of these tests are shown in fig. 22 in which the anneled material (solid line) has an EPR DOS of 0.8 C/cm^2 while that of the sensitized material (dotted line) was 18 C/cm^2.

4 RESULTS

4.1 316NG MATERIAL

4.1.1 Slow Strain Rate Tests

The stress strain curves for the 316 material tested in 1000ppm chloride solution at the various corrosion potentials is shown in fig. 23.

4.1.1.1 Mechanical Properties

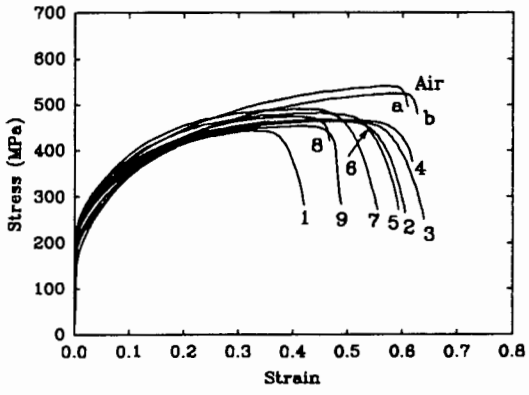

1 = 200mV* 2 = 100mV* 3 = 0mV* 4 = −41mV
5 = −100mV* 6 = −200mV* 7 = −200mV 8 = −450mV
9 = −1200mV a = Perpendicular b = Parrallel

Figure 23 Slow strain rate engineering stress vs. engineering strain curves for the 316NG material tested in air (room temperature) and a range of solutions (75°C). (mV vs SHE)
* Specimens were machined parallel to the forging direction.

The results shown in fig. 23 represent load-deflection data after correcting for the deflection of the test rig. The values of UTS, ϵ_f, ROA and energy to fracture (a numerical integration of the area under the stress strain curve) are given in Appendix C.

The relative effect of the various test potentials can be illustrated by normalising the results with respect to the air test

data obtained from specimens with the same orientation. In this way a normalised value of 1 represents no change from the air test, while a value of less than 1 indicated a degradation in properties. The results of such a normalization process are shown in fig. 24, in which the solid marker indicates the only 316NG test in which stress corrosion cracking is evident from the fractography.

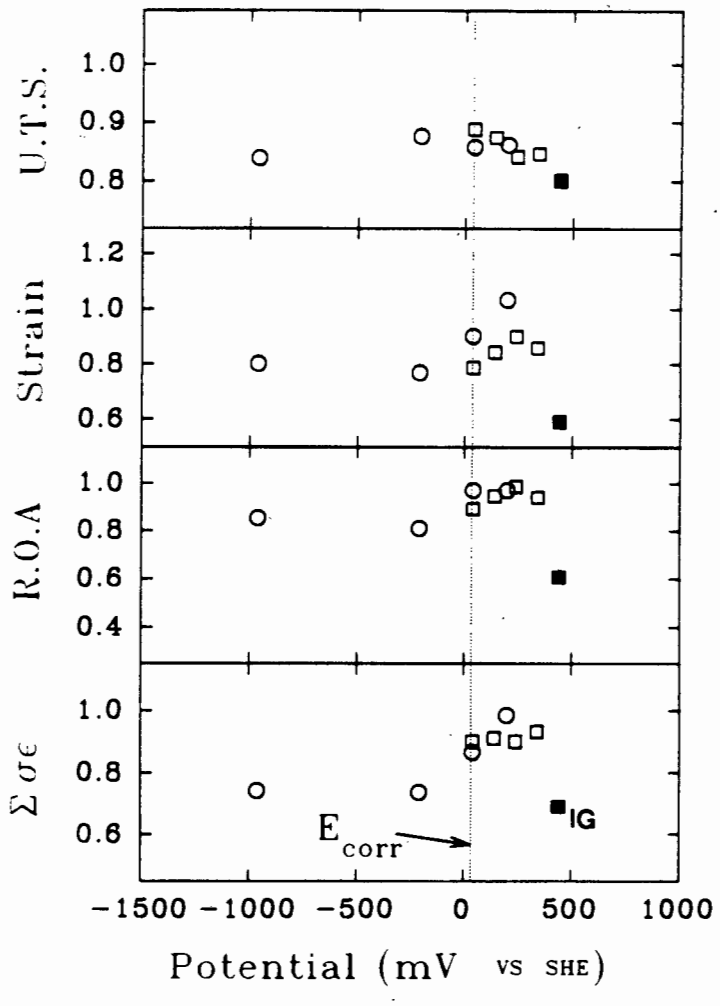

Figure 24 Normalised results for the 316NG material as a function of test potential. Circles are for specimens parallel to the forging direction while squares are for perpendicular ones. The solid marker indicates fractographic evidence of stress corrosion cracking. (Ecorr = +40mV SHE)

4.1.1.2 Fractography

In every case but one the fractography of the 316NG steel indicated ductile failure. The nature of this failure differed depending on the orientation of the specimen with respect to the forging direction. Those specimens which were oriented perpendicularly to the forging direction exhibited cup and cone failure with shear lips accounting for about half of the fracture surface. Closer examination of these failures indicate void coalescence as the initial failure mode. A typical fractograph is shown in fig. 25.

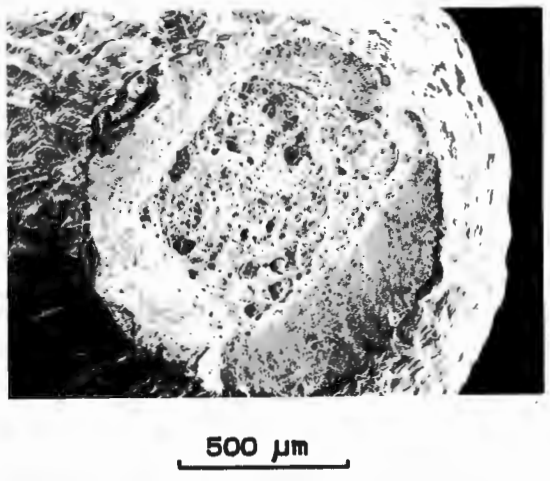

Figure 25 SEM micrograph of cup and cone failure typical of the 316NG specimens machined perpendicularly to the forging direction. Failure results from dimpled tearing of the centre of the specimen, followed by shear of the edge regions.

Parallel ditches separated by ridges dominate the macroscopic appearance of the fracture surfaces for the specimens machined in the direction of forging (fig. 26). Closer examination of these ditches reveals secondary cracks, void coalescence and some shear edges. Fracture surfaces from this specimen orientation exhibit much less reduction in area than those from the perpendicular direction, though the relative change in ROA with respect to the air tests is similar for both orientations.

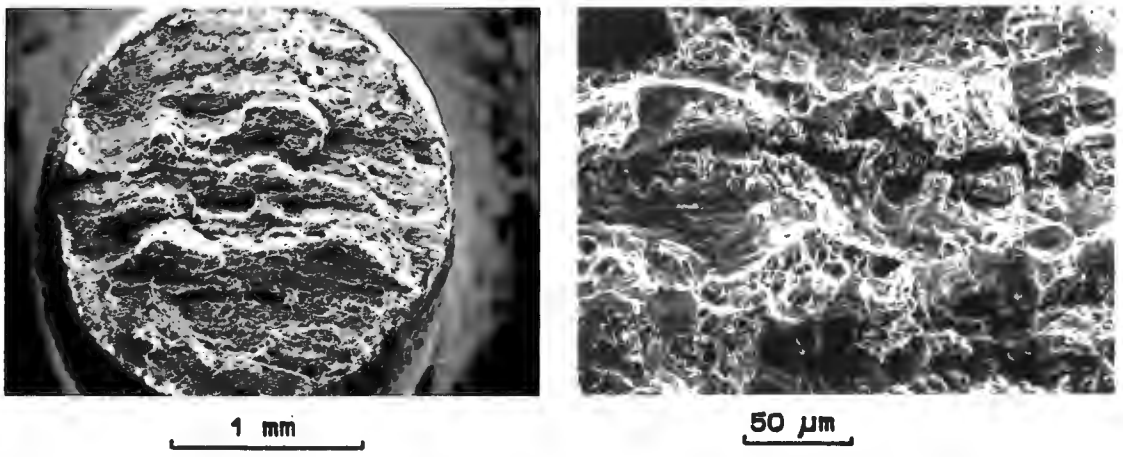

Figure 26 Ductile failure of the specimens machined parallel to the forging direction leads to the formation of ditches and ridges on the failure surface. Secondary cracking in the base of the troughs is evident.

Transverse sections through these specimens (fig. 27) reveal that the failure is due to the formation of tunnels of voids, which grow as the load increases and eventually join up to form the final fracture surface. These tunnels have the same orientation as the ditches on the fracture surface. Tunnels form within the gauge length, and are thus not the result of directional corrosive attack from the surrounding solution.

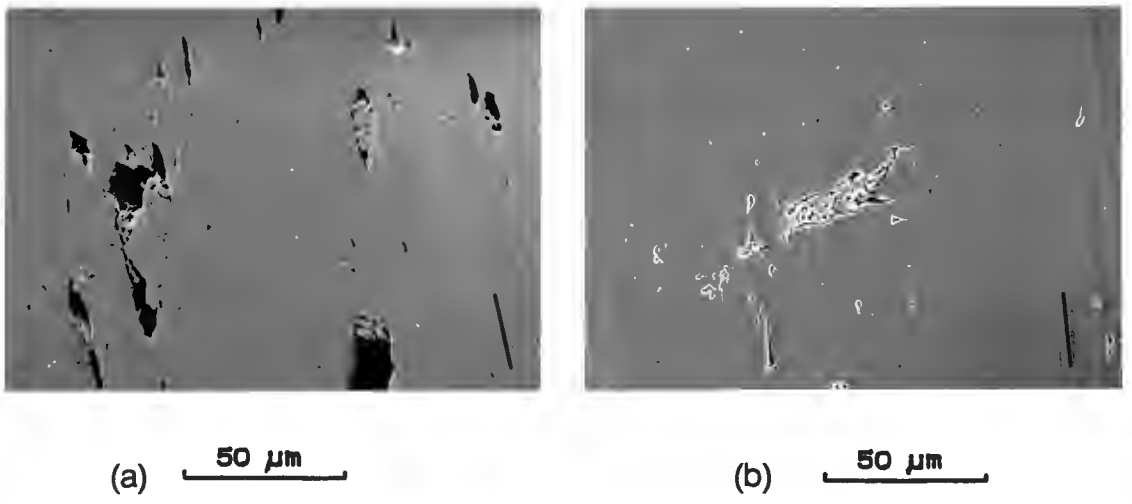

Figure 27 Sectioning the gauge length of the specimens shown in fig. 26 reveals regions of void coalescence, which have the same orientation as the ditches on the fracture surface.
(a) Sectioned across (b) Sectioned along the direction of the ditches. (Lines represent the principle loading axis)

The most anodic test conducted was at +440mV (SHE) and in this instance stress corrosion cracking was indicated. The fracture surface of this test piece is shown in fig. 28. Transverse sectioning of the gauge length of this test piece did not reveal any secondary cracking, and the only sign of pitting was in the necked down region, adjacent to the intergranular fracture area.

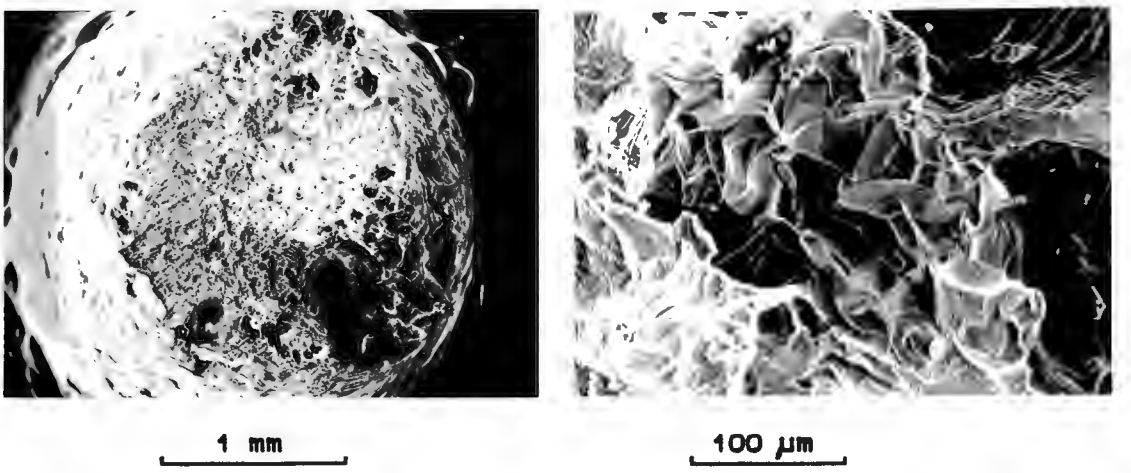

Figure 28 Fracture surface of 316NG tested at +440mV (SHE). Note the small intergranular region shown in the enlargement.

4.1.2 Corrosion Properties

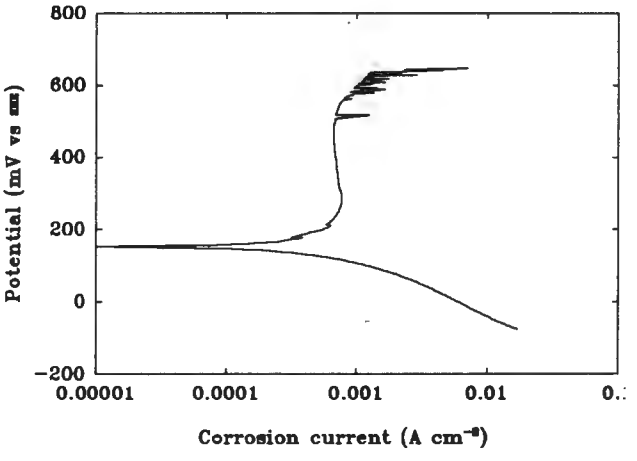

Figure 29 Potentiodynamic scan of 316NG in a solution containing 1000ppm Cl^- ions.

The result of a potentiodynamic scan conducted on the 316NG material in 1000ppm Cl^- solution is shown in fig. 29. From this scan it

can be seen that the free corrosion potential (Ecorr) for this combination of material and environment is around +160mV. Also evident from this scan is the lack of an active region. Below Ecorr the material is cathodically charged, while above this potential passivation dominates until the onset of pitting at potentials above +500mV.

4.1.3 Electrochemical Potentiodynamic Reactivation

The 316NG material was heat treated at 650°C for 1, 8, 24, 36, and 48 hours in an attempt to induce sensitization of the microstructure. The EPR scans generated from these test pieces are shown in fig 30, and the normalised charge per unit area (Pa) are given in Table 6. These can be contrasted with the 304 material (fig. 22 on page 50) and the data from the work of Berneke *et al* [62] in fig. 10 (page 28).

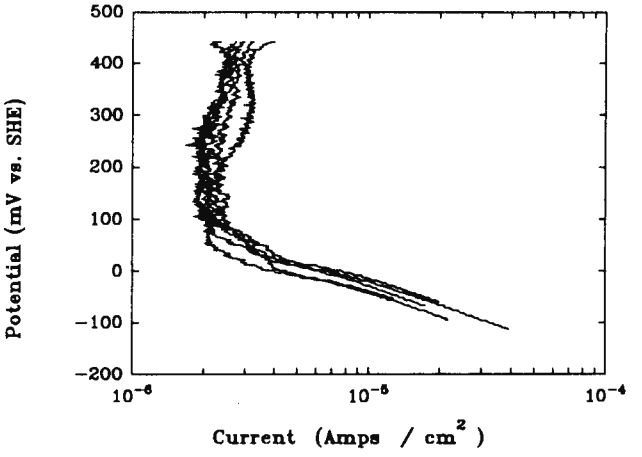

Figure 30 The EPR scans generated after heat treating the 316NG material at 650°C for 1, 8, 24, 36 and 48 hours.

The Pa values for this material are of the same order of magnitude as other workers have found [23,28,62] for nuclear grade 316 stainless steel subjected to similar heat treatments.

Heat treatment	Pa (C/cm2)
1 hr at 650°C	0.035
8 hr at 650°C	0.050
24 hr at 650°C	0.081
36 hr at 650°C	0.016
48 hr at 650°C	0.023

Table 6 Results of the EPR testing of the 316NG material after various heat treatments. Values for Pa represent normalised charge per unit area of grain boundary. (ASTM grain size 5 for all heat treatments)

These specimens were subsequently pollished and etched in oxalic acid in accordance with the ASTM 262 A, to confirm the absence of sensitization. The microstructure of the specimen which had been soaked at 650°C for 24 hours (the highest EPR DOS condition) is shown in fig. 31, and consists of austenite and some delta ferrite. There are no carbides visible on the grain boundaries.

Figure 31 Microstructure of the 316NG material after sensitizing at 650°C for 24 hours. Etched in 10% oxalic acid solution in accordance with ASTM 262 - A.

4.2 A508 MATERIAL

4.2.1 Slow Strain Rate Tests

4.2.1.1 Mechanical Properties

508 – A, Condition HT1

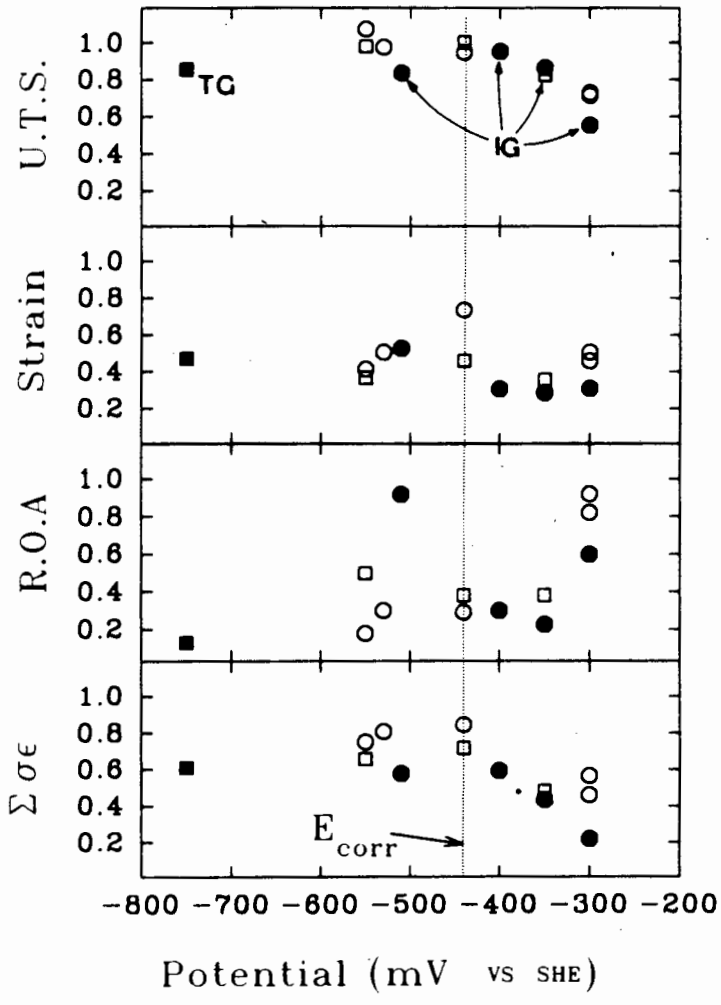

Figure 32 Normalised results for the 508 – A material in the HT1 condition. Circles represent tests in chloride solution, squares represent sulphate tests. (Solid markers indicate tests with fractographic evidence of stress corrosion cracking)

The output (normalised with respect to the air test results) for the 508 – A tested in the HT1 condition (quenched) is shown in

fig. 32. In this diagram the solid markers represent the tests in which fractographic examination reveals indications of stress corrosion cracking. There is a large amount of scatter in the results obtained for the material in this heat treated condition. The only trend which seems to emerge is the systematic degradation in strength and fracture energy as the test potential increases above Ecorr (−440mV SHE).

508−A, Condition HT2

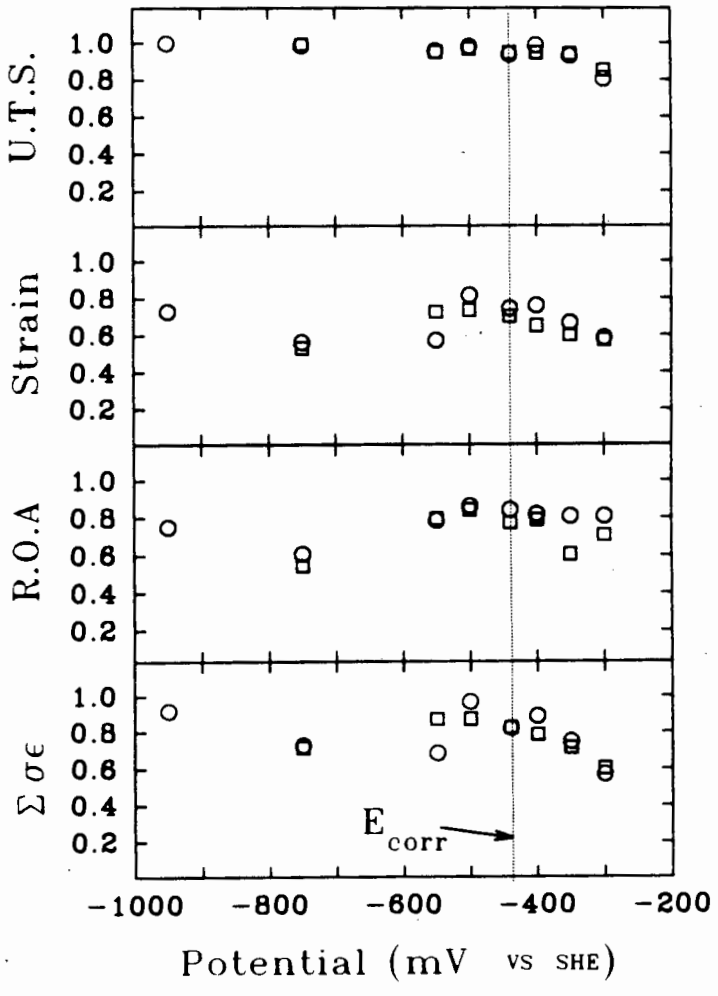

Figure 33 Normalised results for the 508−A material in the HT2 condition. Circles represent tests in chloride solution, squares represent sulphate tests.

Figure 33 shows the normalised results of the tests on the 508−A after tempering for 1 hour at 650°C (HT2 condition). Again the trend indicates a slight degradation of mechanical

properties with increasing anodic test potential. In this case the ductility is also reduced. In general the tests in sulphate solutions produced slightly lower ductility than the chloride tests. These reductions in ductility were not accompanied by any fractographic indications of stress corrosion cracking.

508-A, Condition HT3

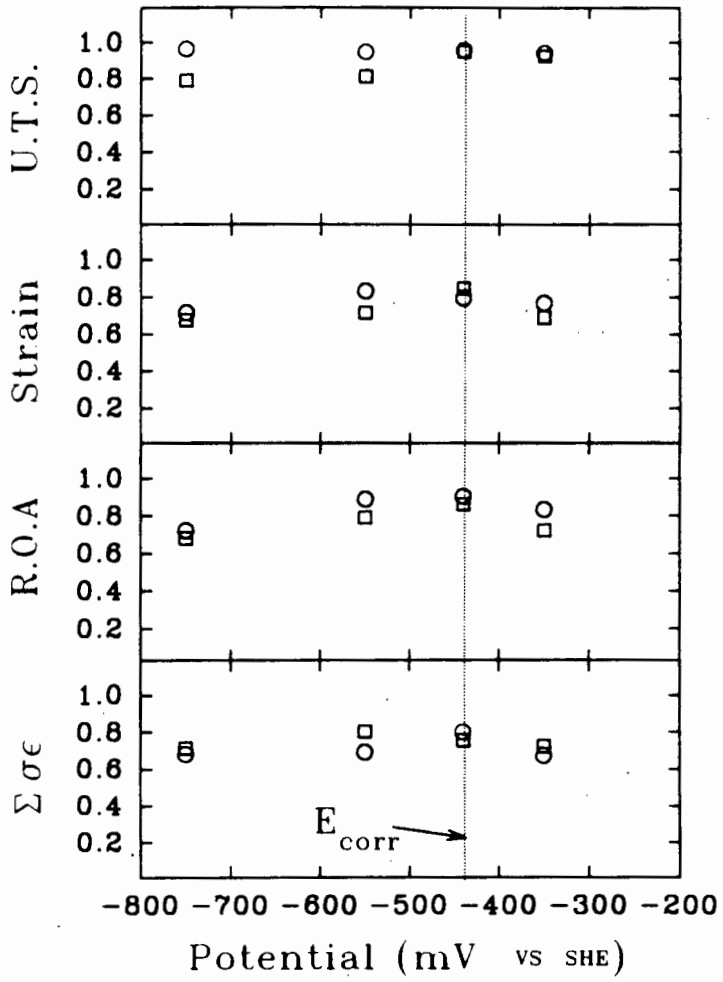

Figure 34 Normalised results for the 508-A material in the HT3 condition. Circles represent tests in chloride solution, while squares represent sulphate solution.

The results for the 508-A material in the HT3 condition are given in fig. 34. The failure mode for all specimens in this set of tests was ductile rupture with shear. In this condition the ductility decreases slightly for both anodic and cathodic test potentials but the strength remains more or less potential

independent. Again the sulphate solution leads to slightly lower properties than the chloride solution.

508 – B, Condition HT3

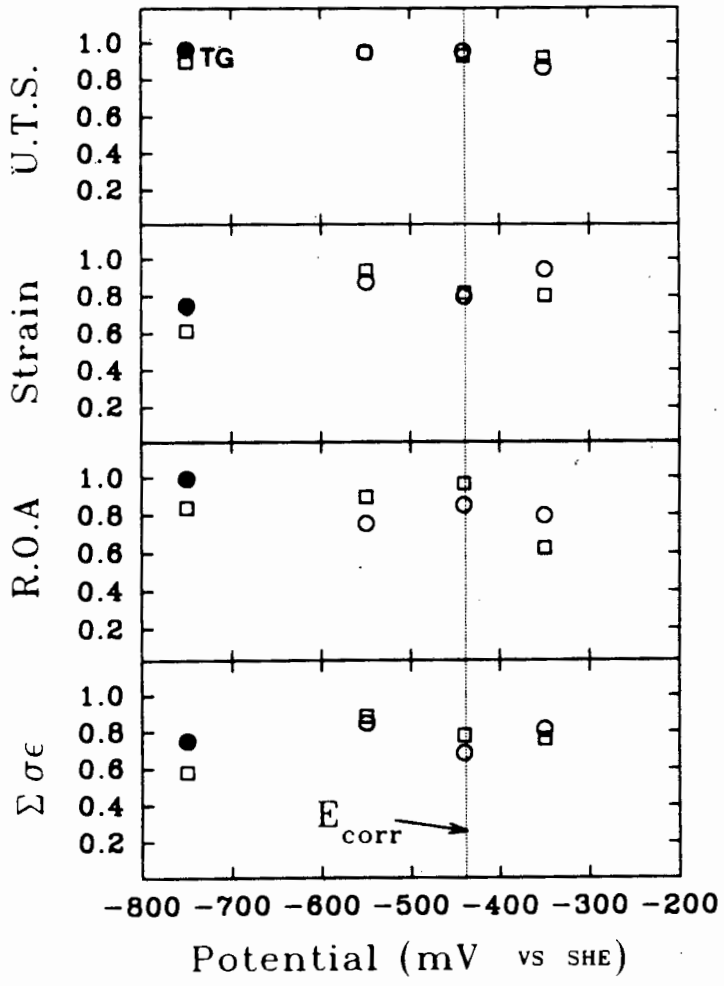

Figure 35 Normalised results for the 508 – B material in the HT3 condition. Circles represent tests in chloride solution, squares represent sulphate tests. Solid marker indicates fractographic indications of stress corrosion cracking.

Normalised results for the 508 – B material are given in fig. 35. The solid point represents a single test in which fractographic examination revealed the presence of a small area of transgranular stress corrosion cracking. In every other instance the failure mode was ductile rupture with shear. In this set of results the strength and the ROA decline on either side of the free corrosion potential (Ecorr = −440mV SHE),

but the strain to fracture indicates increased ductility for mildly anodic and cathodic test potentials. These changes are not of sufficient magnitude to be regarded as being significant.

The specimen which failed with some transgranular fracture had approximately the same reduction of area as the air test specimen, and almost as high a UTS. This, in conjunction with the small proportion of the fracture surface area that was transgranular in nature indicates that the fracture was not dominated by the stress corrosion cracking which occured. This would imply that either cracking initiated late into the test or the strain rate was too high to allow crack growth to proceed once the strain had been localised (either by the presence of the crack or by the onset of necking). This will be discussed further in the next chapter.

4.2.1.2 Fractography

508 – A, Condition HT1

The fractography of the 508 – A in the HT1 condition can be split into two groups, the first group containing specimens which show no fractographic evidence of stress corrosion cracking and the second group containing specimens which do.

In the first group failure is typified by 45° shear planes. In some cases a single shear plane covers the entire fracture surface while in other cases the surface contains two or more intersection planes. Typical examples of these fracture surface morphologies are shown in fig. 36.

Five tests produced fracture surfaces with signs of stress corrosion cracking as indicated next. Intergranular stress

corrosion cracking is noted for four tests in Cl^- solution (under anodic conditions) while transgranular stress corrosion cracking was evident for the $SO_4^=$ solution under a strongly cathodic potential.

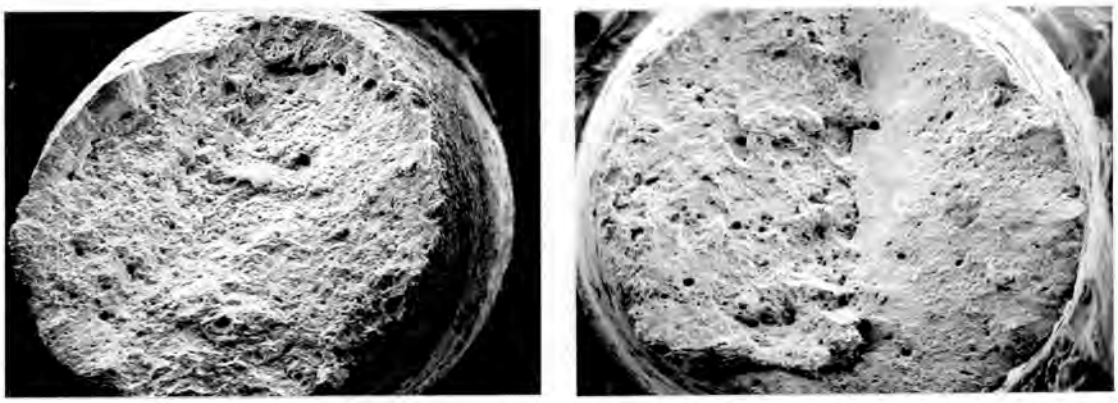

Figure 36 Shear failure of the 508-A material in the HT1 condition, showing (a) single shear plane and (b) multiple intersecting shear planes.

Fractographic examination of the specimen tested at -790 mV (SHE) in 1000ppm $SO4^=$ solution (fig. 37) indicates two adjacent regions of transgranular cleavage. The transgranular region accounts for less that 5% of the fracture surface area. Sectioning of the cathodic test specimens did not reveal any pitting or secondary cracking.

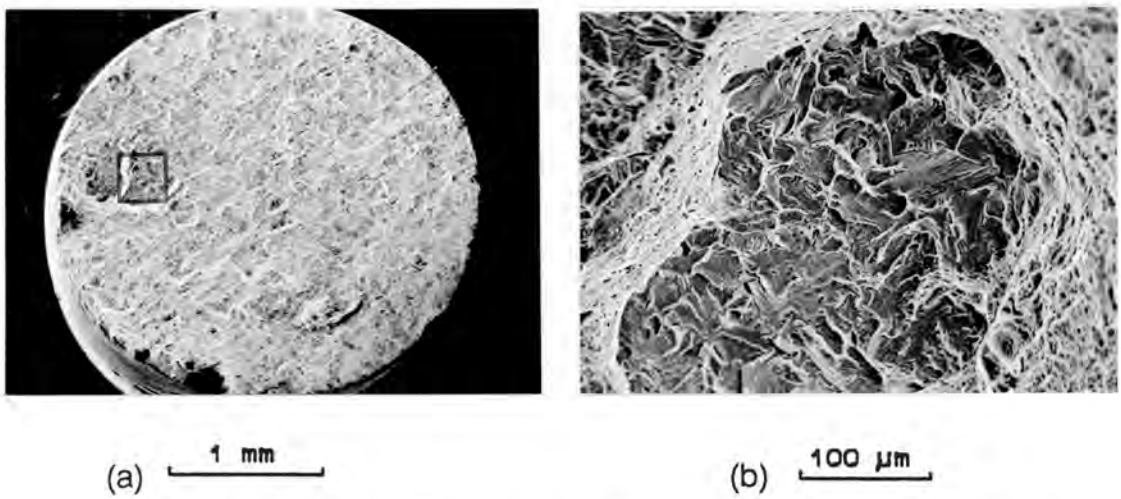

Figure 37 Fracture surface of the 508-A HT1 specimen tested at -750mV (SHE) in 1000ppm $SO_4^{=}$. Transgranular stress corrosion cracking is evident on a region of the fracture surface.

Four specimens tested in chloride solutions exhibited varying extents of intergranular fracture. Figure 38 is the fracture surface of the specimen tested at +300mV (SHE) and shows two intergranular regions separated by a shear failure plane. Closer examination of the intergranular regions (fig. 38b) reveals grain boundary attack and pitting of the surfaces of exposed grains. Intergranular attack was noted for one specimen which was tested at a mildly cathodic potential (70mV below Ecorr) and for three specimens covering a range of anodic test potentials. In every case less than 10% of the fracture surface was intergranular.

Figure 38 Two regions of intergranular attack on the fracture surface of the 508-A material in the HT1 condition tested at +300mV SHE in 1000ppm Cl^- solution. (a) General fracture surface, (b) Close up of the upper intergranular region.

Gauge length sectioning of the specimens tested in sulphate solutions (fig. 39a) under anodic conditions reveals a profusion of wide pits which have an aspect ratio (pit width to depth) of between 2 and 3. Cross sectioning of the gauge lengths of the specimens tested in chloride solution (fig. 39b) indicated some contrasts with the sulphate tested specimens. Firstly, for the anodic test specimens the pit aspect ratio was between 0.8 and 1, indicating that the pits were deeper and narrower than those of the sulphate tests. Secondly, some relatively wide secondary cracks were evident as shown in fig. 40. These cracks were certainly not atomically sharp. This will be discussed further in the next chapter.

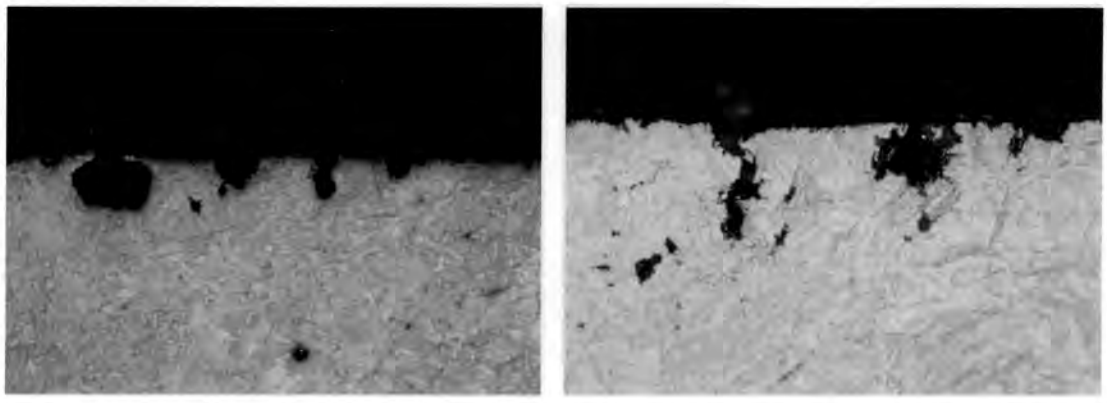

Figure 39 Cross sections through typical pits in the gauge length of the 508-A HT1 specimens tested at -350 mV (SHE) in (a) 1000ppm sulphate ions and (b) 1000ppm chloride ions.

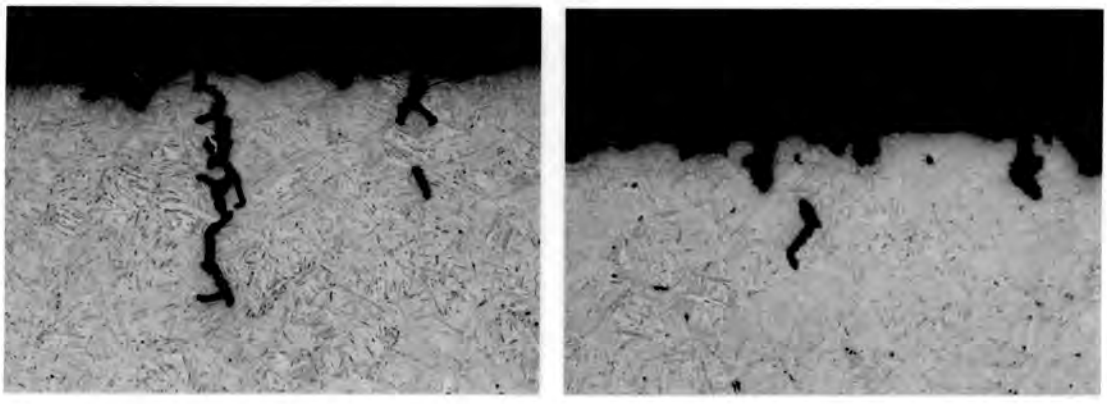

Figure 40 Secondary stress corrosion cracks were evident in the gauge lengths of the specimens tested under anodic conditions in 1000ppm chloride solution. Note the bluntness of the crack front.

508-A, Condition HT2

The fractography of the 508-A in the HT2 condition differs depending on whether the test was conducted under cathodic or anodic conditions.

Below the free corrosion potential the fractography consists of ductile failure with shear lips. Well developed cup and cone fractures from this category of tests are shown in fig 41.

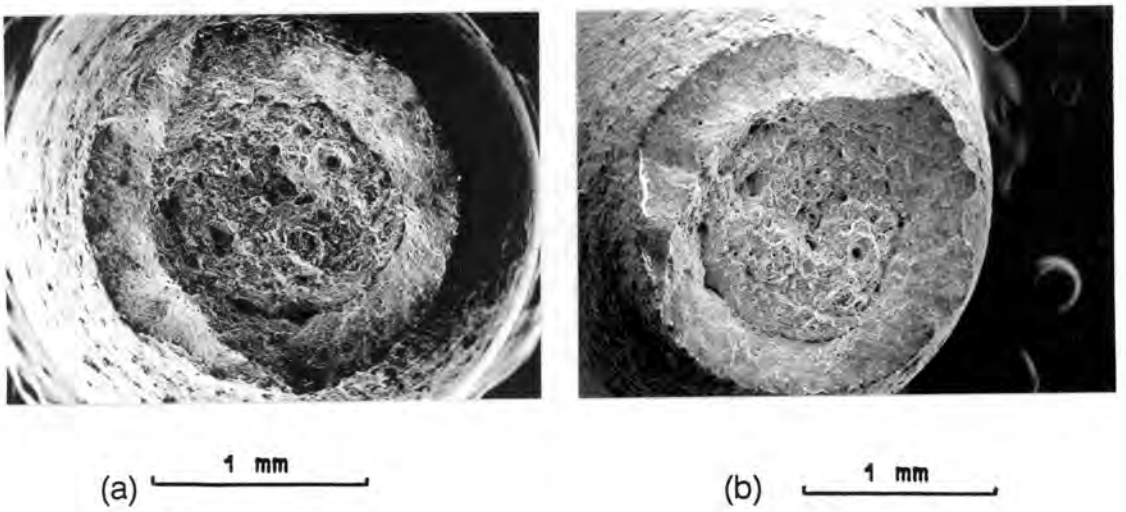

Figure 41 Fracture surface of the 508-A material in the HT2 condition after slow strain rate testing at a test potential of -500mV SHE (60mV below Ecorr). (a) in 1000ppm Cl^- (b) in 1000ppm $SO_4^=$

Tests conducted under mildly anodic conditions (fig. 42) show a flatter fracture surface with less shear lip development. In one test chevron cracks (fig 43a) are evident in the heavily necked region of the gauge length and radial secondary cracking of the fracture surface is apparent (fig 43b).

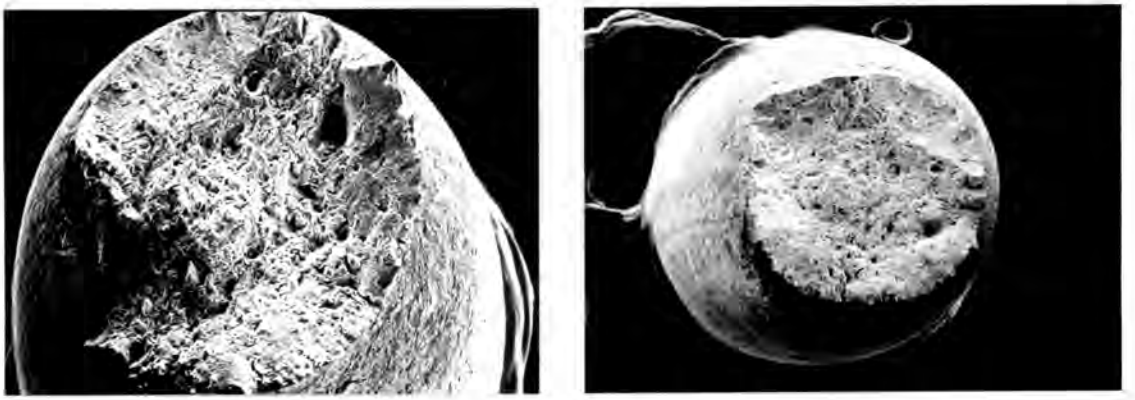

Figure 42 Fracture surface of the 508-A material in the HT2 condition after slow strain rate testing at a test potential of -400mV SHE (40mV above Ecorr). (a) in 1000ppm Cl^- (b) in 1000ppm $SO_4^=$

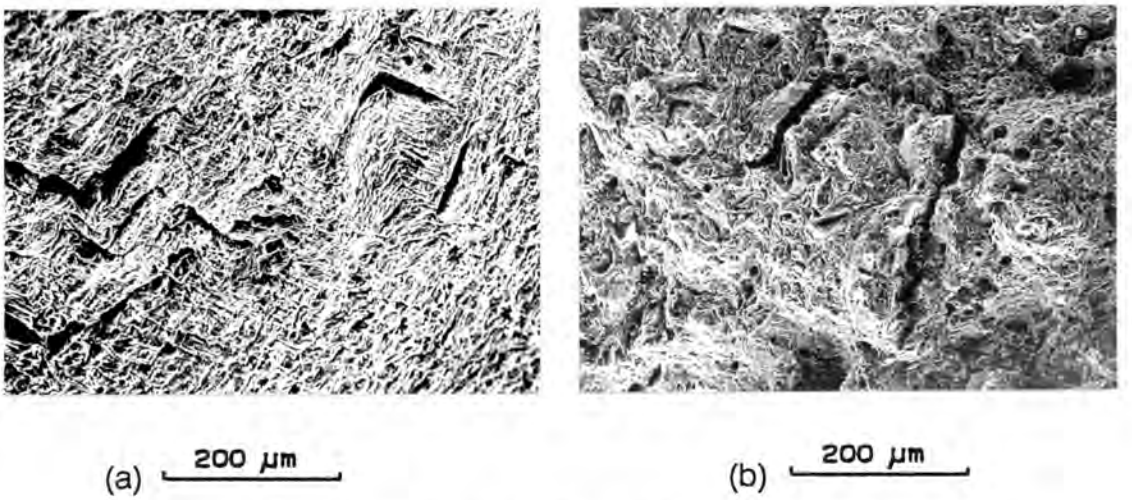

Figure 43 (a) Chevron cracks in the heavily plastically deformed region of the gauge length (508-A, HT2, 1000ppm Cl^- at -400mV SHE) (b) Secondary cracking of the fracture surface (same specimen as in a).

At more positive potentials (fig 44) the fracture surface approaches a single shear plane. Corrosion products adhering to these surfaces (fig 44b) were not removed by the di-amonium hydrogen citrate cleaning process.

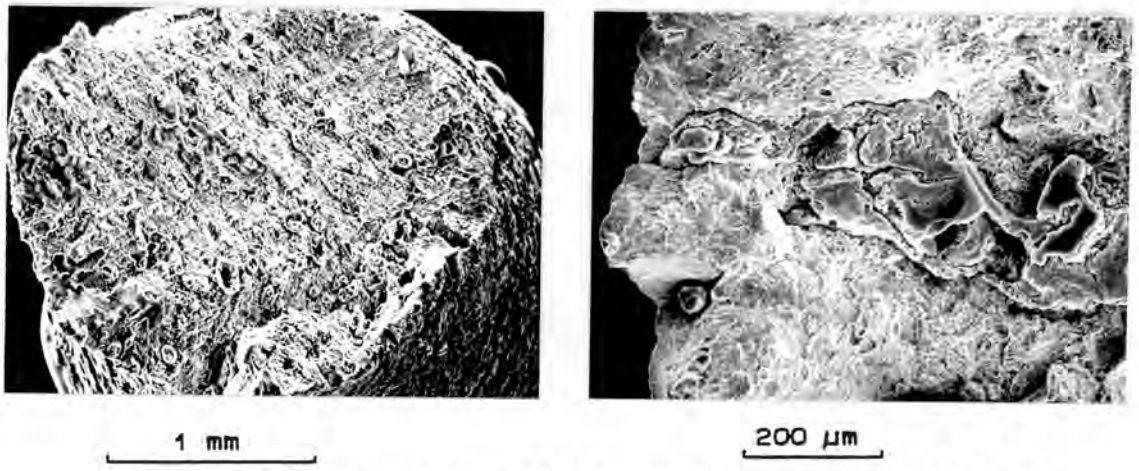

Figure 44 The strongly anodic test specimens show a corroded, ductile surface, covered with corrosion products which resist removal by ultrasonic cleaning in di-amonium hydrogen citrate.

Cross sectioning of the gauge lengths of this batch of specimens did not reveal any secondary cracking. Pitting of the anodic specimens was not noticably different for the two different test solutions.

508 – A, Condition HT3

In the HT3 condition the fractography of the 508 – A material shows little dependence on test conditions covered in this study. In all cases failure is by ductile rupture with shear lips as shown in fig. 45.

Sectioning of the gauge lengths of these specimens did not reveal any cracks.

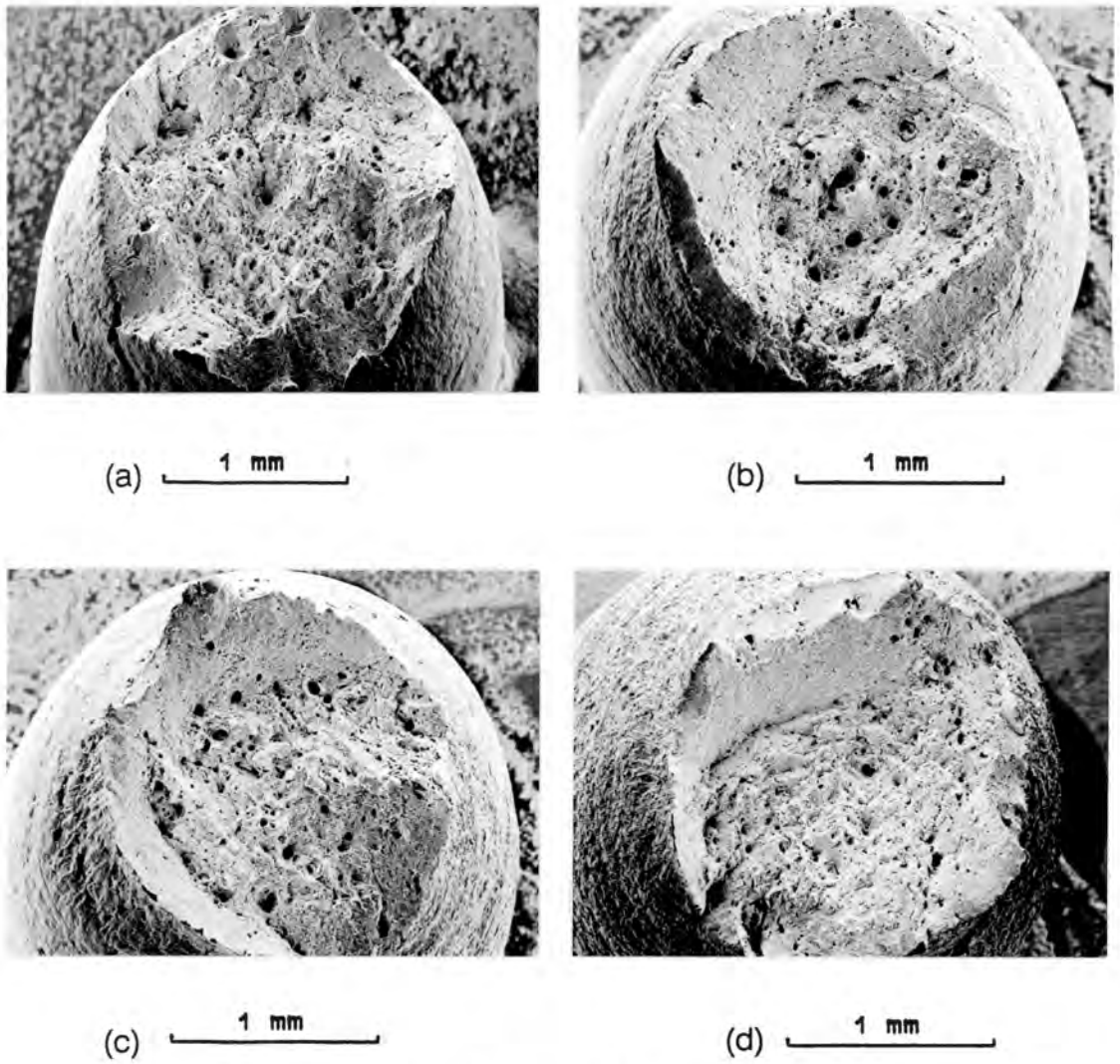

Figure 45 Fractographs of the 508 – A HT3 tests in 1000ppm Cl^- showing ductile failure with shear for all test potentials.
a) = -350mV b) = -440mV (Ecorr)
c) = -550mV d) = -750mV (SHE).

508 – B, Condition HT3

Under increasingly cathodic conditions (fig. 46) the fractography of the 508 – B HT3 material changes from cup and cone ductile fracture (100mV below Ecorr) to shear tearing (300mV below Ecorr) at 45° to the loading axis. This will be discussed in the next chapter.

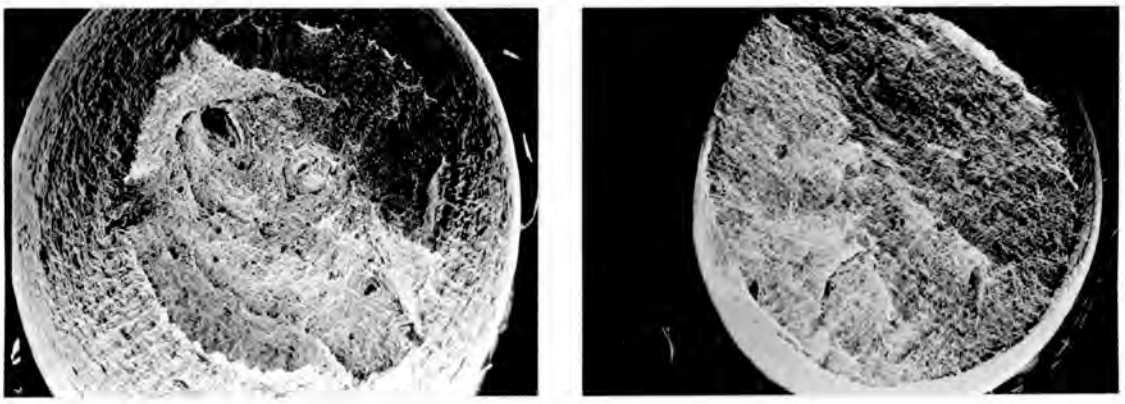

Figure 46 The fractography of the 508-B material (HT3) changes from (a) ductile cup and cone fracture at -550mV SHE (Cl solution) to (b) shear failure at -750mV SHE (Cl solution).

The most cathodic test in the chloride solution caused a small region of transgranular cleavage, with this section of the fracture surface accounting for about 2.8% of the total fracture area (fig. 47). This specimen, like all the others in this batch of tests, did not show secondary cracking when sectioned along the gauge length.

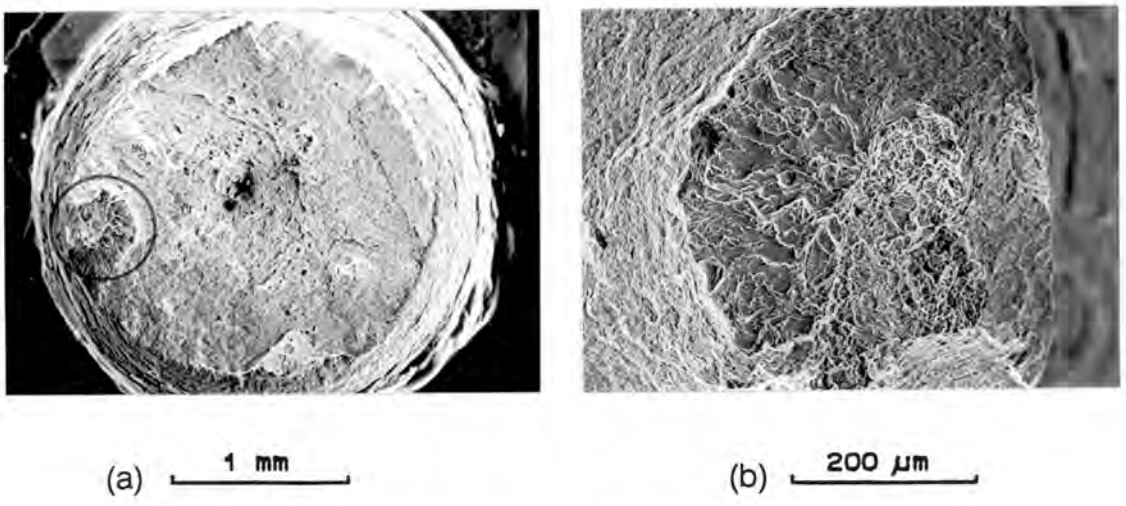

Figure 47 Transgranular stress corrosion cracking on the fracture surface of the 508-B material (HT3 condition) tested at -750mV (300mV below Ecorr) in 1000ppm Cl^- solution.

4.2.2 Rising Load Tests

The load, crosshead position and either alternating current potential drop (ACPD) or clip gauge output were recorded as a function of test duration. Crack growth prior to final fracture was not established by either of these two monitoring methods during any of the tests conducted. The ACPD system produced significant "noise" signals during tests (fig. 48) and these overshadowed any useful output from the equipment, while the clip gauge failed due to the ingress of the test solution in the two tests in which this method of crack growth monitoring was attempted. Fractographic investigation does not indicate any instances of stress corrosion cracking for the material and environments tested.

4.2.2.1 Mechanical Properties

Results of a typical rising load test are shown in fig. 48. The load at fracture, together with the specimen geometry were used to calculate the stress intensity at failure. The results of this testing program are shown in Table 7.

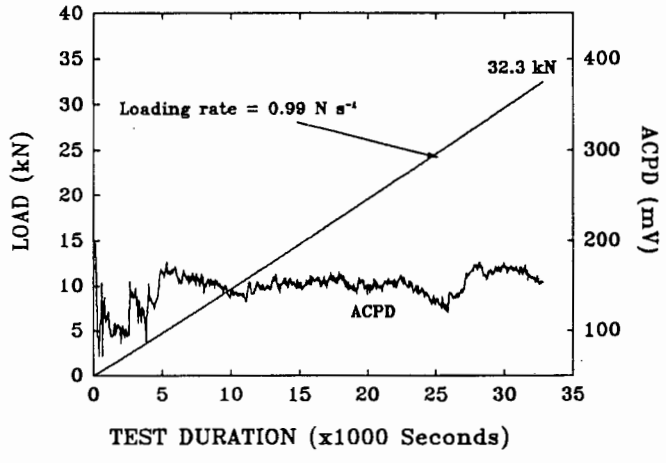

Figure 48 Load and alternating current potential drop (ACPD) vs test duration graph for the 508–A HT2 in 1000ppm Cl^- solution.

The specimens were too thin for the results to be interpreted as valid K_{Ic} values and so the values quoted in Table 7 are candidate K_{Iq} values. While the stress intensity at fracture in the two solutions are not significantly different, they are lower than the value obtained in the air test. The air test was conducted at room temperature while the other tests were all conducted at 75°C.

ENVIRONMENT	TEST	K_{Iq}*
Air	1	118
1000ppm Cl^-	1 2	87 103
1000ppm $SO_4^=$	1 2 3	94 79 103

Table 7 Results of the rising load stress corrosion cracking testing programme. Material is 508-A in the HT2 condition. * Values quoted as K_{Iq} do not meet the specimen geometry validity criterion of K_{Ic} results, i.e. b,B,W > 2.5 K_{Ic}

4.2.2.2 Fractography

Typical fractographs of the rising load tests are shown in fig. 49. In the air and 1000ppm Cl^- tests the transition from pre-crack surface to ductile failure surface is direct, while for one of the three tests in 1000ppm $SO_4^=$ solution (shown in fig. 49c) there was some tearing of the material along the interface between the pre-crack and the ductile failure surface regions.

For the air test and both environments the radius of the plastic zone was 1.5 to 2.5mm. Shear lips (fig. 50) flank the ductile region for all test conditions.

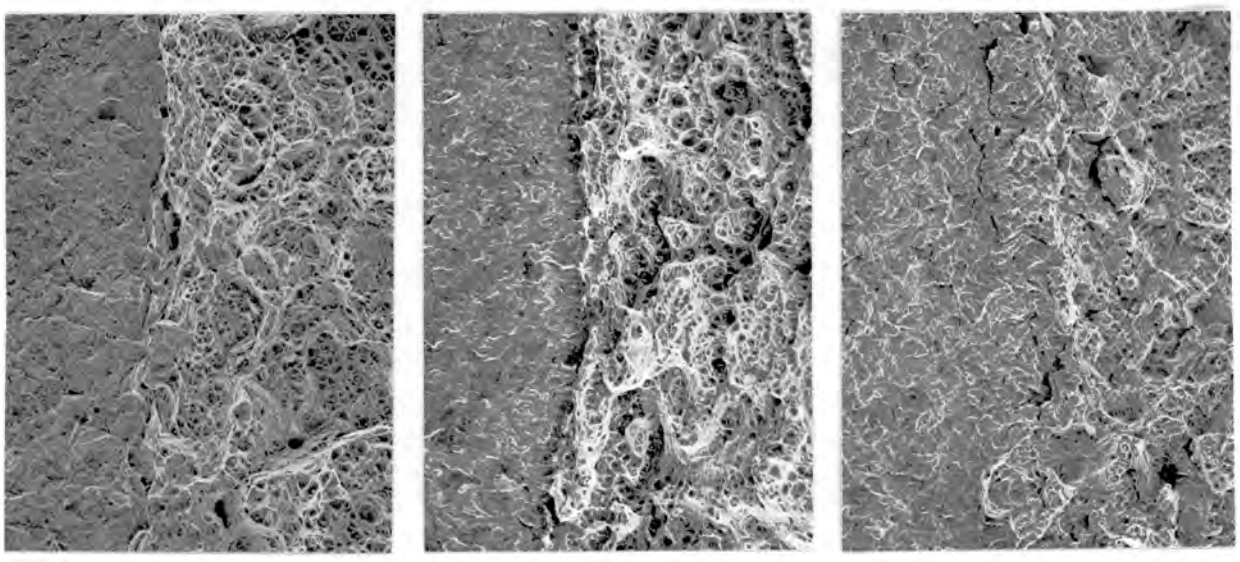

Figure 49 Fracture surfaces of the rising load specimens. Fatigue pre-crack is on the left and the final ductile failure is on the right. (a) Air test (Room temperature). (b) 1000ppm Cl^- at 75°C. (c) 1000ppm $SO4^=$ at 75°C.

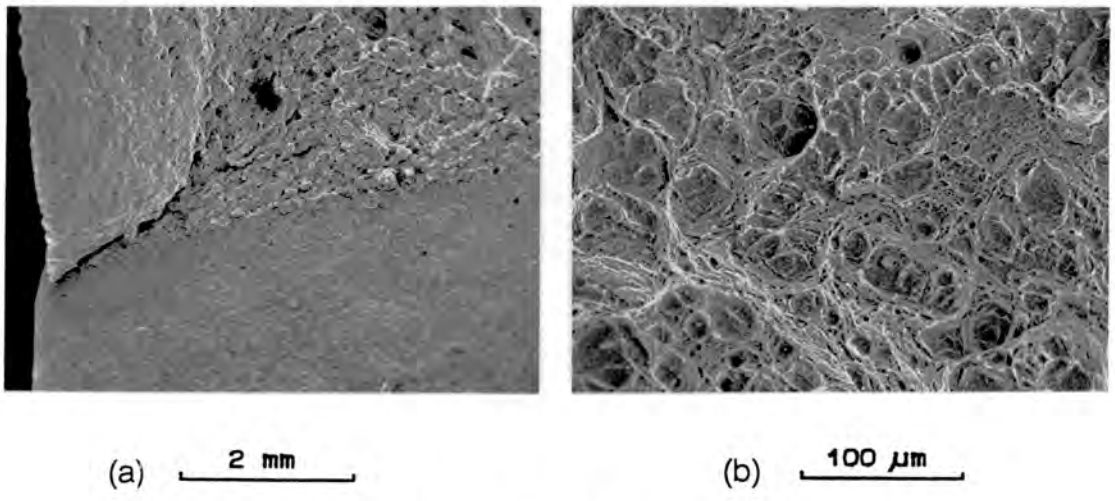

Figure 50 (a) Edges of the failed CT specimens exhibit shear lips. (b) Ductile void coalescence dominates the centre (200um beyond the pre-crack).
(Specimen tested in 1000ppm $SO_4^=$ at 75°C)

5. DISCUSSION

5.1 316NG Material

5.1.1 General Observations

The composition of the 316NG used in this study, in conjunction with the pseudo binary phase diagram (fig. 12, pg. 34) indicates that this cast of 316NG, while being within the range covered by the specifications, has a composition which lies close to the $\gamma/(\gamma+\alpha)$ boundary. Thus it is not surprising that the microstructure contains some delta ferrite stringers. While the austenite is isotropic, the delta ferrite stringers are oriented across the forging direction. During manufacture the delta ferrite, which formed on cooling from the liquid phase, is elongated into stringers by the forging process. Subsequent heat treatment has allowed recrystalisation of the austenite but not of the delta ferrite. This has left the steel with a general matrix of equiaxed austenite which is penetrated by stringers of delta ferrite. This in turn results in anisotropic mechanical properties for the steel.

5.1.2 Sensitization and Corrosion Properties

The results of both the EPR and ASTM tests indicate that none of the heat treatments investigated in this study caused sensitization of the 316NG material. In a study on the sensitization of a 316NG steel of similar composition Sandenberg [28] also reports no measurable sensitization for a range of heat treatments including 100 hours at 700°C. In a steel with a similar composition but more than double the carbon content (0.030 wt. %) Beneke et al [62] found that heat treating at 650°C for 48 hours caused an EPR DOS of 1.0 C cm^{-2}. An EPR DOS of 2 C cm^{-2} is commonly accepted as being the minimum for sensitization [23].

It has been found that sensitization is enhanced by simultaneous thermo and mechanical cycling [73] because of an increase in the nucleation of carbides during high temperature straining. Advani *et al* [19] have shown that transgranular carbide formation is also possible in thermomechanically sensitized low carbon stainless steels. It is felt that further work needs to be done to quantify the response of the AISI 316 stainless steel to more elaborate sensitization heat treatments. This work needs to focus on the effect of simultaneous thermo and mechanical treatments as well as the effect of longer heat treatments at intermediate temperatures (around 550°C) and higher temperatures (up to 700°C).

5.1.3 Slow Strain Rate Testing

Failure of the specimens machined across the forging direction appears to be the result of separation at the delta to gamma interfaces (fig. 27a, pg. 54). As the load increases, strain accumulates at these interfaces due to the plastic mismatch between the delta ferrite stringers and the austenite matrix. At higher strains separation occurs and tunnel shaped voids form within the material. The fractography arises naturally when these tunnels join up to form the final fracture surface. This is analogous with the failure of fibre reinforced composites when loaded perpendicularly to the fibre plane.

The potentiodynamic scan of this material (fig. 29, pg. 55) in 1000ppm Cl^- solution indicates some important points. Firstly, there is no active loop (nose) evident under mildly anodic conditions. When the material is scanned anodically through the free corrosion potential it immediately passivates and does not activate at all until pitting occurs. When this scan is compared with the schematic diagram given in figure 1 (pg. 8) it would seem likely that anodic stress corrosion cracking should only be expected at potentials above 450mV SHE.

The absence of pitting in all tests conducted below 440mV is thus expected. In the test conducted at 440mV the single pit in the necked region could have occurred via one of two sequences of events. In the first scenario pitting initiated early on in the test due to anodic dissolution of the passive film (possibly exacerbated by the presence of a surface or near surface pre-existing defect or inclusion), and necking was later confined to the pitted section of the gauge length because of the reduced cross sectional area. In an alternate scenario local necking late in the test caused a higher than usual anodic dissolution rate (due to continual film rupture in the necking region) resulting in pit initiation. The absence of any other pitting on this specimen would seem to support this second sequence of events. Once initiated, the pit grew because the test potential was so close to the pitting potential of the material.

Sheltered stagnant conditions within the pit, together with the stress concentrating effect of the growing defect allowed the stress corrosion crack to initiate. This crack grew a short distance before gross section yield led to final cup and cone fracture. It seems likely from this sequence of events that initiation was not possible until after the onset of necking. Once initiated, however, this crack was only able to grow a short distance and did not lead to excessive loss of ductility (fig. 24, pg 52). A possible reason for this is discussed now.

Once necking begins in a tensile specimen, strain is concentrated into the necking region and, for a constant crosshead speed, the local strain rate increases. With the specimen geometry used in this study a crosshead speed of 4.5×10^{-8} ms^{-1} lead to an initial strain rate of 3×10^{-6} s^{-1}. However, once necking commences all of the strain is confined to less than 4mm of the gauge length and the strain rate in this region would thus be greater than 1.2×10^{-5} s^{-1}.

It would seem evident that in this test the fine balance between film formation, film rupture and anodic dissolution necessary for stress corrosion crack growth could only be sustained for a short while before the locally accelerating strain rate exceeded some critical value and ductile tearing took over as the active failure mode.

From this explanation two important points emerge. Firstly, crack initiation is not easy in this material and the absence of cracking in tests at lower potentials must not be taken to mean that the material is immune to stress corrosion cracking particularly in the presence of an existing defect. Secondly, it seems likely that cracking would be more severe if tests were conducted at slower strain rates. The strain rate used in this investigation appears to be at the upper end of the range of strain rate for which stress corrosion cracking will occur in this environment.

In future studies of this material it is recommended that slower strain rates be employed. In the present context this would mean either modifying the existing rig to achieve lower crosshead speeds or using specimens with a longer gauge length.

The problem of crack initiation also needs to be addressed. Two possible approaches could be tried.

In the first instance strain could be localised to a section of the gauge length by notching the specimen. An alternate solution would be to follow the lead of Maiya [58] (see page 25) and drill a small hole in the gauge length of the specimens. These approaches could only be used if the crosshead speed of the machine were also reduced to maintain the low strain rates required for stress corrosion cracking.

Another interesting observation can be made when one compares the potential at which cracking occurs in this study with the results of Congleton *et al* [65] shown on page 29. In their results progressively decreasing the test temperature from 300°C down to 100°C caused a double effect. In the first instance the severity of the environmental attack reduces, to the extent that at 100°C it is handily noticeable in the test solution of the cited study (5ppm chloride). Of equal importance to the results of the present study is the effect of temperature on the potential at which the environmental effect is most severe. At 300°C this is at about −350mV (SHE) while at 100°C it is close to +220mV. If one plots these potential-temperature pairs (as has been done in fig. 51) and extrapolates down to 75°C the clear implication is that cracking should be most severe between 400 and 600mV

(SHE). This is consistent with the cracking found in the present study which occurred at +440mV (SHE).

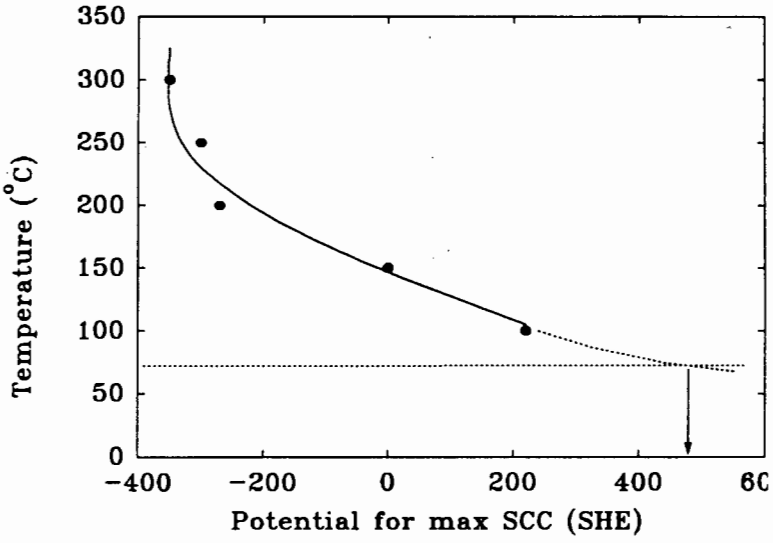

Figure 51 The effect of temperature on the potential at which stress corrosion cracking is most severe for 316NG. (Data after Congleton *et al* [65]).

5.2 508 Material

5.2.1 General Observations

Several aspects of the testing of the 508−III material require consideration in this section. The effects of the various heat treatments on the microstructure and mechanical properties will be discussed first. After this, the slow strain rate tests will be discussed with respect to the effects that test potential and test solution have on the mechanical properties and fractography. A possible link between test solution, pit morphology and cracking severity will be debated. Finally, a discussion of the results of the rising load tests will be presented.

5.2.2 Heat Treatments

When a martensitic steel is heated to some temperature below the Ac_1 temperature carbon is expelled from the body centred tetragonal lattice into the body centred cubic lattice and microscopic particles of cementite nucleate. When this temperature is held for longer times these particles grow through a process of coalescence. This is known as tempering, and serves to reduce the hardness and relieve the internal stresses of the quenched steel. If temperatures close to the Ac_1 temperature are used and enough time allowed the process can lead to the formation of small spheres of cementite surrounded by ferrite and is known as spheroidizing.

In this study the 508-A material was heat treated to three conditions. In the HT1 condition the material is fully martensitic and this is the condition after forging and quenching. Tempering at 650°C for one hour (the HT2 condition) results in limited microstructural change (fig. 16b on page 39) but a significant drop in hardness (Table 4 on page 38). Further heat treatment (HT3) leads to some coalescence of the cementite and a progressive drop in hardness. The 508-B in the HT3 condition (as received) is tempered still further (fig. 16d) and is in the spheroidized condition, with relatively large areas of ferrite surrounded by cementite. From a microstructural point of view this would be the toughest condition for this material.

5.2.3 Slow Strain Rate Testing

From the results of slow strain rate testing of the 508 material, the most general observation to be made is that the intergranular cracking observed in the HT1 condition is mitigated by tempering. In the HT1 condition, stress corrosion cracking was noted in five out of thirteen tests (one instance of TGSCC and four of IGSCC), while of the remaining

thirty one tests (in both HT2 and HT3 conditions), only one instance of stress corrosion cracking (TGSCC) was found. Two things happen during tempering which could be responsible for this change.

Firstly, the ultimate tensile strength of the material is significantly reduced. If intergranular stress corrosion cracking required a certain principal tensile stress state (σ_{crit}) to initiate or grow then in the tempered condition the ultimate strength of the material may not be able to sustain this critical stress and cracking could not occur. This is shown schematically in fig. 52.

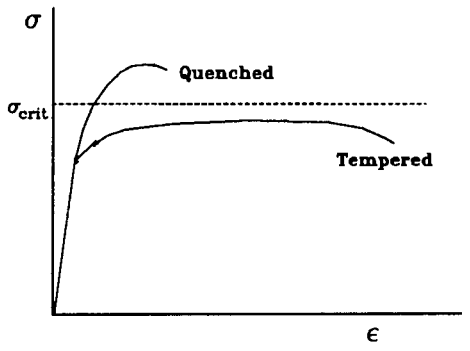

Figure 52 Schematic diagram representing the effect of tempering on the ability of the material to sustain a critical stress necessary for stress corrosion cracking.

Secondly, tempering leads to significant microstructural change. The high internal energy of the martensite is reduced and elements which during forging had segregated to the austenite grain boundaries redistribute. Thus the 'activeness' of the pre-existing active path (the prior austenite grain boundaries) is decreased and intergranular stress corrosion cracking is mitigated.

However, the single instance of transgranular fracture in the 508-B tested in Cl^- solution at -750mV SHE indicates that even for the fully heat treated steel (HT3 condition), environmentally induced cracking can still occur.

It is important to note that the instances of transgranular cracking were all for strongly cathodically polarised tests, while anodic conditions led exclusively to intergranular stress corrosion cracking or ductile rupture.

It is argued that the inter- and transgranular fractures result from totally different mechanisms. Under cathodic conditions the hydrogen evolution reaction (page 15) predominates on the surface of the steel and there is a strong possibility of hydrogen charging. This would lead to hydrogen embrittlement which, in a martensitic steel, is known to manifest itself as transgranular cleavage [74].

This form of hydrogen embrittlement is not, strictly speaking, a corrosion phenomenum, since corrosion by definition involves the oxidation of the metal to metal ions, and cathodic conditions bar this from happening. Additionally, corrosion would start from the surface of the specimen (in contact with the solution) and proceed inwards, while an examination of the two specimens manifesting transgranular failure reveals that the transgranular regions of the fracture surface are surrounded by regions of ductile failure (figs. 37 & 47). This is in contrast to the fractographs published by Hurst et al [5] and Congleton et al [7] in which transgranular *anodic* stress corrosion cracking of 508 pressure vessel steel are seen to initiate from small pits on the extreme edge of the fracture surface. In the present work it would appear that hydrogen entered the steel and caused transgranular cleavage away from the test solution. Thus while the cathodic transgranular failures found in this study are environmental failures they are not true transgranular stress corrosion

cracking since the hydrogen causing the embrittlement was not generated by a corrosion reaction but wat the product of cathodic potentiostatic control.

At potentials above the free corrosion potential, anodic dissolution would be encouraged and local corrosion would initiate in those areas of the surface where weaknesses in the oxide layer and possible surface or near surface inclusions lower the metals resistance. This would lead to local pitting attack, thus providing sheltered, actively corroding enclaves which would be self perpetuating for three reasons. Firstly, a local corrosion cell will be set up, with a potential drop along the length of the pit (the bulk metal surface being cathodic with respect to the corrosion site inside the pit). Secondly, solution mixing will be restricted by the pit geometry and the aggressive solution will thus be able to concentrate in the enclave. Thirdly, the pit will constitute a stress concentration and so the oxide film which forms in the very base of the pit will be subject to higher amounts of plastic deformation than the bulk surface. These three measures together will encourage still further anodic dissolution in the base of the pit.

In the case of the 508-A steel in the HT1 condition it is apparent that general anodic dissolution is further encouraged by a pre-existing corrosion susceptibility associated with the prior austenite grain boundaries. This is either because the general lattice energy is higher (a result of the grain boundary mis-orientation) or because of the segregation of impurity atoms to these regions during forging.

An interesting observation can be made when one considers the morphology of the pits which formed in the two test solutions (fig. 39). Those formed in the sulphate solution were wide and shallow as if active corrosion had concentrated on the sides of the pit, while those which formed in the chloride solution were deep, narrow and jaggered as if the

primary site of anodic dissolution were the very base of the pit. This could be explained by the following hypothesis.

Firstly, anodic dissolution leads to the formation of a small pit or crack. If the environment is very severe then general corrosion will occur equally around its inner surface and the pit will grow in all directions, leading to a hemispherical surface defect. On the other hand, if the environment is mild enough then general corrosion may not be possible and corrosion will primarily occur in regions where film rupture is concentrated (i.e. in the region of highest stress concentration – the base of the defect). In this latter case the defect will grow into a narrow pit and possibly eventually into a stress corrosion crack.

It is thus argued that intergranular stress corrosion cracking does not occur in the sulphate environment because the environment is so harsh that corrosion sites which nucleate, grow into blunt pits. On the other hand, in the milder chloride environment some corrosion sites grow primarily as slip causes film rupture. In this case the cracking mode would be a combination of the slip dissolution and the pre-existing active path models.

When one looks at the shape of the secondary cracks (fig. 40) evident in the gauge lengths of the 508-A HT1 tested in chloride solutions it seems reasonable to conclude that even the chloride solution used in this investigation was too aggressive. The cracks found are surprisingly wide and blunt for stress corrosion cracks.

As mentioned previously, intergranular stress corrosion cracking requires directed anodic dissolution, where the direction is guided by the principal tensile stress (i.e. dislocations pile up at the grain boundaries thus raising the grain boundary energy fields still further). Thus cracking is the fine balance between ductile slip and anodic dissolution. Anodic dissolution without slip will lead to pitting and general

corrosion, while slip without dissolution will lead to ductile failure. This is in keeping with the quantitative model for crack growth developed by Ford [1] in which the crack growth rate depends on a trade off between the kinetics of passivation and the dynamic strain rate of the crack tip.

In these tests in the HT1 condition it seems evident that anodic dissolution had the upper hand, particularly in the sulphate solution. Taking this argument one logical step further would imply that cracking would be made more severe in one of two ways; by increasing the strain rate or by decreasing the aggressiveness of the environment.

Pitting was also noted for anodic tests in the HT2 and HT3 conditions, though in both of these conditions the pits were very shallow and wide. The absence of deep pits and secondary cracks indicates that the material is resistant to crack initiation in these conditions of environment and material condition, however nothing can be stated categorically about the stability of an existing defect from these tests.

In all of these tests it will be noticed that the results in the test solutions were almost always normalised to a value of less than one. This means that all tests in the solutions lead to decreased ductilities and lower strengths than the air tests. This is ascribed to the fact that the air tests were conducted at room temperature and all of the environmental tests were conducted at 75°C.

5.2.4 Rising Load Testing

Due to time and material constraints, rising load tests were only conducted on the 508-A material in the HT2 condition at the free corrosion potential. This represents a small subset of the conditions covered in the slow strain rate testing program. In these tests no indication of crack growth before sudden failure was found, however the threshold stress intensity at

failure was lower in both solutions than the laboratory air tests. In the absence of fractographic evidence of stress corrosion cracking or hydrogen embrittlement it is felt that this apparent drop in toughness is a function of the different test temperatures (25°C for the air test and 75°C for the environmental tests) rather than a direct result of the environment on the failure mode.

These results augment those of the slow strain rate testing. It is evident that even in the presence of a pre-existing defect, active crack growth does not occur in these solutions at 75°C when tested at the free corrosion potential.

6. CONCLUSIONS

1. The 316NG material is very resistant to sensitization. Heat treating at 650°C for up to 48 hours did not lead to any signs of sensitization when subjected to the oxalic acid etch test, and the highest EPR DOS obtained was 0.08 C/cm^2.

2. The 316NG investigated in this study is very resistant to stress corrosion cracking in the environments in which it was tested. In this regard it is up to the standard of material studied in other work cited in the open literature. Anodic stress corrosion cracking was only found at potentials within 100mV of the pitting potential.

3. Intergranular attack is evident in the 508-A material in the HT1 condition (Quenched) when subject to slow strain rate testing at anodic potentials in 1000ppm chloride solution.

4. Cracking of the 508-A is hindered by harsher environments because general corrosion prevents the development of deep pits, thus mitigating against the formation of both an occluded cell and a severe stress concentrator.

5. In the HT2 condition (Tempered) of the 508-A steel, environmental crack growth of pre-existing defects does not occur in either of the solutions at or above the free corrosion potential.

6. Transgranular hydrogen embrittlement is evident in the 508-A steel when the potential of the test specimen is cathodically polarised by more than 200mV. This hydrogen embrittlement is independant of the heat treated condition of the steel.

REFERENCES

1 P.M. Scott. A review of environment sensitive fracture in water reactor materials. Corrosion Science (25), 1985, 583-605.

2 J.R. Weeks, B. Vyas, S. Isaacs. Environmental factors influencing stress corrosion cracking in boiling water reactors. Corrosion Science, (25), 757-768.

3 M.E. Indig, J.L. Nelson. Electrochemical measurements and modeling predictions in boiling water reactors under various operating conditions. Corrosion NACE, (47), 1990.

4 Escom Technical Brochure "Koeburg - Energy for teh Future", The publications section, Communications department, Escom, January 1990.

5 P. Hurst,, D.A. Appleton, P. Banks, A.S. Raffel. Slow strain rate stress corrosion tests on A508-III and A533B steel in de-ionized and PWR water at 563K. Corrosion Science, (25), 1985, 651-671.

6 W.A. Van Der Sluys, R.H. Emanuelson. Environmental acceleration of Fatigue Crack Growth in Reactor Pressure Vessel Material and Environments. Environmentally assisted cracking, ASTM STP 1049, 117-135, 1990

7 J. Congleton, T. Shoji, R.N. Parkins, The stress corrosion cracking of reactor vessel steel in high temperature water, Corrosion Science, (25), 1985, 633-649.

8 D.R. Tice. A review of the U.K. collaborative programme to test the effect of mechanical and environmental variables on environmentally assisted crack growth of PWR pressure vessel steels. Corrosion Science, (25), 1985, 705-743.

9 J.H. Payer, W.E. Berry, W.K. Boyd. Evaluation of slow strain rate stress corrosion test results. Stress corrosion cracking - The slow strain rate technique, ASTM STP665. 1979, 61-77

10 C.L. Briant. Metallurgical aspects of environmental failures. Elsevier. Oxford. 1985.

11 R. W. Staehle, The theory of stress corrosion cracking. p223, NATO, Brussels, 1971.

12 E.L. Hall, C.L. Briant, Chromium depletion in the vicinity of carbides in sencitized austinitic stainless steels, Metallurgical Transactions A, 15A, May, 793-811, 1984.

13 E.C. Bain, R.H. Abon, J.J.B. Rutherford. Trans. American Steel Treating Society. (21) 1933. 481-503

14 C.L. Briant, R.A. Mulford, E.L. Hall, Sensitization of austenitic stainless steels, 1) Controlled Purity Alloys., Corrosion, 38, 9, 468 - 477, 1982.

15 N. Parvathavarthini, R.K. Dayal; S.K. Seshardi, J.B. Gnanamoorthy. Influence of prior deformation on the sensitization of AISI304 stainless steel and applicability of EPR technique, Br. Corros, J., 26, 1, 67-76, 1991.

16 A.H. Advani, D.G. Atteridge, L.E. Murr, S.M. Bruemmer & R. Chelakara, Deformation effects on chromium diffusivity and grain boundary chromium depletion development in type 316 stainless steels, Scripta Metallurgica, 25, 461 - 465, 1991.

17 A.H. Advani, L.E. Murr, Deformation site spacific nature of strain-induced transgranular carbide precipitation in type 316 stainless steels, Scripta Metallurgica, 25, 349 - 353, 1991.

18 A.H. Advani, D.G. Atteridge, L.E. Murr, S.M. Bruemmer & R. Chelakara. Deformation effects on intergranular carbide precipitation and transgranular chromium depletion in type 316 stainless steel. Corrosion NACE (47) No 12. 1991. 939-947.

19 A.H. Advani, L.E. Murr, D.G. Atteridge, & R. Chelakara. Mechanisms of deformation induced grain boundary chromium depletion (sensitization) development in type 316 stainless steels. Metallurgical Transactions A. (22A) 1991. 2917-2934.

20 Sedriks. The corrosion resistance of Fe-Cr-Ni-Mo alloys. Intermantional Metals Review. 27, 6, 1982.

21 ASTM Standard practices for detecting susceptibility to intergranular attack in austenitic stainless steels., ASTM A262.

22 T.M. Devine, B.J. Drummond. Use of accelerated intergranular corrosion tests and pitting corrosion tests to detect sensitization and susceptibility to IGSCC in high temperature water of duplex 308 stainless steel. Corrosion NACE, (37), 1981,104-114.

23 W.L. Clark, R.L. Cowan, W.L. Walker. Comparative methods for measuring the degree of sensitization of stainless steel. ASTM STP 656, 1978

24 V. Cihal. A potentiokinatic reactivation method for predicting the ICC and IGSCC sensitivity of stainless steels and alloys. Corrosion Science, 1978, 737-743.

25 A.P. Majidi, M.A. Streicher. Potentiodynamic Reactivation Method for detecting sensitization in AISI 304 and 304L stainless steels, Corrosion, 40, 8, 393-408, 1984.

26 R.C. Newman, R.P.M. Procter. Stress corrosion cracking - Silver Jubilee Review, Br. Corr. J., 25, 4, 259-269, 1990.

27 T. Inazumi, G.E.C. Bell, E.A. Kenik, K. Kiuchi. Evaluation of radiation induced sensitization of austenitic stainless steels using electrochemical potentiokinetic reactivation technique EPR, Corrosion, 46, 10786-792, 1990.

28 R.F. Sandenbergh. Evaluation of the degree of sensitization in type 316LNG, 304L and 308/309 stainless steels. Laboritory for Materials Science and Metallurgical Engineering Incorpteated Report, 31/01/1991.

29 R.D. Knutsen, A. Ball. The influence of inclusions on the corrosion resistance of a 12wt% chromium steel. Corrosion NACE, 47 (5) 1991. 359-368

30 Avner S.H. Introduction to Physical Metallurgy. McGraw-Hill Kogakusha Ltd. Tokyo. 1974.

31 C.D. Kim, B.E. Wilde, A review of the constant strain rate stress corrosion cracking test. Stress corrosion cracking-The slow strain rate technique, ASTM STP665. 1979, 97-112

32 G. Buzzanca, E. Caretta, L. Meini, R. Pascal and C. Ronchetti. A contribution to the interpretation of the strain rate effect on type 304 stainless steel intergranular stress corrosion cracking. Corrosion Science 25 (8/9) 1985 805-813.

33 D.D. Macdonald. Viability of hydrogen water chemistry for protecting in-vessel components of boiling water reactors. Corrosion NACE, 48 (3) 1992. 194-205

34 L.G. Ljungberg, D. Cubicciotti, M. Trille. Effects of some seldom noticed water impurities on stress corrosion cracking of BWR construction materials. Corrosion NACE. 45 (3). 1989. 215-221.

35 S. Szklarska-Smialowska, G. Cragnolino. Stress corrosion cracking on sensitized 304 stainless steel in oxygenated pure water at elevated temperatures (Review). Corrosion NACE 36 (12). 1980. 653-665.

36 E.G. Coleman, D. Weinstein, W. Rostoker. Acta Met. 9. 1961, 491.

37 M. Kowaka. Metal Corrosion Damage and Protection Technology. New York, Allerton Press, 1990.

38 P. Marshell. Austenitic Stainless Steels. Microstructure and Mechanical Properties. Elsivier Applied Science Publishers. London. 1984.

39 R. Kerr F. Solana I.M. Bernstein A.W. Thompson. Microstructural effects on the stress corrosion cracking behaviour of medium and high strength steels. Metallurgical Transactions, 18A 1987, 1011-1022

40 T. Shoji, H. Takahashi, S. Aizawa, M. Saito. Effect of sulphate contamination, sulphur in steel and strain rate on critical cracking potentials for SCC of pressure vessel steels in pressurized high temperature waters. Proceedings of the 3rd international symposium on environmental degradation of materials in nuclear power systems - water reactors, Edited by G.J. Theus and J.R.Weeks. 251-258. 1988

41 J.H. Bulloch. Environmental assisted cracking phenomena in reactor pressure vessel steel - the role of manganese sulphide segregation. Proceedings of the 3rd international symposium on environmental degradation of materials in nuclear power systems - water reactors, Edited by G.J. Theus and J.R.Weeks. 261-268. 1988

42 P. Combrade, M. Foucault. On the role of Sulfur on the dissolution of pressure vessel steels at the tip of a propagating crack in PWR environments. Proceedings of the 4th international symposium on environmental degradation of materials in nuclear power systems - water reactors. Edited by D. Cubicciotti. Pages 8.48-8.63. 1989

43 H.L. Ewalds and R.J.H. Wanhill. Fracture Mechanics. Edward Arnold Press. 1985. Page 98 & 99

44 S.P. Lynch. Metallographic contributions to understanding mechanisms of environmentally assisted cracking, Metallography, 23, 147-171, 1989.

45 K. Sieradzki, R.C. Newman. Stress Corrosion Cracking, J. Phys. Chem. Solids, 48, 11, 1101-1113, 1987.

46 G.M. Scamans, P.R. Swann. Corrosion Science, 18, 983-989, 1978.

47 W.F. Flanagan. P. Bastias, B.D. Lichter, A theory of transgranular stress-corrosion cracking, Acta Metall, 39, 4, 695-705, 1991.

48 ASTM G39-79 (1984). Standard practice for preperation and use of bent-beam stress corrosion specimens.

49 ASTM G30-72 (1984). Standard practice for making and using U-bend stress corrosion specimens.

50 B.E. Wilde. Corrosion. 25, 1969, 359.

51 ASTM STP 626

52 S. Abe, M. Kojima, Y. Hosoi. Stress corrosion cracking susceptibility index, I_{SCC}, of austenitic stainless steels in constant strain rate test. Stress Corrosion Cracking - The slow strain rate technique. ASTM STP 665. 1979. 294-304.

53 R.N. Parkins. Development of strain rate testing and its implications. Stress Corrosion Cracking - The slow strain rate technique. ASTM STP 665. 1979. 5-25.

54 H. Buhl. Validity of the slow strain rate test method in the stress corrosion cracking research compared with conventional testing techniques. Stress Corrosion Cracking - The slow strain rate technique. ASTM STP 665. 1979. 333-346.

55 W.J. Daniels. Comparative findings using the slow strain rate, constant flow stress, and U-bend stress corrosion cracking techniques. Stress Corrosion Cracking - The slow strain rate technique. ASTM STP 665. 1979. 347-361.

56 W. Yang, M. Zhang, G. Zhao, J. Congleton, A comparison of U-bend and SSR procedures for assessing the SCC resistance of type 304SS in high temperature water. Corrosion, 47, 4, 1991, 226-233.

57 W. Yang, M. Zhang, G. Zhao, J. Congleton, An AES investigation of the surface films formed on stress corrosion test specimens of type 304 stainless steel in high temperature water. Corrosion Science. 33 (1). 1992. 89-102.

58 P.S. Maiya. Plastic strain, environmental and crevice effects on SCC initiation and propagation in type 316NG and 304 stainless steel. Corrosion NACE. 45 (11). 1989. 915-924.

59 J..A. Beavers, G.H. Koch. Limitations of the Slow strain rate test for stress corrosion cracking testing. Corrosion. 48 (3) 1992. 256-264.

60 B.F. Brown, C.D. Beachem, Corrosion Science, 5, 1965, 745

53 P.S. Maiya, W.J. Shack. Stress corrosion cracking susceptibility of AISI 316 NG and 316 stainless steel in an impurity environment. Corrosion NACE. Vol 41 (11). 1985.

62 R. Berneke, R.F. Sandenbergh. The influence of Nitrogen and Molybdenum on the sensitization properties of low carbon austenitic stainless steels. Corrosion Science. 29 (5). 1989.

63 J. Congleton, H.C. Shih, T. Shoji, R.N. Parkins. The stress corrosion cracking of type 316 stainless steel in oxygenated and chlorinated high temperature water. Corrosion Science. 1984. 769-788.

64 J. Congleton, W. Zheng, H. Hua. The stress corrosion cracking behaviour of annealed type 316 stainless steel in low oxygen 5ppm chloride content water at 300 °C. Corrosion Science. Vol 30 (6/7). 1990.

65 J. Congleton, W. Zheng, H. Hua. Stress corrosion cracking of annealed type 316 stainless steel in high temperature water. Corrosion NACE, Vol 46 (8). 1990.

66 J.D. Atkinson. The effect of corrosion potential on fatigue crack growth rates in pressure vessel steels exposed to PWR primary water environments. Proceedings of the 4th international symposium on environmental degradation of materials in nuclear power systems - water reactors.Edited by D. Cubicciotti. Pages 8.64-8.74. 1989

67 P. Combrade, M. Foucault. On the role of Sulfur on the dissolution of pressure vessel steels at the tip of a propagating crack in PWR environments. Proceedings of the 4th international symposium on environmental degradation of materials in nuclear power systems - water reactors. Edited by D. Cubicciotti. Pages 8.48-8.63. 1989

68 P.M. Scott, A.E. Treswell, S.G. Druce. Corrosion fatigue of pressure vessel steels in PWR environments - Influence of steel sulphur content. Corrosion NACE. 40 (7) 1984.

69 V.G. Rivlin, G.V. Raynor. Int. Met. Rev. 1980. (1) 21-28.

70 F.C. Hull. Weld. J. Res. Suppl. 1973, 52 (5), 193s-203s.

71 Standard specifications for quenched and tempered vacuum-treated carbon and alloy steel forgings for pressure vessels. ASTM A508/A 508/M - 86. Volume 01.04 1987.

72 R.W.K. Honeycombe.Steels, Microstructure and properties. Edward Arnold. 1981

73 D.G. Atteridge, S.M. Bruemmer, R.E. Page. Evaluation of welded and repair-welded stainless steel for LWR service. NUREG/CR–3613 Vol 2. TI85 013660. 1984.

74 J.R. Scully. P.J. Moran. Influence of strain on hydrogen assisted cracking of cathodically polarised high-strength steel. ASTM STP 1049. 1990. 5-29.

APPENDIX A

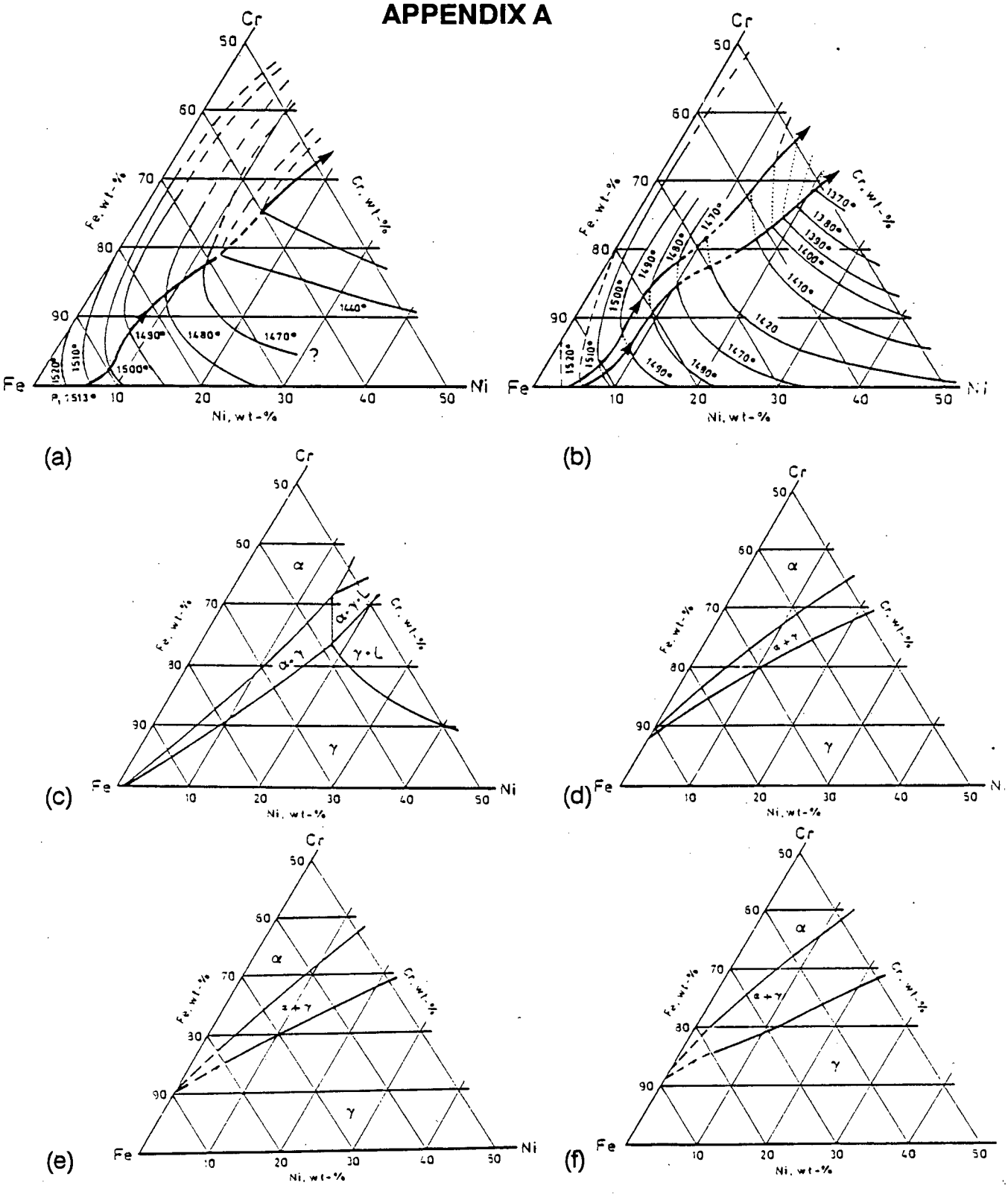

FIGURE A1 Isothermal sections through the Fr-Cr-Ni ternary phase system. (a) Liquidus projection (b) Solidus projection (c) 1400°C, (d) 1300°C (e) 1200°C (f) 1100°C *(Continued overleaf...)*

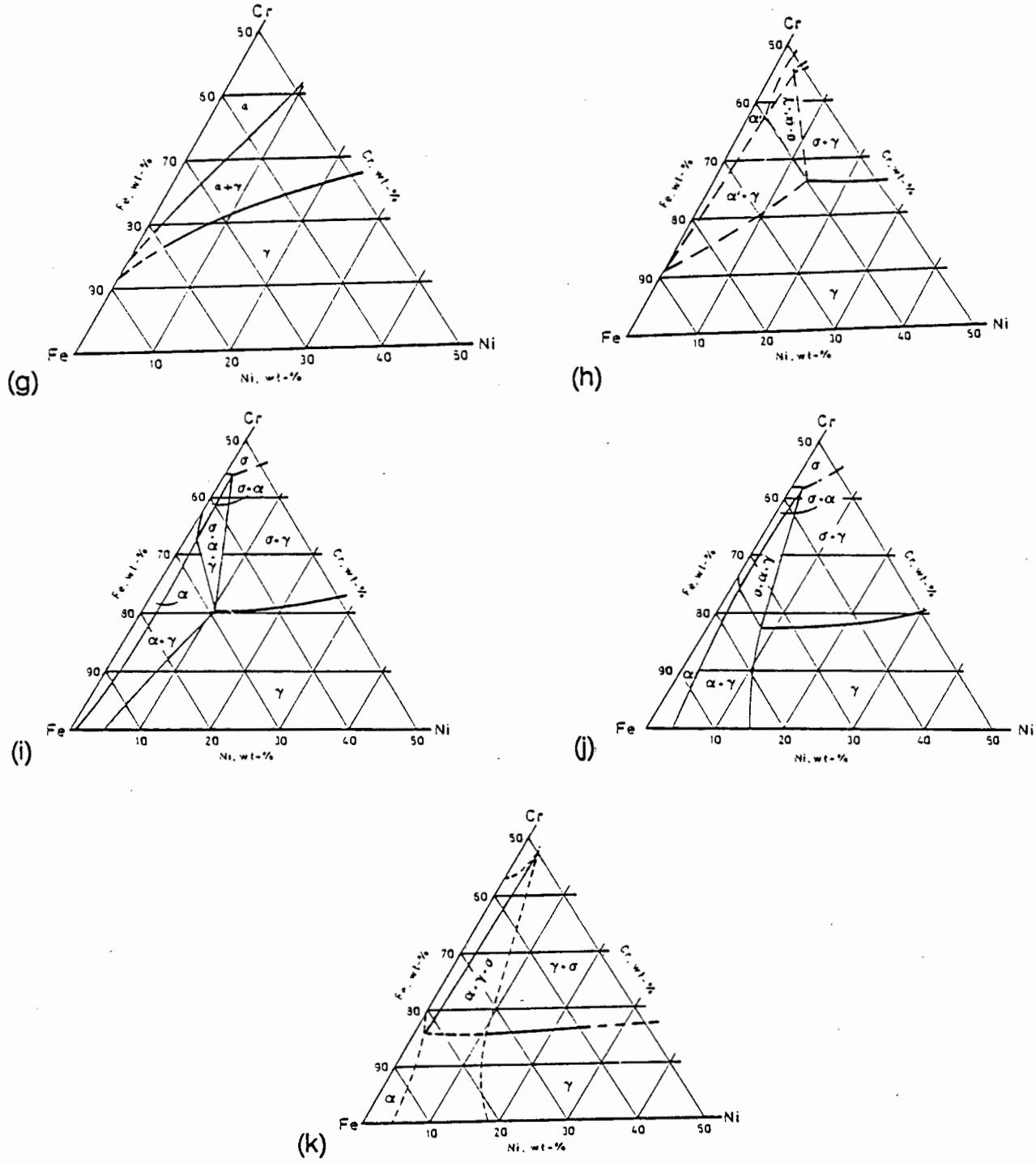

FIGURE A1 Isothermal sections throught the Fr-Cr-Ni ternary phase system. (g) 1000°C (h) 900°C (i) 800°C (j) 650°C (k) 550°C.

APPENDIX B

ADCARD.PAS (UNIT)

Source code for the A-D conversion card unit writen in turbo Pascal 5.5. This unit defines codes used by all the other programmes utalised in this project.

```
UNIT ADCard;

INTERFACE
      Uses Crt;

      TYPE CardMode = (Five_Five, Zero_Ten, Ten_Ten);

      VAR CardResult : Integer;
        Mode : CardMode;

   PROCEDURE BEEP;
   FUNCTION SAMPLE (Channel,Average:Integer) : REAL;
   PROCEDURE SetDA (volts : Real; Channell : INTEGER);
   FUNCTION CardError (Result:INTEGER) : String;

{***********************************************}
IMPLEMENTATION
{***********************************************}

FUNCTION ADSAMPLE (channel:INTEGER): INTEGER;
 VAR I:INTEGER;

BEGIN
  PORT [$702] := (channel SHL 4) + 2; {channel selection and}
                        {clear software-clock bit }
   PORT [$702] := (channel SHL 4) + 3;{channel selection and}
                        {setting of software-clock bit }
   FOR I:=1 TO 6 DO
   BEGIN              {loop until end of conversion }
   END;
   ADSAMPLE := ((PORT[$701] AND $0F) SHL 8) + PORT[$700];
END;

{***********************************************}

FUNCTION SAMPLE (Channel,Average:Integer) : Real;

Var SampleTotal,Ans : Real;
   Loop : Integer;

BEGIN
   IF (Channel <0) OR (Channel > 15) THEN
   BEGIN
      CardResult := 1;
      Beep;
      EXIT;
   END;
   IF Average < 1 THEN
   BEGIN
      CardResult := 2;
      Beep;
      EXIT;
   END;
   CardResult := 0;
   PORT[$703] := $92;
   PORT[$70B] := $9B;
   SampleTotal := 0;
   FOR LOOP:= 1 TO (Average) DO
   BEGIN
      SampleTotal := (ADSample (Channel) + (SampleTotal));
   END;
   Ans := SampleTotal / Average;
   CASE Mode OF
   Five_Five : BEGIN
      Sample := (Ans-2048) *10000/4095;
   END;
   Zero_Ten : BEGIN
      Sample := Ans * 10000/4095;
   END;
   Ten_Ten : BEGIN
      Sample := (Ans-2048) *20000/4095;
   END;
   ELSE BEGIN
      CardResult := 5;
   BEEP;
   EXIT;
   END;
END; {Case}
END;

{***********************************************}

PROCEDURE SetDA (volts : Real; Channell : INTEGER);

VAR
   da_msb,da_lsb,temp  : INTEGER;
   UpperPort, LowerPort : INTEGER;

BEGIN
   IF (volts < -10) OR (Volts > 10) THEN
   BEGIN
      CardResult := 3;
      Beep;
      Exit;
   END
   ELSE CardResult := 0;
   CASE Channell OF
   1 : BEGIN
      UpperPort := $714;
   END;
   2 : BEGIN
      UpperPort := $715;
   END;
   3 : BEGIN
      UpperPort := $70D;
      LowerPort := $70C;
   END;
   4 : BEGIN
      UpperPort := $711;
      LowerPort := $710;
   END;
   ELSE
   BEGIN
      CardResult := 4;
      Beep;
      EXIT;
   END;
   END; {case}
   Temp := ROUND((volts*(2048/-10))+2048);
   da_msb := temp SHR 4;
   da_lsb := (temp SHL 4) AND $F0;
   Port[UpperPort] := da_msb;
   IF (Channell = 3) OR (Channell = 4) THEN
   Port[LowerPort] := da_lsb;
END;

{***********************************************}

Procedure BEEP;

begin
   Sound(220);       { Beep }
   Delay(200);       { For 200 ms }
   NoSound;          { Relief! }
end;

{***********************************************}

FUNCTION CardError (Result:INTEGER) : String;

BEGIN
   CASE Result OF
   1 : CardError := 'Channell out of range';
   2 : CardError := 'Cant Average this Number of readings';
   3 : CardError := 'Voltage out of range';
   4 : CardError := 'Invalid output channell';
   5 : CardError := 'Card MODE not set: Five_Five, 0/10, 10/10 ';
   END; {case}
END;


END. {of the unit...}
```

SCC.PAS (PROGRAMME)

Source code for the programme used to control the slow strain rate test rig. This programme samples the load and displacement at 1 min intervals during a test and stores the results in an ASCII text file. Data relevant to the test is stored in the file SCC-DATA.SET which must be in the default directory of the A: drive. This file conforms to the following format...

```
1000        (Load Cell Gain)
1           (LVDT Gain)
0.492       (Load cell cal. factor)
5           (LOAD CELL Voltage)
0.796       (LVDT Cal. factor)
15          (Gauge Length)
3           (Gauge diameter)
3e-6        (Desired strain rate)
```

```
PROGRAM StressCorrosionCracking;
USES Dos,Crt,ADCard,Forms;

TYPE Q=STRING [80];
     Main = ARRAY [1..2,1..30] OF REAL;

  VAR LoadGain, StrainGain, LoadCalFactor, LoadInptVolts,
  StrainCalFactor, GaugeLength, GaugeDiam, StrainRate,
  Area, LoadFactor, StrainFactor, Speed, D_A : REAL;
  Load0, Strain0 : REAL;
  Ended, Testing : BOOLEAN;
  FileError,Count,SaveTimes : INTEGER;
  DataArray:Main;
  FailureStr : Q;
  SameFile : String[20];
  Out:TEXT;
  Outpt : File of real;

{Procedure to put text at a spacific location in a spacific color}
PROCEDURE Puts (x,y,TC:INTEGER; Str:Q);
BEGIN
  GOTOXY(x,y);
  TEXTCOLOR (TC);
  WRITE (Str);
  TEXTCOLOR(Black);
END;

{This places the blinking curser in the upper lefthand corner of
the screen}
PROCEDURE Home;
BEGIN
  TextBackground (16);
  Puts(1,1,LightGray,'');
END;

{This returns an explanation (in text) of the dos error code
number}
Function FindError(ErrNo:INTEGER) : Q;
  VAR Inpt : String [5];
  BEGIN
    Case ErrNo OF
      2 : FindError := 'File not found ';
      3 : FindError := 'Path not found ';
      5 : FindError := 'File access denied ';
     15 : FindError := 'Invalid drive number ';
     100 : FindError := 'Disk read error ';
     101 : FindError := 'Disk write error ';
     150 : FindError := 'Disk is WRITE Protected ';
     152 : FindError := 'Drive not ready ';
     155 : FindError := 'Bad File Name ';
     160 : FindError := 'Device WRITE fault ';
     ELSE
     BEGIN
       STR (ErrNo,Inpt);
       FindError := 'Dos error Number : '+Inpt;
     END;
    END; {case}
  END;

{this creates the disk file SCC-DATA.SET if it was not available}
PROCEDURE MakeFile;
Var DataInfo : String[10];
BEGIN
  Window(19,7,57,17);
  Home;
  ClrScr;
  Window(17,6,55,16);
  Color(BackColor);
  ClrScr;
  Puts (8,2,White,'**** Data Entry ****');
  GotoXY(1,4);
  TextColor(White);
  Assign (out,'a:\SCC-DATA.SET');
  Rewrite (out);
  Write (' LoadCell Gain              : ');
  ReadIn (DataInfo); WriteIn (out,DataInfo);
  Write (' LVDT Gain                  : ');
  ReadIn (DataInfo); WriteIn (out,DataInfo);
  Write (' Load Calabration Factor    : ');
  ReadIn (DataInfo); WriteIn (out,DataInfo);
  Write (' Loadcell input voltage     : ');
  ReadIn (DataInfo); WriteIn (out,DataInfo);
  Write (' LVDT Calabration Factor    : ');
  ReadIn (DataInfo); WriteIn (out,DataInfo);
  Write (' What is the gauge length   : ');
  ReadIn (DataInfo); WriteIn (out,DataInfo);
  Write (' and the gauge diameter (mm) : ');
  ReadIn (DataInfo); WriteIn (out,DataInfo);
  Write (' Enter the strian rate      : ');
  ReadIn (DataInfo); WriteIn (out,DataInfo);
  Close (out);
  Window(1,1,80,25);
END;

{This reads the machine (and other) constants from the file
          a:\scc-data.set }
PROCEDURE DataRead;
VAR Inpt : TEXT;
  Ch : CHAR;
BEGIN
  Puts (20,20,black,'  Reading SCC-DATA.SET  ');
  REPEAT
  {$I-} {turn IO error checking off}
  ASSIGN(Inpt,'A:\SCC-DATA.SET');
  RESET(Inpt);
  {$I+}  {turn IO error checking back on again}
  FileError := IOResult;
  If FileError < > 0 THEN
  BEGIN
    BEEP;
```

```
      Color(ForeColor);
      If FileError = 2 then
      Puts(15,23,RED,'  '+FindError(FileError)+'  ENTER - Retry,
                Q - quit,  C - Create  ')
      ELSE Puts (15,23,red,'    '+FindError(FileError)+'  ENTER -
                              Retry, Q - quit    ');
      Home;
      Repeat until keypressed;
      ch := Readkey;
      IF UpCase(ch) = 'Q' THEN
      BEGIN
         {$F+}
         TextColor(LightGray);
         ClrScr;
         Halt;
      END;
      IF UpCase(ch) = 'C' THEN MakeFile;
   END;
   UNTIL FileError = 0;
   READLN(Inpt,LoadGain);
   READLN(Inpt,StrainGain);
   READLN(Inpt,LoadCalFactor);
   READLN(Inpt,LoadInptVolts);
   READLN(Inpt,StrainCalFactor);
   READLN(Inpt,GaugeLength);
   READLN(Inpt,GaugeDiam);
   READLN(Inpt,StrainRate);
   CLOSE (Inpt);
END;

{calculates the area, machine speed and callabration factors}
PROCEDURE FactorsCalculate;
BEGIN
   Area:=Pi*(SQR(GaugeDiam/2));
   LoadFactor:=(((1/LoadInptVolts)*LoadCalFactor*9.8)/Area);
   StrainFactor:=(((1/StrainGain)*(1.256/1000))/GaugeLength);
   Speed:=StrainRate/(3.135e-7/GaugeLength); {Speed setting
                                 on the machine}
END;

{This is the procedure which prompts for test data to write to the
output file}
PROCEDURE EnterTestData;  {Uses forms unit in OOPDEMO of
turbo V5.5}
type
   TestData = record
   Date : string[28];
   SpecimenType: string[28];
   TestWater: string[28];
   Potential: string[28];
   Temp: string[28];
   FileName: String[20]
   end;

CONST
   GeneralTest : TestData=( {this constant is the default values}
   Date : ' 01-01-92';          {for all this data and could be}
   SpecimenType : '_________';      {changed as required}
   TestWater : ' Distilled & Aerated';
   Potential : '- mV';
   Temp : ' 75°C ';
   FileName : 'A:\Test.PRN');

var
   F: Form;  {form is defined as an object in the FORM.PAS unit}
   P: TestData;
   Ch : Char;
   ProblemStr, Inpt : Q;

BEGIN
   Color(BackColor);
   ClrScr;
   Color(ForeColor);
   GotoXY(1, 1); ClrEol;
   Write('              Enter the test data relavent to this test.');
   GotoXY(1, 25); ClrEol;
   Write('                              F2 = done');
   F.Init(30, 3, 74, 14);
   F.Add(New(FStrPtr, Init(3, 3, '  Test Date ', 28)));
   F.Add(New(FStrPtr, Init(3, 5, '   Material ', 28)));
   F.Add(New(FStrPtr, Init(3, 6, '      Water ', 28)));
   F.Add(New(FStrPtr, Init(3, 7, '  Potential ', 28)));
   F.Add(New(FStrPtr, Init(3, 8, 'Temperature ', 28)));
   F.Add(New(FStrPtr, Init(3, 10,' File to save to ',23)));
   P := GeneralTest;
   F.Put(P);
   F.Show(True);
   if F.Edit = CSave then F.Get(P);
   F.Done;
   NormVideo;
   WITH P DO
      REPEAT
{$I-}          {have to turn input output checking off...}
      Assign (out,FileName);
      Rewrite (out);
{$I+}          {...and on again to prevent programme hanging}
      FileError := IOResult;  {if there is a FileError }
      If FileError <> 0 THEN      {FileError = 0 = no problem}
      BEGIN
         BEEP;
         Color(ForeColor);
         Puts(15,25,RED,'  '+FindError(FileError)+'  RETURN to
                              retry, Q to Quit  ');
         Home;
         Repeat until keypressed;
         ch := Readkey;
         IF UpCase(ch) = 'Q' THEN
         BEGIN
            {$F+}
            TextColor(LightGray);
            ClrScr;
            Halt;
         END;
      END;
   UNTIL FileError = 0;
   Color(ForeColor);  GotoXY(1,25); ClrEol;
   WITH P DO
   BEGIN
      Writeln(out,'Date        :,,',Date);
      WriteLn(out,'Specimen Type:,,',SpecimenType);
      WriteLn(out,'Water Type  :,,',TestWater);
      WriteLn(out,'Potential   :,,',Potential);
      WriteLn(out,'Temperature :,,',Temp);
   END;
   Writeln (out);
   Close (out);
   SameFile := P.FileName;
END;

{flush the array out and fill it with zero's}
PROCEDURE Empty_the_Array;
BEGIN
   FillChar (DataArray,SizeOf(DataArray),0);
   Count := 0;
END;

PROCEDURE Initialize;
BEGIN
   Ended := False;
   Testing := False;
   D_A := 10000/4096;   {Digital to annalog conversion (Digit-
                        4096=10000mV) }
   SaveTimes := 0;
   Empty_the_Array;
   Count := 1;
   Mode := Zero_Ten;          {D-A card configuration 0-10V
                        (ADCard unit)}
   Load0 := 0; Strain0 := 0;
END;

{This uses the function Sample(Channell,Average_of) in the
ADCard unit}
PROCEDURE SampleAll (ReadingNo:INTEGER);
VAR Temp1, Temp2 : REAL;
BEGIN
   DataArray[1,ReadingNo] :=
         (Sample(3,300)-Load0)*LoadFactor;
   DataArray[2,ReadingNo] :=
         (Sample(2,300)-Strain0)*StrainFactor;
END;

{This saves the contents of the array (test data) to the end of the
out file}
PROCEDURE SaveAll;
VAR loop : integer;
BEGIN
   Append (out);
   For Loop := 1 to 30 DO
   BEGIN
      IF Loop MOD 5 = 0 THEN
      BEGIN
         Write(out,(SaveTimes*30)+Loop,',');
         Write(out,DataArray[1,loop]:5:3,',');
         Writeln(out,DataArray[2,loop]:5:5);
      END;
   END;
   Close (Out);
   SaveTimes := SaveTimes+1;
   Empty_the_array;
END;


{Name is self explanatory...}
PROCEDURE WasteTime;
VAR Min0,Sec0, Hr,Min,Sec,Frac : WORD;
   Info : STRING[4];
```

```
    WatchFlag : BOOLEAN;
    ch : Char;
BEGIN
    Window(50,19,60,20);
    Color(ForeColor);
    ClrScr;
    GetTime (Hr,Min,Sec,Frac);
    Min0 := Min;
    Sec0 := Sec;
    WatchFlag := True;
    REPEAT
    BEGIN
        GetTime (Hr,Min,Sec,Frac);
        IF Sec > Sec0 THEN
        BEGIN
            TextColor(Red);
            GotoXY(1,1);
            Writeln('  TIME');
            Write('  ',Hr,':',Min,':',Sec);
            GotoXY(1,1);
            Sec0 := Sec;
        END;
        IF Min = Min0+1 THEN WatchFlag := False;
        IF Min < Min0 THEN Watchflag := False;
        IF Keypressed THEN
        BEGIN
            ch := ReadKey;
            IF (ch='t') then watchflag := false;
            IF ch=#0 THEN                    {check for CTRL or ALT}
            BEGIN
                Ch := ReadKey;               {Alt-X keys}
                If ch=#045 THEN
                BEGIN
                    Ended:=TRUE;
                    FailureStr := 'Operator Interrupt.';
                    Watchflag := False;
                END;
            END;
        END;
    END;
    UNTIL Watchflag = False;
END;

PROCEDURE DisplayStatus;
Var Info : STRING[10];
BEGIN
    Window(1,1,80,25);
    Color(ForeColor);
    GotoXY(1, 1); ClrEol;
    Write('        Slow Strain Rate Test in progress. Please Don''t
                                TOUCH.');
    GotoXY(1, 25); ClrEol;
    Write('                        <Alt-X> to end.');
    Window(4,5,30,19);
    Home;
    ClrScr;
    Window(3,4,28,18);
    Color(ForeColor);
    ClrScr;
    Puts(4,2,Blue,' PRESENT TEST STATUS:');
    Puts(4,3,Blue,'~~~~~~~~~~~~~~~~~~~~~~~~');
    Puts(3,6,Magenta,'LOAD (MPa) :');
    Puts(3,8,Magenta,'STRAIN (%) :');
    Puts(3,12,Black,'Run Time :');
    Str(SaveTimes*30+Count,Info);
    Puts(14,12,Black,Info+' mins');
    TextBackground(Cyan);
    Str(DataArray[1,Count]:5:3,Info);
    Puts(16,6,Black,' '+Info+' ');
    Str(DataArray[2,Count]:5:3,Info);
    Puts(16,8,Black,' '+Info+' ');
    Window(1,1,80,25);
END;

PROCEDURE RunTest;
BEGIN
    SampleAll (Count);
    IF DataArray[1,count]>200 THEN Testing := TRUE;
    IF (DataArray[1,count]<100) and (Testing = true) THEN
    BEGIN
        Ended := TRUE;
        FailureStr := 'Specimen Broke';
        Exit;
    END;
    IF DataArray[1,count]>1300 THEN
    BEGIN
        Ended := TRUE;
        FailureStr := 'Loadcell overload';
        Exit;
    END;
    If Count MOD 30 = 0 THEN
     SaveAll;
    DisplayStatus;
    Count:=Count+1;
    WasteTime;
END;

PROCEDURE StartTest;
VAR Out : TEXT;
    Info : string[5];
    Ch : Char;
BEGIN
    Str(Speed:5:0,info);
    Puts (40,14,Black,'Machine speed = '+Info);
    Puts (25,22,White,'"Y" to start.');
    Home;
    REPEAT
        REPEAT UNTIL KeyPressed;
        CH := ReadKey;
    UNTIL UpCase(ch)='Y';
    Puts(23,22,LightGray,' Test is running... ');
    Load0 := Sample(3,300);
    Strain0 := Sample(2,300);
END;

PROCEDURE Introduction;
VAR Ch : Char;
BEGIN
    Color(BackColor);
    ClrScr;
    Color(ForeColor);
    GotoXY(1, 1); ClrEol;
    Write('  SLOW STRAIN RATE TESTING PROGRAMME  v1.00');
    GotoXY(1, 25); ClrEol;
    Write(' By - M. Gammon.                          1992');
    Window(10,6,75,19);
    Home;
    ClrScr;
    Window(8,5,73,18);
    Color(ForeColor);
    ClrScr;
    Writeln; Writeln; Writeln;
    Writeln ('  This programme will sample the load and strain on
                                the specimen');
    writeln ('  in the slow strain rate rig at one minute
                 intervals,and shut');
    Writeln ('  the system off when the specimen breaks.');
    Writeln ('  The load cell and LVDT  calabration  data must be in
                                        a file on');
    Writeln ('  the A: drive called SCC-DATA.SET.');
    Writeln;
    Writeln ('          Strain = Channel 2;    Load = Channel 3.');
    Puts (20,2,Blue,'****  INTRODUCTION  ****');
    Puts (39,13,blue,'Space bar to continue...');
    Repeat
        Repeat until keypressed;
        Ch := ReadKey;
    Until ch = ' ';
    Window(1,1,80,25);
END;

PROCEDURE EndingScreen;
BEGIN
    Window(20,18,50,22);
    Home;
    ClrScr;
    Window(18,17,48,21);
    TextBackground(yellow);
    ClrScr;
    Puts(4,2,Blue,'*** THIS TEST IS OVER ***');
    Puts(2,3,Black,'REASON : '+FailureStr);
    Window(1,1,80,25);
    Puts(22,21,LightGray,'ENTER to exit programme');
    Textbackground(black);
    Textcolor(lightgray);
END;

BEGIN
    Home;
    ClrScr;
    SetDA (0,1);
    Introduction;
    DataRead;
    FactorsCalculate;  {LoadCell & Strain factors...}
    EnterTestData;     {Date, soln, Pot, °C, File...}
    Initialize;        {Counter, array=0's, ended= x, AD card mode}
    StartTest;
    REPEAT
        RunTest;
    UNTIL Ended;
    SaveAll;
    SetDA (10,1);
    EndingScreen;
    Readln;
    ClrScr;
END.
```

ESH.PAS (PROGRAMME)

Source code for the programme written to sample test data from the ESH universal testing machine. This programme samples up to 8 channels from the A-D card at specified time intervals and stores the data in an asci text file for importation into a spreadsheet programme.

```
PROGRAM ESH_Testing;
USES Dos,Crt,ADCard;

CONST MaxChan = 8;
   D_A : Real = 10000/4096;
        {Digital to annalog conversion (Digit-4096=10000mV)}
   CardRange : CardMode = Ten_Ten;
        {D-A card configuration 0-10V (ADCard unit)}
   BufSize = 30;  {Number of readings before saving to disk}

TYPE Q = String[30];
    Main = array[0..MaxChan, 1..BufSize] OF Real;

VAR Sec0, Hr, Min, Sec, Frac : Word;
   DataArray : Main;
   TopChan, Count, Savetimes : Integer;
   RunTime, PrevTime, SamplePeriod, Mean_Of : Integer;
   Ended : BOOLEAN;
   Today : String[12];
   N, SameFile : String[20];
   Out:TEXT;
   Outpt : File of real;
   ExitSave : Pointer;

{*********************************************************}

{This returns a text explanation of the dos error code number}
Function FindError(ErrNo:INTEGER) : Q;
VAR Inpt : String [5];

BEGIN
   Case ErrNo OF
   2 : FindError := 'File not found ';
   3 : FindError := 'Path not found ';
   5 : FindError := 'File access denied ';
   15 : FindError := 'Invalid drive number ';
   100 : FindError := 'Disk read error ';
   101 : FindError := 'Disk write error ';
   150 : FindError := 'Disk is WRITE Protected ';
   152 : FindError := 'Drive not ready ';
   155 : FindError := 'Bad File Name ';
   160 : FindError := 'Device WRITE fault ';
   ELSE
   BEGIN
      STR (ErrNo,Inpt);
      FindError := 'Dos error Number : '+Inpt;
   END;
   END; {case}
END;

{*********************************************************}

PROCEDURE EnterTestData;

Var Filename,Code,SpecimenType,
   Comment1,Comment2,Comment3 : String[20];
   S : PathStr;
   y,m,d,dow : word;
   Yr,Mo,Day : String[4];
   Ch : Char;
   FileError : Integer;

BEGIN
   GetDate (y,m,d,dow);
   Str(y,Yr); Str(m,Mo); Str(d,Day);
   Today := Day+'/'+Mo+'/'+Yr;
   Window (40,4,77,15);
   TextColor (LightGray);
   Write ('Test Code : '); Readln (code);
   Write ('Specimen : '); Readln (SpecimenType);
   Write ('Comment 1 : '); Readln (comment1);
   Write ('Comment 2 : '); Readln (comment2);
   Write ('Comment 3 : '); Readln (comment3);
   WINDOW (1,5,39,15);
   Repeat
      Write ('File name : ');
      REPEAT
         GotoXY (14,1);
         Readln (FileName);
      UNTIL FileName <> '';   {They must enter something!}
      S := FSearch (FileName,GetEnv('PATH'));
      IF S<>'' THEN     {Does the file already exist?}
      BEGIN
         Beep;
         Writeln (' File already exists,');
         Writeln (' Please start again... ');
         Delay (1500);
         ClrScr;
      END;
   UNTIL S = '';

   REPEAT
      {$I-}     {have to turn input output checking off...}
      Assign (out,FileName);
      Rewrite (out);
      {$I+}     {...and on again to prevent programme hanging}
      FileError := IOResult;   {if there is a FileError }
      If FileError <> 0 THEN {FileError = 0 means no problem}
      BEGIN
         BEEP;
         Writeln (FindError(FileError));
         Writeln (' RETURN to retry, Q to Quit ');
         Repeat until keypressed;
         ch := Readkey;
         IF UpCase(ch) = 'Q' THEN
         BEGIN
            {$F+}
            TextColor(LightGray);
            ClrScr;
            Halt;
         END;
         GotoXY (1,2);
         Write ('     ');
      END;
   UNTIL FileError = 0;   {We have a new file name thats OK}
   BEGIN
      Writeln(out,'Date :,,',today);
      Writeln(out,'Test code :,,',Code);
      WriteLn(out,'Specimen Type:,,',SpecimenType);
      WriteLn(out,'Water Type :,,',Comment1);
      WriteLn(out,'Potential :,,',Comment2);
      WriteLn(out,'Temperature :,,',Comment3);
   END;
   Writeln (out);
   Writeln (Out,'Data Readings');
   Close (out);
   SameFile := FileName;
   REPEAT
      GotoXY (1,3);
      Writeln ('Reading Channels 1 to ? ');
      GotoXY (23,3);
      Readln (TopChan);
      If TopChan > MaxChan Then Beep;
   UNTIL TopChan <= MaxChan;
   Write ('Sampling Period (s) : '); Readln (SamplePeriod);
   Window(1,1,80,25);
END;

{*********************************************************}

{flush the array out and fill it with zero's}
PROCEDURE Empty_the_Array;
BEGIN
   FillChar (DataArray,SizeOf(DataArray),0);
   Count := 0;
END;
{*********************************************************}
```

```
PROCEDURE Initialize;

BEGIN
   Ended := False;
   SaveTimes := 0;
   IF SamplePeriod < 10 THEN
   Mean_Of := 500 ELSE
   Mean_Of := 5000;
   Empty_the_Array;
   Count := 1;
   Runtime := 0;
   PrevTime := 0;
   Mode := CardRange;
END;

{*********************************************************}

{This uses the function Sample(x,y) in the ADCard unit}
PROCEDURE SampleAll (ReadingNo:INTEGER);
   VAR Loop : Integer;
BEGIN
   For Loop := 1 TO TopChan DO
   BEGIN
      DataArray[Loop,ReadingNo] := Sample(Loop,Mean_Of);
      If Cardresult <>0 THEN Writeln (CardError (CardResult));
   END;
END;

{*********************************************************}

{This adds the contents of the array (testdata) to the end of the
output file}

PROCEDURE SaveAll;
   VAR loop,Chan : integer;
BEGIN
   Append (out);
   For Loop := 1 to BufSize DO
   BEGIN
      FOR Chan := 0 to (TopChan-1) DO
      BEGIN
         Write(out,DataArray[Chan,loop]:5:5,',');
      END;
      Writeln(out,DataArray[TopChan,loop]:5:5);
   END;
   Close (Out);
   SaveTimes := SaveTimes + 1;
   Empty_the_array;
END;

{*********************************************************}

{Name is self explanatory...}
PROCEDURE WasteTime;
   VAR Info : STRING[4];
      WatchFlag : BOOLEAN;
      ch : Char;
BEGIN
   WatchFlag := True;
   REPEAT
      BEGIN
         GetTime (Hr,Min,Sec,Frac);
         IF (Sec > Sec0) THEN
         BEGIN
            RunTime := RunTime + (Sec-Sec0);
            Sec0 := Sec;
         END;
         IF (Sec < sec0) THEN
         BEGIN
            RunTime := RunTime + (60-Sec0 + Sec);
            Sec0 := Sec;
         END;
         If RunTime >= PrevTime + SamplePeriod THEN
         BEGIN
            DataArray[0,Count] := RunTime;
            WatchFlag := False;
            PrevTime := RunTime;
            Sec0 := sec;
         END;
         IF Keypressed THEN
         BEGIN
            ch := ReadKey;
            IF (ch = 't') then watchflag := false;
                        {increment 1 min and take readings}
            IF ch = #0 THEN        {check for CTRL or ALT}
            BEGIN
               Ch := ReadKey;   {Alt-X keys}
               If ch = #045 THEN
               BEGIN
                  Ended: = TRUE;
                  SaveAll;
                  Watchflag := False;
               END;
            END;
         END;
      END;
   UNTIL Watchflag = False;
END;

{*********************************************************}

PROCEDURE StartTest;
   VAR Out : TEXT;
      Info : string[5];
      Ch : Char;
      Loop : Integer;
BEGIN
   GotoXY (1,12);
   Writeln ('     Y to Start Test');
   REPEAT
      REPEAT UNTIL KeyPressed;
      CH := ReadKey;
   UNTIL UpCase(ch) = 'Y';
   GoToXY (33,25);
   TextColor (Black);
   TextBackground (White);
   Write('<Alt-X> to END');
   TextColor (White);
   Textbackground (Black);
   GotoXY (1,11);
   Write ('Time (s) ');
   FOR loop := 1 to TopChan DO
   BEGIN
      Str (loop,N);
      Write ('Chan '+N+' ');
   END;
   Writeln;
   Writeln ('_________ ... _________');
   Window (3,13,78,24);
END;

{*********************************************************}

PROCEDURE DisplayLine;
   Var Loop : Integer;

BEGIN
   For Loop := 0 to TopChan DO
   BEGIN
      GotoXY (Loop*8,WhereY);
      Write (DataArray[Loop,Count]:5:0);
   END;
   Writeln;
END;

{*********************************************************}

PROCEDURE RunTest;
BEGIN
   REPEAT
      SampleAll (Count);
      DisplayLine;
      If Count MOD BufSize = 0 THEN SaveAll;
      Count: = Count + 1;
      WasteTime;
   UNTIL Ended;
END;

{*********************************************************}

PROCEDURE Introduction;
   VAR Ch : Char;
BEGIN
   TextColor(Black);
   ClrScr;
   TextBackGround(White);
   GotoXY(1, 1); ClrEol;
   Write('  E. S. H. DATA AQUISITION PROGRAMME V1.00');
   GotoXY(1, 25); ClrEol;
   Write(' Writen by M. Gammon.        1992');
   TextBackGround (Black);
   Window(10,6,75,19);
   ClrScr;
   Window(8,5,73,18);
   TextColor(White);
   ClrScr;
   Writeln; Writeln ('    **** INTRODUCTION ****');
   Writeln;
   Writeln ('This programme will sample upto 8 channels of the PC_30 card ');
   writeln ('at set time intervals and store the voltages recorded in a file');
   Writeln (' for future importation into a spreadsheet programme.');
   Writeln (' You will be asked for data relavent to the test as well as a ');
   Writeln (' file name for storage and the channel numbers to monitor. ');
   Writeln (' THE PC-30 CARD MUST BE CONFIGURED AS 0 TO 10 VOLTS... ');
   Writeln;
```

```
    WriteIn ('Space bar to continue...');
    Repeat
       Repeat until keypressed;
       Ch := ReadKey;
    Until ch = ' ';
    TextColor (Black);
    ClrScr;
    Window(1,1,80,25);
END;

{*********************************************************}

PROCEDURE EndingScreen; ; clears test mode screen settings
BEGIN
    Window(1,1,80,25);
    ClrScr;
    TextColor (LightGray);
    TextBackground(Black);
END;

{*********************************************************}

PROCEDURE MyExit ; FAR;
BEGIN
    EndingScreen;  {Clears the test mode screen settings}
    IF NOT Ended THEN
    BEGIN
       SaveAll;
       WriteIn ('<Ctrl-Break>');
       WriteIn ('This test has been abborted... ');
       Beep;
    END;
    GotoXY (1,10);
END;

{*********************************************************}

BEGIN
    ExitSave := ExitProc;
       ExitProc := @MyExit;
          ClrScr;
          Introduction;
             EnterTestData;  {Date, soln, Pot, °C, File...}
                Initialize;{Counter, array=0's,
                            ended = x, AD card mode}
                StartTest;
             GetTime (Hr,Min,Sec,Frac);
          Sec0 := Sec;
       RunTest;
    EndingScreen;
END.
```

APPENDIX C

508-A : HT3	Potnetial		Resultant Values				Normalised values			
TEST CON	SCE	SHE	UTS	Strain	Produc	ROA	UTS	Strain	Produc	ROA
1000ppm SO4	-590	-350	618	15.7	91	52	0.924	0.770	0.722	0.732
1000ppm SO4	-680	-440	635	16.2	95	62	0.949	0.794	0.754	0.861
1000ppm SO4	-790	-550	543	17.0	101	57	0.812	0.833	0.802	0.792
1000ppm SO4	-990	-750	528	14.6	90	49	0.789	0.716	0.714	0.681
1000ppm Cl	-590	-350	631	14.1	85	60	0.943	0.691	0.675	0.833
1000ppm Cl	-680	-440	641	17.3	101	65	0.958	0.848	0.802	0.903
1000ppm Cl	-790	-550	634	14.6	87	64	0.948	0.716	0.690	0.889
1000ppm Cl	-990	-750	645	13.8	86	52	0.964	0.676	0.683	0.722
Air Test			669	20.4	126	72				

508-B : HT3	Potnetial		Resultant Values				Normalised values			
TEST CON	SCE	SHE	UTS	Strain	Produc	ROA	UTS	Strain	Produc	ROA
1000ppm SO4	-590	-350	558	15.3	80.6	44	0.919	0.801	0.760	0.625
1000ppm SO4	-680	-440	564	15.6	82.7	68	0.929	0.817	0.780	0.966
1000ppm SO4	-790	-550	575	17.9	93.9	63	0.947	0.937	0.886	0.895
1000ppm SO4	-990	-750	545	11.7	61.6	59	0.898	0.613	0.581	0.838
1000ppm Cl	-590	-350	525	18.0	86.2	56	0.865	0.942	0.813	0.795
1000ppm Cl	-680	-440	579	15.2	72.5	60	0.954	0.796	0.684	0.852
1000ppm Cl	-790	-550	576	16.7	89.9	53	0.949	0.874	0.848	0.753
1000ppm Cl	-990	-750	585	14.3	79.8	70	0.964	0.749	0.753	0.994
Air Test			607	19.1	106	70.4				

APPENDIX C

508-A : HT1	Potnetial		Resultant Values				Normalised values			
TEST CON	SCE	SHE	UTS	Strain	Produc	ROA	UTS	Strain	Produc	ROA
1000ppm SO4	-590	-350	990	3.1	53.1	25	0.825	0.356	0.483	0.380
1000ppm SO4	-680	-440	1203	4.0	79.0	19	1.003	0.460	0.718	0.380
1000ppm SO4	-790	-550	1176	1.2	72.4	25	0.980	0.368	0.658	0.496
1000ppm SO4	-990	-750	1026	4.1	67.1	6	0.855	0.471	0.610	0.197
1000ppm Cl	-100	140	741	4.9	37.4	30	0.549	0.563	0.340	0.600
1000ppm Cl	-540	-300	982	4.4	62.1	30	0.727	0.506	0.565	0.600
1000ppm Cl	-540	-300	744	2.7	24.1	46	0.551	0.310	0.219	0.920
1000ppm Cl	-540	-300	962	4.0	50.5	41	0.713	0.460	0.459	0.820
1000ppm Cl	-590	-350	1038	2.5	47.9	16	0.865	0.287	0.435	0.225
1000ppm Cl	-640	-400	1286	2.7	65.4	15	0.953	0.310	0.595	0.300
1000ppm Cl	-680	-440	1136	6.4	92.9	19	0.947	0.736	0.845	0.290
1000ppm Cl	-750	-510	1129	4.6	63.6	46	0.836	0.529	0.578	0.920
1000ppm Cl	-770	-530	1319	4.4	89.0	15	0.977	0.506	0.809	0.300
1000ppm Cl	-790	-550	1288	3.6	82.7	9	1.073	0.414	0.752	0.180
AIR TEST			1200	8.7	110.0	50.0				

508-A : HT2	Potnetial		Resultant Values				Normalised values			
TEST CON	SCE	SHE	UTS	Strain	Produc	ROA	UTS	Strain	Produc	ROA
1000ppm SO4	-540	-300	733.0	11.5	81.3	48	0.852	0.575	0.602	0.708
1000ppm SO4	-590	-350	809.0	12.0	96.5	41	0.941	0.600	0.715	0.605
1000ppm SO4	-640	-400	815.0	13.0	106.2	53.5	0.948	0.650	0.787	0.789
1000ppm SO4	-680	-440	815.0	14.0	111.4	52.4	0.948	0.700	0.825	0.773
1000ppm SO4	-740	-500	834.0	14.7	117.7	57.1	0.970	0.735	0.872	0.842
1000ppm SO4	-790	-550	818.0	14.5	117.9	54	0.951	0.725	0.873	0.796
1000ppm SO4	-990	-750	854.0	10.6	96.8	35	0.993	0.530	0.717	0.546
1000ppm Cl	-540	-300	692	11.7	77.2	54.7	0.805	0.585	0.572	0.807
1000ppm Cl	-590	-350	802	13.3	101.3	54.7	0.933	0.665	0.750	0.807
1000ppm Cl	-640	-400	851	15.2	120.4	55.5	0.990	0.760	0.892	0.819
1000ppm Cl	-680	-440	806	14.9	111.2	57.1	0.937	0.745	0.824	0.842
1000ppm Cl	-740	-500	846	16.3	131.0	58.5	0.984	0.815	0.970	0.863
1000ppm Cl	-790	-550	825	11.4	92.8	53.3	0.959	0.570	0.687	0.786
1000ppm Cl	-990	-750	850	11.2	98.4	41.2	0.988	0.560	0.729	0.608
1000ppm Cl	-1190	-950	860	14.6	123.9	51	1.000	0.730	0.918	0.752
Air Test			860.0	20.0	135.0	67.8				

APPENDIX C

316NG	Potential		Resultant Values				Normalised values			
Specimen Orientation	SCE	SHE	UTS	Strain	Produc	ROA	UTS	Strain	Produc	ROA
Parallel	*****	-960	454	49	195.5	59	0.839	0.803	0.855	0.743
Parallel	-450	-210	474	47	194.2	56	0.876	0.770	0.812	0.738
Parallel	-200	40	464	55	227.9	67	0.858	0.902	0.971	0.867
Parallel	-41	199	466	63	258.9	67	0.861	1.033	0.971	0.984
Perpendicular	-100	140	483	60	255.6	87	0.873	0.845	0.947	0.911
Perpendicular	-200	40	491	56	241.0	86	0.888	0.789	0.893	0.901
Perpendicular	0	240	465	64	266.4	86	0.841	0.901	0.987	0.901
Perpendicular	100	340	468	61	254.0	89	0.846	0.859	0.941	0.932
Perpendicular	200	440	443	42	164.0	66	0.801	0.592	0.607	0.691
Air parallel			541	61	263.0	69				
Air Perpendicular			553	71	270.0	95.5				